ADVANCED FUNCTIONAL MATERIALS
www.afm-journal.de

Perylene-Based Dyes in Dye-Sensitized Solar Cells: Structural Development and Synthetic Strategies

*Marco Giordano, Francesca Cardano, Claudia Barolo, Guido Viscardi, and Andrea Fin**

The versatile absorption and fluorescence properties alongside the outstanding chemical and photostability make the rylene-based derivatives one of the most investigated compounds in the field of third-generation solar cells. Over the last 25 years, an intensive research activity has made the rylene-based derivatives one of the most interesting and modular class of sensitizers in the dye-sensitized solar cells. This critical analysis compares and discusses the state of the art of the rylene-based dyes, starting from the pioneering studies on the perylene bisimides to the latest *N*-annulated rylene derivatives. The focus of this review is to discuss the structure-to-properties relationship highlighting how critical points have been overcome and what are the most recent approaches toward the achievement of novel record efficiencies in the dye-sensitized solar cells.

1. Introduction

World energy consumption is a daily modern-society challenge. The 600 BTU (British Thermal Unit) values, currently used, are expected to rise by 50% by 2050: the socio-economic growth requests energy sources that are still, unfortunately, based on fossil fuels.[1] The environmental impact of fossil fuels represents the main drawback for their use as a long-term solution and their shortages and costs result in additional weak properties. Renewable and economic energy sources are the only possibilities for a sustainable global development.[2] Photovoltaic technology is considered one of the most promising option among the renewable energy solution.[2,3] Sun is the most powerful energy source available, every year it provides the earth with 174 petawatts (PW) of energy: the sun provides more energy to the earth in 1 h than the earth/humans' energy needs of a whole year.[4] The photovoltaic technologies have therefore been a hot topic in the international research and politics over the last twenty years due the almost "unlimited power", the global availability, and the low cost.[5,6]

A photovoltaic cell (PV) is an electrical device converting the sun's incident light directly into electricity by using photovoltaic effect. Several technologies have been developed over the years after the first crystalline silicon solar cell reported by Chapin et al. in 1954 following this concept.[7] The first-generation solar cells are based on monocrystalline or polycrystalline silicon, they achieve efficiencies of over 25%, and they are dominating the PV global market.[8] Their production remains limited regarding sustainability, but the reduced production costs enforce their competitiveness.[8,9] Over the years, different PV technologies have been developed: thin-film solar cells, based on semiconductor materials such as gallium arsenide and copper indium gallium selenide (CIGS) and the latest third-generation technologies including dye-sensitized solar cells (DSSC), organic solar cells (OSC), quantum dots solar cells (QDSC), and perovskite solar cells (PSC).[10–21] DSSCs result in today's most consolidated technology reaching conversion efficiencies above 14%.[22] DSSCs remain attractive thanks to low-cost materials, easy-to-scale manufacturing, versatile design (colors and patterns), high performance and stability under low or diffuse light conditions, and lower performance than other third-generation technologies.[8,13,22–25]

New interesting DSSC-based approaches like i) textile-DSSCs for wearable electronics, ii) semi-transparent DSSCs for the application in agrivoltaic systems (AVs), and iii) colorless and transparent DSSCs for the building integration photovoltaics (BIPVs) are indeed in constant development.[26–28]

1.1. DSSC Structure and Working Principle

A typical DSSC (**Figure 1a**) is a multicomponent photoelectrochemical device constituted by several components: i) a transparent glass sheet covered by a conductive indium-tin oxide (ITO) or fluorine-tin oxide (FTO) layer used as anode substrate; ii) a mesoporous oxide layer, typically TiO_2, deposited on the substrate to transfer electrons; iii) a sensitizer adsorbed on the

M. Giordano, F. Cardano, C. Barolo, G. Viscardi, A. Fin
Department of Chemistry
University of Torino
Via Pietro Giuria 7, Torino 10125, Italy
E-mail: andrea.fin@unito.it
C. Barolo
NIS Interdepartmental Centre
University of Torino
Via Gioacchino 15/a, Torino 10125, Italy
C. Barolo
ICxT Interdepartmental Center
University of Torino
Lungo Dora Siena 100, Torino 10153, Italy

The ORCID identification number(s) for the author(s) of this article can be found under https://doi.org/10.1002/adfm.202411230

DOI: 10.1002/adfm.202411230

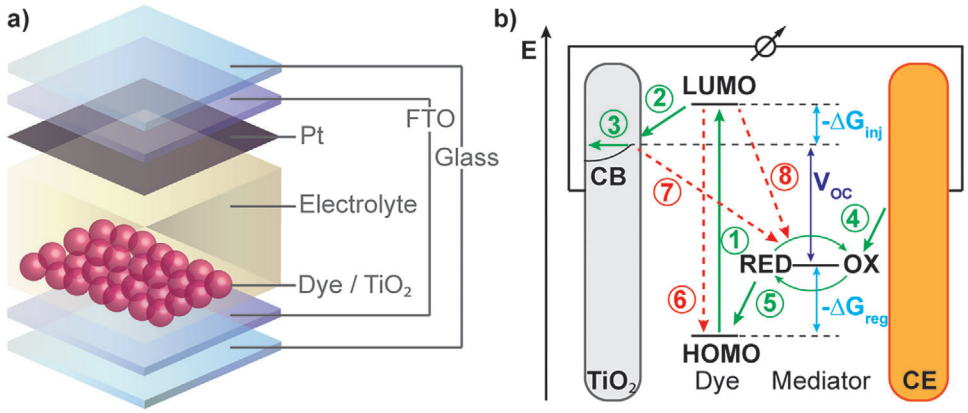

Figure 1. a) Schematic overview of a classic DSSC highlighting the different components. b) Schematic overview of charge transfer processes in DSSCs. 1) Photoexcitation, 2) electron injection, 3) electron migration, 4) redox couple regeneration, 5) dye regeneration, 6) deactivation of the excited state, 7) geminate electron recombination, and 8) non-geminate electron recombination. $-\Delta G_{inj}$ and $-\Delta G_{reg}$, are the driving force energy for electron injection and dye regeneration, respectively. $-\Delta G_{inj}$ is defined by the potential difference between the conduction band of semiconductor and LUMO level of the dye while, $-\Delta G_{reg}$ is defined by the potential difference between the HOMO level of the sensitizer and the redox couple.

mesoporous oxide layer to harvest incident light; iv) an electrolyte for the recovery of dye, typically based on triiodide/iodide redox couple or on the most performant cobalt- and copper-based complexes; v) a counter electrode made of a conductive layer glass sheet coated with a catalyst, typically platinum, to catalyze the redox couple regeneration reaction and collect the electrons from the external circuit.[13,29–33]

The operating principle in DSSCs under light involves four main processes with different time scales (Figure 1b): i) the photoexcitation of the sensitizer followed by the electron injection from the dye excited-state to the conduction band (CB) of the semiconductor (fs up to ps); ii) the dye regeneration (ns up to µs); iii) the electron transport toward collection (ms); iv) the diffusion of the redox mediator to/from the counter electrode (ms up to s).[31] Nevertheless, some undesirable reactions as the deactivation of the excited state of the dye, the geminate, and the non-geminate electron recombination can occur beside the desired electron transfer processes resulting in efficiency's losses.[34–36]

The photovoltaic conversion efficiency (PCE) is correlated to the short circuit photocurrent density (J_{SC}), the open circuit voltage (V_{OC}), the fill factor of the cell (FF), and the intensity of the incident light (P_{in}), as shown by the Equation (1):

$$PCE = \frac{J_{SC}\ V_{OC}\ FF}{P_{in}} \tag{1}$$

The fill factor is the ratio between the maximum power obtained with the device and the theoretical maximum power (J_{SC} V_{OC}), it can vary between 0 and 1 and describes the electrical and electrochemical losses during cell's operation. Another fundamental measurement of the performance of a DSSC is the "external quantum efficiency", usually called the Incident Photon to Current Conversion Efficiency (IPCE). The IPCE value corresponds to the photocurrent density produced in the external circuit under monochromatic illumination of the cell divided by the photon flux that strikes the cell. IPCE values provide practical information about the monochromatic quantum efficiencies of a DSSC and is calculated by Equation (2):

$$\text{IPCE} = 1240\ [eV\ nm]\ \frac{J_{SC}\ \left[mA\ cm^{-2}\right]}{\lambda\ [nm] \cdot P_{in}\ (\lambda)\ [mW\ cm^{-2}]} \tag{2}$$

The successful production of current relies on reaching a quantitative yield of electron injection and dye regeneration, but it also requires the minimization of the undesired recombination processes. Each unfavorable deactivation path requires to be at least 10^3 times slower than the favorable pathway to reach 99 + % yield.[34]

The optimization of each component and process previously described is required to achieve high efficiencies. Over the years, each component of the device was in depth investigated. Most recently, conversion efficiencies above 15% were achieved by pursuing different strategies covering the development of new sensitizers, novel composite photoanodes, and copper-based electrolytes, up to the co-sensitization approach.[22,37–40]

A great attention was dedicated to the improvement of dye properties.[13] The ideal photosensitizer should fulfill some essential characteristics: i) the dye should have a panchromatic absorption spectrum with a high molar extinction coefficient; ii) strong anchoring groups are required to bind the dye onto the semiconductor surface; iii) the LUMO level of the sensitizer should be higher in energy than the conduction band edge of semiconductor to lead to an efficient electron injection; iv) optimized molecular structure is off importance to avoid unfavorable aggregation phenomena; v) high photo- and thermal stability are required.[41] Many classes of dyes were tested starting from the ruthenium-based complexes with the goal to fulfill these requirements.[42,43] Porphyrin, phthalocyanine, metal-free organic dyes including coumarins, indolines, triarylamines, polymethines, are just few examples.[44–52] Among these molecules, perylene-based dyes were intensively studied for their i) remarkable photophysical properties; ii) outstanding conductive behavior; iii) exceptional chemical, thermal, and photostability; iv) easy tunability of the optical and physical properties.[53–66] Over

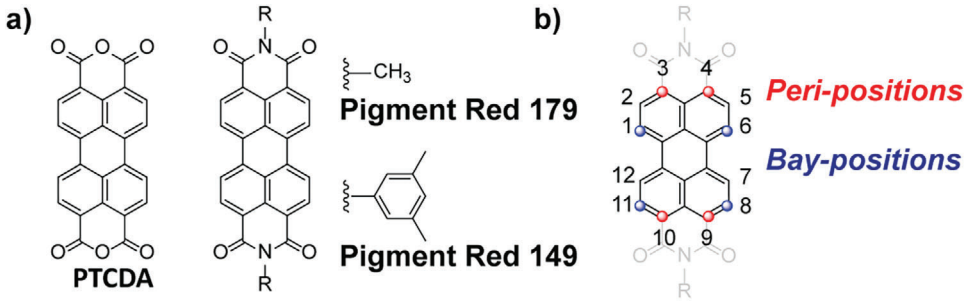

Figure 2. a) Chemical structures of **1** and PDIs widely used as industrial pigments. b) Basic molecular structures of the **1** highlighting the different reactive sites.

their application as sensitizer in DSSCs, perylene-dyes were also widely exploited in fully-organic solar cells (OSCs), in organic field-effect transistors (OFETs) technologies, in bioimaging applications, in organic light-emitting diode technologies (OLED) and in luminescent solar concentrators (LSCs).[16,67–82] In this review, we provide a complete overview on the use of perylene-based dyes in DSSCs, highlighting the relationship between the molecular design and the photovoltaic performance for a useful overview and an outline for future research strategies.

2. Synthesis

It is important to highlight how the photophysical and electrochemical properties of rylene dyes can be tuned via several synthetic strategies before examining the application in DSSCs. A general overview on the main synthetic strategies to modify both perylene imides and *N*-annulated perylene derivatives will be herein discussed, highlighting the state-of-the-art strategies to synthetize the main building blocks and the final dyes. The synthetic functionalization of the perylene core could be essentially described by two complementary pathways. The most functional synthetic approach aims on conferring solubility to the perylene scaffolds by replacing the anhydride moieties with the imide functions on the molecular edges. The strategic insertion of the imides not only confers higher processability to the material but can also provide additional functionalities, reactive groups, linkers for further synthetic steps, and chemical decorations as later discussed in this review. In a complementary manner, the other synthetic approach is strictly related to the tuning of the photophysical and electrochemical features of the dyes by the functionalization of perylene core with various substituents following a common halogenation stage. The straightforward halogen insertion on the dye core facilitates and widens the possible further functionalization that has a remarkable effect on the photophysical, and electrochemical properties of the final dye as discussed in the following sections. The combination of these two strategies along with appropriate molecular design allows the preparation of symmetrical, asymmetrical, core-extended perylene-based dyes bearing various substituents on the dye scaffold and either one or two functional amides on the dye edges suitable for application in many research fields and applications.[67–82] Additional details on the reactivity and synthesis of rylene-derivatives can be found in other literature resources.[50,56–62]

2.1. Synthesis of Perylene Imides

Perylene-3,4,9,10-tetracarboxylic acid diimide derivatives (PDIs) were introduced in 1912 in the dyes industry where the perylene-3,4,9,10-tetracarboxylic dianhydride **1**, was first synthetized and further reacted to prepare brilliant red dyes used in vat dyeing processes on cellulosic fiber (**Figure 2a**). Four decades later industrial scale production of PDIs started to fulfill the demand of this chromophore family due to their versatility and stability as pigments.[53,83] The pivotal common starting material of all PDIs, **1**, is a flat symmetrical oligo aromatic scaffold bearing two anhydride functions at the so-called peri-positions, which are, by reaction with functionalized amines, condensed to the corresponding imines and play a crucial role in the physical properties of the final dyes (e.g., solubility, hydrophilicity). The four core positions on the perylene, named bay positions, are instead used to tune the photophysical properties by extending the π-system or introducing various functional substituents (Figure 2b).

The first approach, leading to the development of high-performance industrial pigments based on **1**, were described for the preparation of Pigment Red 179 and Pigment Red 149 (Figure 2) by a classical imidization reaction on both anhydride sites to obtain the symmetrical PDIs as **2** (**Scheme 1**).[51,84] These molecules were characterized by high photostability, brilliant color but poor to no solubility in most organic solvents, as most pigments. Therefore, substitutions at the imide sides with various alkyl or aryl moieties were explored to improve their processability.[60] Long branched alkyl chains or *ortho*-substituted aryl groups were particularly effective as solubilizers since their out of plane geometry was reported to lower PDIs aggregation, mostly driven by π–π stacking phenomena.[60,85,86] The solubility of these bulky-substituted PDIs was reported as good in halogenated solvents (e.g., dichloromethane, chloroform) but poor in polar media (e.g., water, alcohols) that were often exploited to precipitate and collect the desired products. Symmetrical PDIs as **2** were commonly synthetized by high-temperature condensation of **1** with aniline or aliphatic primary amines in high-melting point solvents such as imidazole or quinoline using zinc acetate as catalyst. This synthetic approach allowed large-scale production in high isolated yields (> 80%) after relatively simple purification by precipitation in polar solvents.[54,60,64]

Unsubstituted PDIs **2** are usually characterized by i) a strong vibronically structured absorption maxima ≈525 nm, ii) molar extinction coefficients $\approx 10^5$ $M^{-1}cm^{-1}$, iii) fluorescence spectra with small Stokes-shift, and iv) outstanding fluorescence

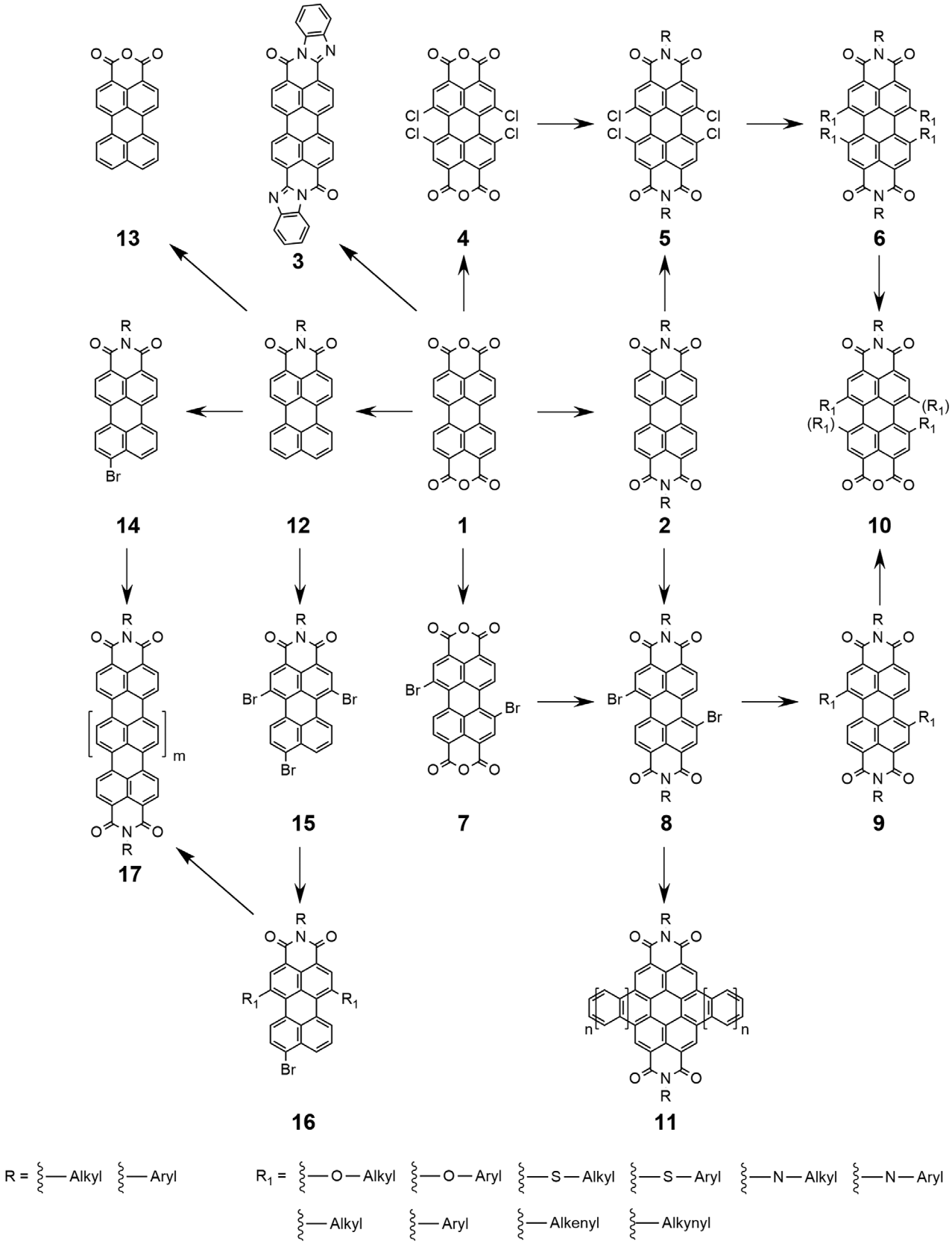

Scheme 1. Synthesis and modification of perylene imide derivatives.

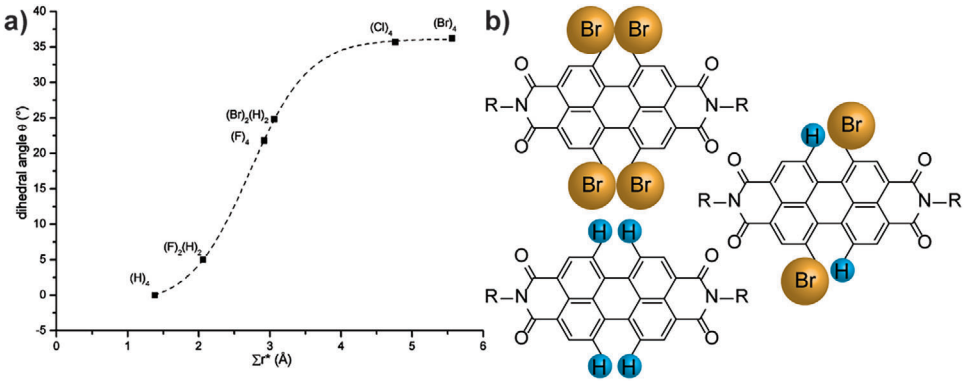

Figure 3. a) Dependence of the dihedral angle and the apparent overlap for different halogen-substituted perylene diimides; b) Chemical structures for different substituted perylene diimides. Reproduced with permission Copyright 2007, American Chemical Society.[88]

quantum yield, higher than 95%.[64,67] In general, the solubility and the supramolecular interactions could be addressed by the functionalization at the imide sites, while these modifications are not affecting the fundamental photophysical or electrochemical features such as absorption/fluorescence maxima and HOMO/LUMO levels of **2**. In few cases, like for **3**, the imidization performed with aromatic diamines provided the extension of the aromatic core of **1** depicted by a remarkable bathochromic shift and a higher molar extinction coefficient compared to **2**.[62]

An important breakthrough to broaden the functionalization and, consequently, the applications of PDIs was represented by the introduction of a selective electrophilic aromatic halogenation of the perylene core.[87] While activating reactive sites, the halogenation of the bay positions induces a distortion on the PDI planar scaffold, depicted by an increase of the dihedral angles in the bay area, which is related to the number and type of halogen atoms (**Figure 3**).[88]

The tetrachlorinated **4** is commonly synthetized from **1** by an electrophilic substitution with chlorosulfonic acid and a catalytic amount of iodine at 70 °C for 20 h, leading to a quantitative yield of almost pure product with minimal contamination of pentachlorinated analog.[89] Similar result can be obtained for the preparation of the PDI **5** starting from **2**.[90] The insertion of bromine, instead of chlorine, requires harder conditions as reported by BASF for the preparation of **7** in fuming sulfuric acid at high temperature (> 80 °C) for 18 h.[91] An insoluble mixture of 1,7, and 1,6 dibrominated regioisomers with traces of tribrominated compound in ratio 76:20:4 is obtained and purified after the subsequent imidization step.[92] The halogenated dianhydride **4** and **7** can be easily converted to the corresponding imines **5** and **8** in *N*-methyl-2-pyrrolidone (NMP) as solvent and a catalytic amount of acetic or propionic acid. It is worth nothing that generally aromatic amines require higher temperature and longer reaction time to react compared to the alkyl ones.[64] Similarly to **5**, **8** can be also obtained in milder conditions followed by recrystallization starting from **2**.[93]

An alternative way to tune the PDI photophysical features is represented by the lateral core extension on **8** to get **11** as coronene diimide ($n = 0$) and dibenzocoronene diimide ($n = 1$) by Sonogashira reaction with alkynes and subsequent aromatization with 1,8-diazabicyclo[5.4.0]undec-7-ene (DBU).[62,63] In a similar logic, the extension of the π-system along the main molecular axis is reported as a useful approach to modulate the molecular dipole moment and the photophysical properties of the dyes.

The halogenated **5** and **8** pave the way to tune the properties of di and tetra-substituted PDI as **6** and **9** by traditional nucleophilic substitution or metal-catalyzed coupling like Suzuki, Stille, Sonogashira, and Heck couplings.[64] Functionalization at the bay positions with phenols, thiophenols, and alcohols is reported to red-shift the absorption maximum while preserving the emission features. Substitution with amines provides large bathochromic shift but lowers both the fluorescence and photostability properties.[54,57,94]

Perylene monoamide (PMI) as **12** are the key structures to pursue this strategy and can be directly obtained from **1**.[95–97] The direct mono imidization to isolate **12** in a single step is carried out in autoclave over a day at high temperature (180–190 °C) and under pressure (15 bar). Reactions with hindered aromatic amines such as 2,5-di-*tert*-butylphenylamine or 2,6-di-*iso*-propilphenylamine led to the desired products in better yield (almost 50%) than reactions whit aliphatic amines (< 30%).[97,98]

Subsequent mild or hard bromination conditions provides the selective single brominated **14** or the tri brominated **15** as versatile building blocks for the π-system extension.[99,100] The brominated bay positions in **15** can be selectively reacted, as previously described, to insert donor groups as in **16** with poor yields generally below 35%.[61] Both the brominated PMI **14** and **16** can be further coupled and aromatized to prepare larger rylene diimides **17** as terrylene diimide (m = 1), quaterrylene diimide (m = 2), pentarylene diimide (m = 3) and hexarylene diimide (m = 4) that are usually characterized by excellent photophysical properties but very low solubility in many organic solvents.[62,63,101,102] The extension of the rylene core moves the absorption maxima toward the near infrared region of the spectra and increases the molar extinction coefficient in linear dependence with the number of naphthalene units (**Figure 4**a,b).

Finally, looking at the application as a sensitizer, the presence of a strong anchoring group as an anhydride on the dye structure is essential to maximize the device results.[103] As mentioned, NDIs suffer from poor processability; therefore, the hydrolysis of the solubilizing imide group to the corresponding anhydride, as in **10** and **13**, is usually performed as the last synthetic step.[54]

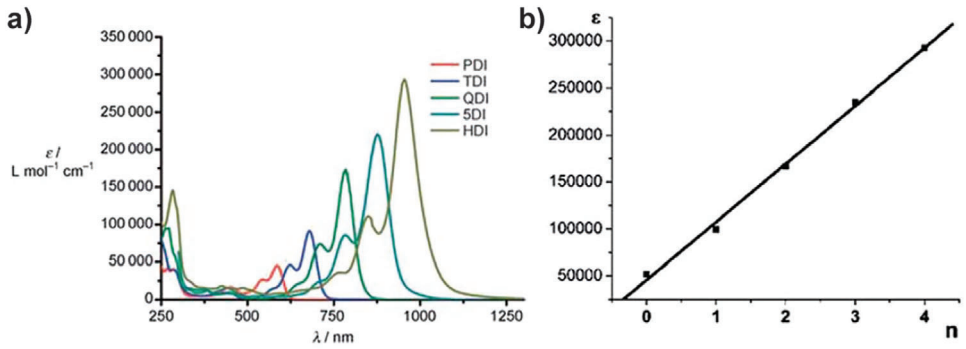

Figure 4. a) Absorption spectra shift rylene diimides as number of fused naphthalene units. b) Correlation between the number of naphthalene units and the molar extinction coefficient. Reproduced with permission Copyright 2014, Royal Society of Chemistry.[63]

2.2. Synthesis of N-Annulated Perylene

π-extended heteroarenes containing nitrogen or chalcogens in fused aromatic rings are deeply investigated for their optoelectronic properties and their potential application in organic field-effect transistors (OFETs), light emitting diodes (LEDs), and photovoltaic devices.[104] *N*-annulated perylene (NP) derivatives have been successfully employed in DSSCs as sensitizers due to their electron-rich nature as an ideal electron donor structure that can be further functionalized (**Figure 5**).

The first reported synthesis of *N*-annulated perylene is a two steps procedure reported by Looker in 1972.[105] The mononitration of **18** to the resulting 1-nitroperylene **19** was carried out using fuming nitric acid in 1,4-dioxane at 60 °C for 30 min followed by the final heterocyclic annulation in triethyl phosphite for 2 h to obtain **20**. While the second step occurs with high yield (> 80%), the first one is limited by the formation of the 3-nitroperylene regioisomer that lowers the yields to 30%. To date, this is the most straightforward procedure to synthetize **20**, a key intermediate in the synthesis of other hetero-annulated perylenes **21** and **22**.[63] The introduction of nitrogen in **20** does not induce a significant change in the packing motif compared to perylene **18** (**Scheme 2**). The crystal structure of **20** exhibits a nearly planar molecular conformation with a packing arrangement consisting of edge-to-face dimers (**Figure 6a**).[65]

On the other hand, the hetero-annulation leads to a hypsochromic shift of the absorption maxima and to a lower molar extinction coefficient of **20** respect to **18** (Figure 6b). As for most unsubstituted perylene dyes, the planar structure in **20** induces a strong π–π interaction lowering the dye solubility. To overcome this limitation, *N*-alkylation or *N*-arylation strategies were reported to confer acceptable solubility of the dyes **23**. The former is an established and efficient procedure (yields > 90%) that usually occurs using a strong base as sodium hydride, alkylbromide as alkylating agent at high temperature while, the latter usually exploits the Ullmann coupling.[106,107] The alkyl- or aryl-*N*-annulated **23** can be further functionalized by classical bromination with *N*-bromosuccinimide (NBS) to obtain the corresponding mono **24** or di brominated **25** derivatives at position 3 and 11 in high yields.[106,108] As mentioned for **8**, the halide presence on the *N*-annulated perylene core of **24** and **25** allows further functionalization by metal-catalyzed coupling reactions. Another interesting strategy consists in the direct mono-formylation of **23** to **26** that can further react in a Knoevenagel condensation to install a cyanoacrylic acid, one of the best-performing anchoring group in DSSCs.[103,108]

Another interesting synthetic strategy, starting from brominated **24** allows the preparation of polycyclic aromatic hydrocarbon (PAH) based on the *N*-annulated perylene scaffold, nowadays among the best-performing sensitizers in DSSCs. A classical Stille coupling on **24** provides the biaryl product **27** with a functionalized thiophene that undergoes a subsequent Grignard reaction to provide a tertiary alcohol moiety in **28**. A final intramolecular Friedel-Crafts cyclization catalyzed by a solid acid catalyst led to the formation of the PAH *N*-annulated perylene isomers **29a** and **29b** in a 2:1 ratio (Scheme 2).[109]

In this section, the most general synthetic strategies for the preparation and functionalization of perylene diimides, monoimides, or *N*-annulated derivatives were discussed. The symmetrical nature of the perylene core along with the poor

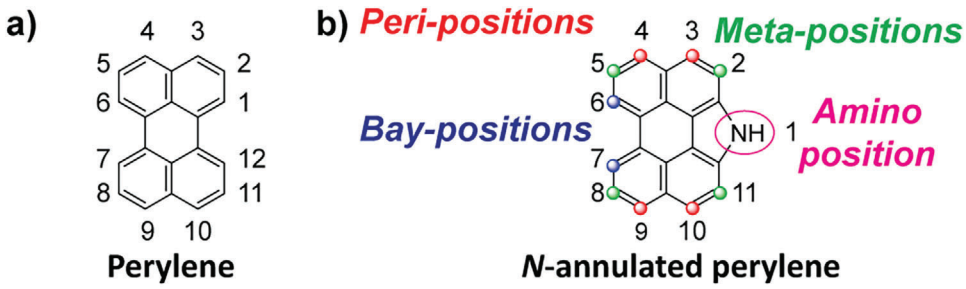

Figure 5. a) Chemical structures of perylene and b) of a *N*-annulated perylene.

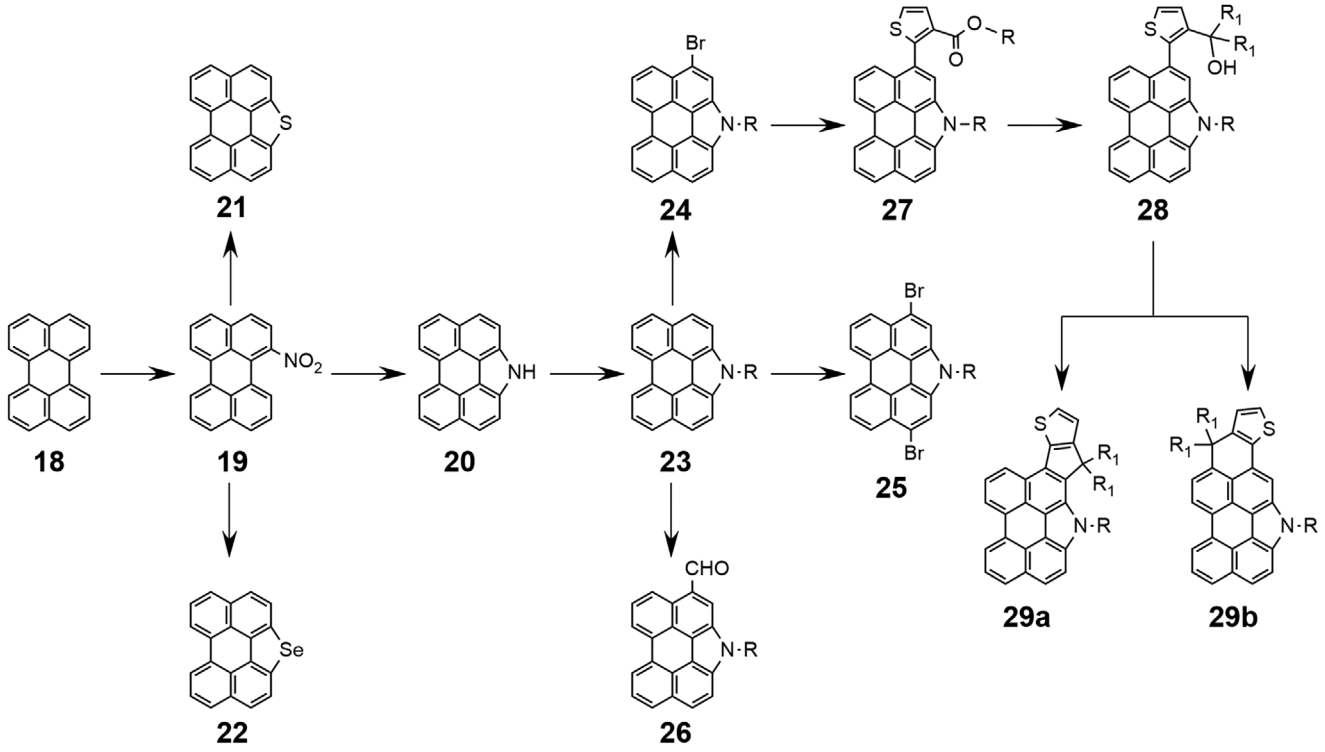

Scheme 2. Synthesis and modification of *N*-perylene derivatives.

processability of the planar scaffolds are the key parameters that require a careful evaluation in the dyes design and in the synthetic pathways rationale to maximize the final output. Obviously, peculiar structures or functional groups can limit if not completely hamper the discussed strategies and require case by case evaluation.

3. Perylene Imides-Based Dyes in DSSCs

Perylene imides were, at first, introduced as sensitizes in 1996 when an electron injection rate of 190 fs was reported for 2,5-bis(*tert*-butyl)-9-methylphosphonic acid perylene adsorbed on nanocrystalline TiO_2.[110] This brilliant result confirmed the versatility of perylene derivatives in which the high emission can facilitate the time-related emission experiments used to measure charge injection rates promoting the use of perylene dyes in DSSC.

3.1. Perylene Diimide Derivatives

The first ever photovoltaic application of perylene dyes was carried out with the sensitizers **30**–**32** onto SnO_2.[111] The dyes were anchored on a 2.5 µm thick nanoporous SnO_2 film on FTO glass through their carboxylic acid groups. A solution of LiBr (0.5 M),

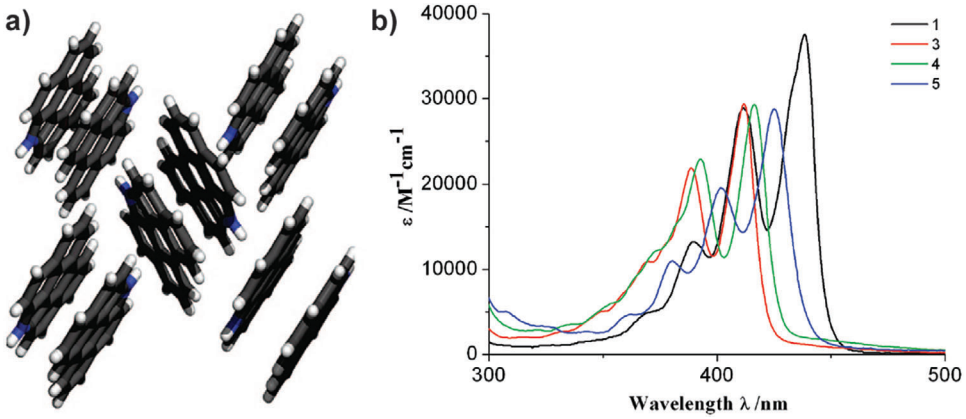

Figure 6. a) The sandwich-herringbone arrangement of *N*-annulated perylene. b) UV–vis absorption spectra of hetero-annulated perylene in chloroform. Reproduced with permission Copyright 2008, American Chemical Society.[65]

Br_2 (0.05 M), and 4-*tert*-butylpyridine (0.2 M) in 80/20 (v/v) ethylene carbonate/propylene carbonate was used as electrolyte and a platinum-coated F-SnO_2 glass substrate as the counter electrode. Cells containing the sensitizer **31** could reach a maximum IPCE of ≈30% in the 458–488 nm spectral region and an overall power conversion efficiency of 0.89%. PDI **32**, bearing a carboxylic group on each phenyl ring rather than directly linked on the perylene core, was efficiently adsorbed on the SnO_2 showing comparable spectral properties to **31**. Nevertheless, **32** exhibited a small short-circuit photocurrent density (≈100 µm cm^{-2}) most likely due to the different dye orientation on the surface, driven by the orthogonal disposition between the anchoring phenyl group and the perylene core.[111] This first work highlighted the potentialities of PDI derivatives in dye sensitized solar cells, despite the lower efficiency compared to the optimized ruthenium complexes-based devices. To better understand the sensitizing behaviour of perylene derivatives, Li et al. studied TiO_2 nanocrystalline films sensitized by **31** and **33** reporting a maximum IPCE of 40% (440–530 nm) for **31** and of 14% (460–510 nm) for **33**. Additionally, the effect of bromine-doping of the TiO_2 nanocrystalline film was discussed for the first time, highlighting a decrease of IPCE values (about a tenth of the non-dopped) and a red-shift of around 20 nm for the wavelength with the maximum quantum yield compared with the non-doped films (**Scheme 3**).[112]

Until then, only carboxylic groups on the PDI scaffold were tested as anchoring group, however, the anhydride moieties can easily react with inorganic semiconductors, such as TiO_2. Icli et al. prepared a series of PMI sensitizers **34–38** varying the substituents on the imide side to evaluate their photovoltaic performance in DSSCs.[113] Dyes with longer and branched alkyl chains achieved higher device efficiencies since hindered alkyl chains prevented self-aggregation of the dye and reduced the charge recombination with the electrolyte.[114,115] Among the tested dyes, **34** was the best performer by reaching an efficiency of 1.61% under AM 1.5 solar light (photovoltaic parameters of *Z907* standard: J_{sc} = 18.02 mA cm^{-2}, V_{oc} = 0.550 V, FF = 0.42, PCE = 4.22%).[113] PMI **38** yields double efficiency value compared to **37** due to the stronger electron donating character of the aromatic ring in comparison to the cyclohexyl substituent. This effect resulted in better electron injection to TiO_2 conduction band for **38**.[113] In the whole series **34–38** the electron transfer from the sensitizer to the conduction band of the semiconductor was not efficient enough because of the absence of a strong intermolecular push-pull effect since the sensitizer consisted of ordinary chromophores bearing an anchoring group (Scheme 3).

Imahori et al. have introduced pyrrolidines as electron-donating groups in the 1,6-position of the perylene core **39–42**, to overcome the poor electron injection and improve the efficiency of perylene sensitizers.[116] The results on these structures led to a couple of benefits. The strong electron-donating ability of the pyrrolidine groups shifted both first oxidation and reduction potentials, generating a more exothermic electron injection from the excited singlet state to the conduction band of TiO_2 electrode along with a bathochromic shift of the absorption maximum. The bay-substituents prevented the dye aggregation on the TiO_2 surface lowering the intermolecular charge recombination, resulting in the highest efficiency of 2.6% under AM 1.5 solar light with **39**. The effect of the pyrrolidine substituents could be further emphasized by simply comparing the devices differences between **39** (PCE 2.6%) and the analog sensitizer **37** (PCE 0.6%). Similarly, the linker effect appeared clear by comparing the device efficiency between the anhydride anchored **39** and **40** (PCE 2.6 and 1.5% respectively) with benzoic acids linked **41** and **42** (PCE < 0.02%) that suffered from lower electron injection due to a larger distance from the dye to the anchoring site.[111]

Following the work of Imahori, Odobel et al. prepared a series of sensitizers **43–50** to correlate the effect of the position and nature of the anchoring groups, the presence of a fused benzimidazole moiety on the perylene scaffold, and the nature of electron-donating substituents on the bay positions to the final device performances.[117] DSSCs sensitized with **43–50** reached efficiencies from 0.2% to 2.3% (photovoltaic parameters of *N3* standard obtained with 0.1 M 4-TBP-based electrolyte: J_{sc} = 13.7 mA cm^{-2}, V_{oc} = 0.663 V, FF = 0.62, PCE = 5.59%).[117] The highest performances were systematically obtained with the sensitizers anchored through the anhydride acid group in **45**, **47–50** showing a better electronic communication with the TiO_2 conduction band (Scheme 3).

The notable difference in the device performances in **43** and **46** was related to the presence of electron-rich groups, a phenoxy and a benzimidazole respectively, and their relative positions to the anchoring site, opposite in **43** and on the fused ring on **46**. As a result, the electronic coupling in the excited-state was reduced, since the electronic density shifted away from the electron rich moieties to reach the most electron-withdrawing group that unfortunately is too far from the TiO_2 surface. The extension of the π-system in **44**, **46**, and **47** led to a similar bathochromic shift of the absorption spectra in all three dyes, while the concurrent presence of the anchoring sites on the benzimidazole in **44** and **46** lowered the devices performances compared to **47** in which the extension of the conjugated system was opposite to the linkage moiety. Looking at the substituent in the bay positions, the presence of four phenoxy groups in **45–48** provided similar effects as two piperidine rings in **49** and **50** along with less dye aggregation, confirming the stronger electron density of the *N*-piperidinyl substituted perylenes compared to the *O*-aryl substituted analogs.[112] Interestingly, the two isomers **49** and **50** exhibited a slightly different behaviour. The HOMO level in **49** was more destabilized compared to **50** by the *trans*-*N*-piperidinyl substituents that was depicted by a lower energy gap resulting in a red-shifted transition and a lower oxidation potential. Vice versa, the *cis*-*N*-piperidinyl substituents lowered the aggregation on TiO_2 surface explaining the higher efficiency of the *cis* isomer **50** versus **49**.

The substituents versatility at the imide edge was also investigated by Palomares et al. by introducing an azacrown moiety in **51** to selectively bind lithium ions to improve the control of ions in the electrolyte and therefore the device performances.[118,119] Under simulated sun light, the DSSCs assembled with **51** showed higher voltages but lower photocurrent compared to the control prepared with **52**. This behavior led to a shift of the TiO_2 conduction band edge due to the complexation of the lithium ions with the aza crown ether, which could be responsible of the formation of dipole at the semiconductor surface (Scheme 3).

As mentioned above, the presence of bulky substituents on the bay position of the perylene core was shown to lower the self-aggregation on the TiO_2 surface and to reduce the charge

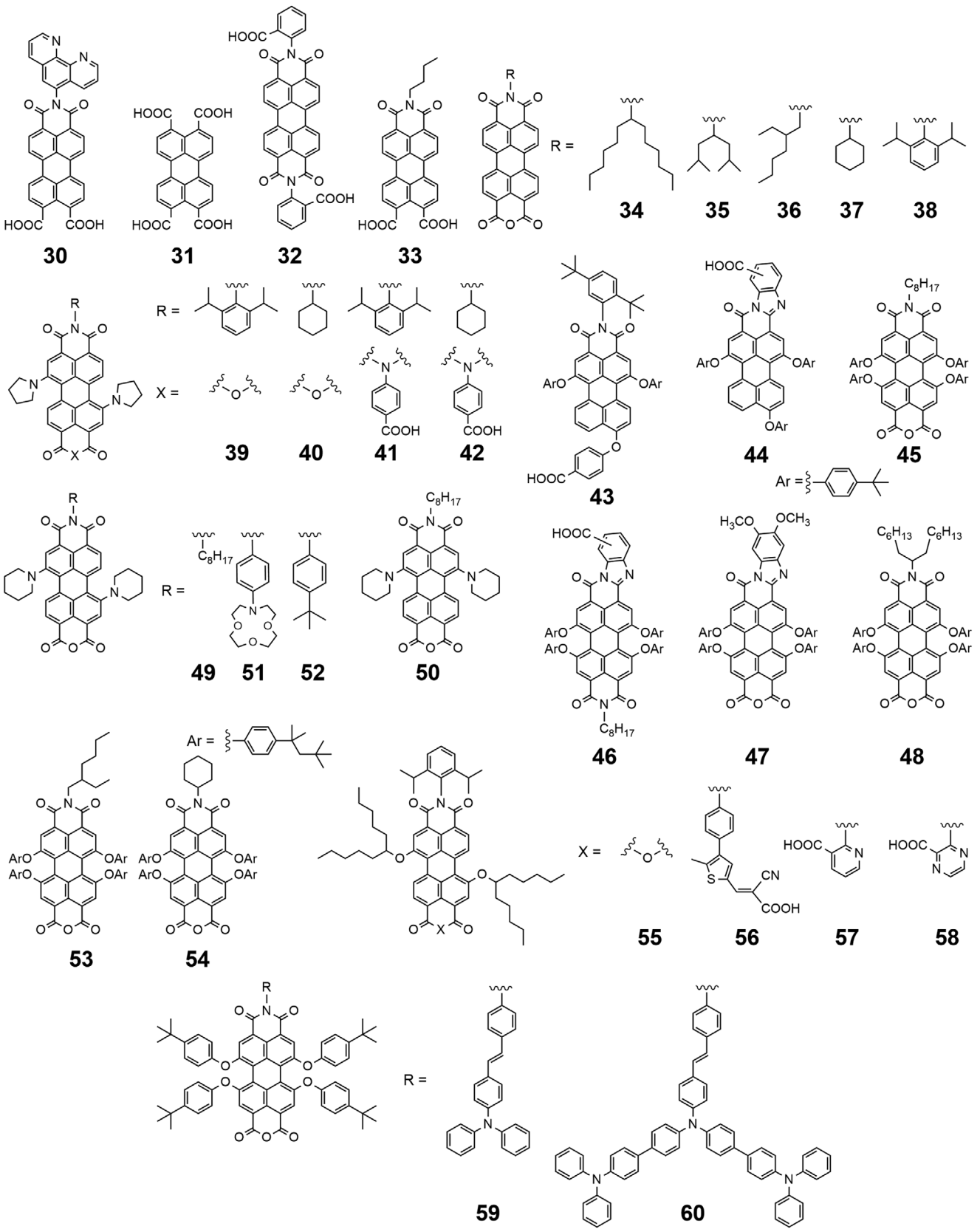

Scheme 3. Perylene diimide-based dyes.

recombination. Over the last years, many interesting studies were reported focussing on this molecular aspect to improve the DSSC performances. The 4-*tert*-octylphenoxy substituent, introduced for the first time by Müllen et al. on the perylene core, represented one of the best bulky-substituents to prevent the aggregation.[102] Few years later, Palomares et al. and Sharma et al. reported detailed correlations among the dye loading, the charge recombination, and the effect of the deoxycholic acid (DCA) on the photovoltaic performance using PMI decorated with the same bulky phenoxy derivative in **53** and **54**.[120,121] Sensitizers **53** was deposited on a 12 µm thick TiO_2 film (8 + 4 µm of scattering layer) on FTO glass varying the dye-loading times. The electrolyte was made by a solution of BMII (0.6 M), I_2 (0.05 M), LiI (0.1 M), and TBP (0.1 mM) in 15/85 (v/v) valeronitrile/acetonitrile. The highest efficiency of 3.15% was reached for the film sensitised for 5 h.[120] Shorter dye-loading time showed both less photocurrent and voltage, demonstrating the key role of the recombination between the photo-injected electrons and the oxidized electrolyte on the overall device efficiency. Interestingly, longer dye-loading time did not involve either a decrease of the electron injection or of the cell voltage, in contrast with the usual trend of other organic dyes (**Table 1**).[115]

Dye **54** was also employed in the evaluation of the deoxycholic acid (DCA) effect as co-adsorber on the photovoltaic performance.[122] A 12 µm thick TiO_2 film on FTO glass was dyed by a solution of sensitizer **54** (0.5 mM) with and without DCA (10 mM) in THF for 24 h. The co-adsorption of DCA resulted in a significant improvement of photocurrent and a slight increase of the open circuit voltage that led to an overall better efficiency. An efficiency of 4.48% was achieved, which represents the highest value among the DSSCs sensitized with perylene diimide derivatives.[121]

Slightly less hindered *O*-alkyl branched substituents dyes **55**–**58** were tested by Dinçalp et al. reporting quite low device efficiencies in the 0.009–0.067% range under AM 1.5 solar light (photovoltaic parameters of *Z907* standard: J_{sc} = 11.87 mA cm^{-2}, V_{oc} = 0.700 V, FF = 0.56, PCE = 4.66%).[123] The low efficiencies were elated to the strong electron-withdrawing nature of imide group, limiting the photo generated electrons transfer from the donor-side to the anchoring-side of the dye. PDIs with pyridine **57** and pyrazine **58** anchoring moieties led to overall better photovoltaic parameters compared to the sensitizer with cyanoacrylic acid anchoring group **56**. These differences were related to the lower LUMO level of **57** (−3.61 eV) and **58** (−3.58 eV) compared to **56** (−3.75 eV), corroborating the key role played by the distance between the chromophore core and the anchoring site. The best efficiency was achieved with **55** with bearing a anhydride acid group anchoring site, highlighting their already reported advantages (Scheme 3).

Among the latest strategies applied to improve the device performance with perylene-based dyes, the functionalization of one imide with a strong electron-donating group such as triphenylamine (TPA) showed interesting results. TPA is a bulky aromatic group well-known to prevent dye-aggregation and to improve the intramolecular electron transfer, leading to an overall improvement of the photovoltaic performance.[50,124–126]

Insuasty et al. reached the efficiencies of 1.00% and 1.30% applying the TPA functionalized PMI **59** and **60**, further highlighting the electron-donating group effect on the photovoltaic performance.[127] However, compared to **39** and **40**, the latest sensitizers show worse efficiency, confirming that the insertion of electron-donating group on the bay position is more effective to better the device performance (Scheme 3).

PDI derivatives show good results in the assembly of several devices, justifying the generally development and further investigation of perylene dyes in the dye-sensitized solar cells field. The presence of an electron-withdrawing group on both sides of the molecule represents one of the main drawbacks of PDIs that prevents a preferential directed photo-generated charge transfer from the molecule toward the conduction band of the metal oxide. This represents the main reason that led to the development of new dyes based on the PMI that allow to design a molecule with a strong push-pull effect. Other key parameters highlighted by the recent experimental results are directed to optimize the dye-anchor site distance, to limit the dye aggregation due to the flat core and to improve the sensitizer solubility to achieve optimal dyeing results.

3.1.1. Multi-Chromophores Systems

An interesting strategy to improve the photovoltaic efficiency is based on multi-chromophores system where suitable molecular design provides dyes characterized by a broad absorption spectra and high molar absorption coefficients.

A first application of this approach based rylene dyes was reported by Tian et al. by merging an NMI and a PMI to bipyridine ligand in **61** and **62** to extend the absorption properties of ruthenium complexes.[128] The photophysical features of **61** and **62** were better than the ruthenium-based dyes alone, but the devices efficiencies reached only 3.08% and 1.75%, respectively.[13] The main responsible for these low efficiency was found in the electron-withdrawing nature of the imide groups, weakening the electrons mobility toward the semiconductor conduction band. Moreover, dye **61** showed higher performance than **62**, which worse efficiency was due to the lower adsorption on TiO_2 due to the larger PMI scaffold (**Scheme 4**).

Similar approach, but operating on the PDI bay positions, was described by Meng et al. linking cyanine unit **63** to a benzo[*e*]indole unit **64** thorough an acetylene linker. In addition to the excellent optical properties, both sensitizers **63** and **64** showed efficiencies of 0.34% and 1.38%, respectively because of an improper intramolecular charge transfer direction caused by the strong electron-withdrawing nature of the imide group. The slightly better conversion efficiency of **64** depended just on its higher LUMO level compared to **63**.

A supramolecular dyad formation, by self-assembly via metal-ligand coordination, was reported by Saha et al. using PMI and Zn-porphyrin or Zn-phthalocyanine as chromophores.[130,131] A 5 µm thick TiO_2 film was first sensitized by PMI solution (0.15 mM in CH_2Cl_2) and later immersed in the Zn-porphyrin or Zn-phthalocyanine solution (2 mM in CH_2Cl_2) to form the supramolecular assembly. A solution of 0.06 M I_2, 1.0 M LiI in propylene carbonate was used as electrolyte. The supramolecular dyads **65** and **66** reached the efficiencies of 1.10% and 2.20%, respectively. The remarkable efficiency shown by dyad **66** was attributed to the better electron-donating ability of Zn-phthalocyanine compared to Zn-porphyrin that led to a

Table 1. Photovoltaic performance of DSSCs employing perylene diimide-based dyes.

Dye	λ_{MAX} (sol) [nm]	ε [$M^{-1}cm^{-1}$]	λ_{MAX} (film) [nm]	IPCE [%] [range/nm]	J_{SC} [mA cm^{-2}]	V_{OC} [V]	FF	PCE [%]	Electrolyte	References
30	510 (NMP)	–	485 (SnO_2)	> 25% (450–525)	3.26	0.45	45.5	0.89	I^-/I_3^-	[111]
31	479 (NMP)	–	492 (TiO_2)	40% (440–530)	–	–	–	–	I^-/I_3^-	[112]
34	–	–	–	> 55% (430–530)	9.79	0.300	55	1.61	I^-/I_3^-	[113]
35	–	–	–	> 45% (450–500)	8.40	0.300	46	1.16	I^-/I_3^-	[113]
36	–	–	–	> 30% (425–525)	6.73	0.26	37	0.65	I^-/I_3^-	[113]
37	524 (Toluene)	–	–	> 25% (425–500)	4.1	0.251	58	0.60	I^-/I_3^-	[113]
38	–	–	–	> 10% (450–550)	0.24	0.273	60	0.37	I^-/I_3^-	[113]
39	708 (CH_2Cl_2)	45 600	–	> 30% (575–725)	7.8	0.54	63	2.6	I^-/I_3^-	[116]
40	708 (CH_2Cl_2)	35 870	–	> 15% (575–700)	4.6	0.51	64	1.5	I^-/I_3^-	[116]
41	708 (CH_2Cl_2)	42 000	–	–	–	–	–	< 0.02	I^-/I_3^-	[116]
42	704 (CH_2Cl_2)	42 300	–	–	–	–	–	< 0.02	I^-/I_3^-	[116]
43	517 (CH_2Cl_2)	31 900	490 (TiO_2)	–	2.6	0.424	66	0.72	I^-/I_3^-	[117]
					0.6 [a]	0.440 [a]	83 [a]	0.22 [a]		
44	560 (CH_2Cl_2)	37 400	551 (TiO_2)	–	0.9	0.336	71	0.21	I^-/I_3^-	[117]
					0.13 [a]	0.369 [a]	79 [a]	0.04 [a]		
45	578 (CH_2Cl_2)	45 600	536 (TiO_2)	–	5.3	0.443	63	1.47	I^-/I_3^-	[117]
					4.1 [a]	0.520 [a]	76 [a]	1.64 [a]		
46	602 (CH_2Cl_2)	66 000	–	–	1.0	0.434	60	0.26	I^-/I_3^-	[117]
					0.3 [a]	0.461 [a]	81 [a]	0.11 [a]		
47	626 (CH_2Cl_2)	27 400	582 (TiO_2)	–	2.9	0.401	65	0.76	I^-/I_3^-	[117]
					2.9 [a]	0.456 [a]	71 [a]	0.96 [a]		
48	581 (CH_2Cl_2)	27 800	525 (TiO_2)	–	6.8	0.494	62	2.09	I^-/I_3^-	[117]
					6.2 [a]	0.550 [a]	67 [a]	2.29 [a]		
49	692 (CH_2Cl_2)	18 000	684 (TiO_2)	–	5.9	0.380	48	1.08	I^-/I_3^-	[117]

(*Continued*)

Table 1. (Continued)

Dye	λ_{MAX} (sol) [nm]	ε [$M^{-1}cm^{-1}$]	λ_{MAX} (film) [nm]	IPCE [%] [range/nm]	J_{SC} [mA cm^{-2}]	V_{OC} [V]	FF	PCE [%]	Electrolyte	References
4.9 [a]	0.450 [a]	64 [a]	1.42 [a]							
50	648 (CH_2Cl_2)	11 300	600 (TiO_2)	–	7.6	0.412	62	1.96	I^-/I_3^-	[117]
					3.2 [a]	0.433 [a]	69 [a]	0.96 [a]		
51	698 (CH_2Cl_2)	23 400	640 (TiO_2)	–	–	–	–	–	I^-/I_3^-	[118]
	680 (ACN)	–								
52	683 (CH_2Cl_2)	22 900	–	–	–	–	–	–	I^-/I_3^-	[118]
53	580 (CH_2Cl_2)	–	525 (TiO_2)	–	9.20	0.52	65.87	3.15	I^-/I_3^-	[120]
54	510 (THF)	–	530 (TiO_2)	60% (550–600)	10.8	0.68	61	4.48	I^-/I_3^-	[121]
55	543 ($CHCl_3$)	–	–	–	0.289	0.350	47	0.067	I^-/I_3^-	[123]
56	528 ($CHCl_3$)	–	665 (TiO_2)	–	0.07	0.320	42	0.009	I^-/I_3^-	[123]
57	528 ($CHCl_3$)	–	671 (TiO_2)	–	0.099	0.390	47	0.018	I^-/I_3^-	[123]
58	527 ($CHCl_3$)	–	671 (TiO_2)	–	0.117	0.410	52	0.025	I^-/I_3^-	[123]
59	586 ($CHCl_3$)	35 600	–	> 5% (480–570)	2.13	0.635	72.3	1.00	I^-/I_3^-	[127]
60	588 ($CHCl_3$)	44 900	–	> 20% (500–550)	2.89	0.638	68.9	1.30	I^-/I_3^-	[127]
61	418 (DMF)	12 900	440 (TiO_2)	> 35% (400–475)	2.64	0.40	58	3.08	I^-/I_3^-	[128]
62	580 (DMF)	45 000	575 (TiO_2)	> 20% (460–525)	1.35	0.42	62	1.75	I^-/I_3^v	[128]
63	589 (ACN:EtOH 1:1)	82 000	555 (TiO_2)	11% (435)	1.24	0.350	59	0.34	I^-/I_3^-	[129]
64	464 (ACN:EtOH 1:1)	75 000	450 (TiO_2)	≈ 2% (500–700)	4.54	0.380	58	1.38	I^-/I_3^-	[129]
65	–	–	415 (TiO_2)	–	5.51	0.410	49	1.10	I^-/I_3^-	[130]
66	–	–	680 (TiO_2)	–	10.0	0.460	50	2.20	I^-/I_3^-	[131]
67	528 (DMSO)	–	495 (TiO_2)	≈ 10% (545)	0.526	0.406	49	0.116	I^-/I_3^-	[142]
68	525 (DMSO)	–	495 (TiO_2)	≈ 8% (545)	0.362	0.387	53	0.083	I^-/I_3^-	[142]
69	385 ($CHCl_3$)	17 900	400 (TiO_2)	> 40% (570–625)	7.54	0.59	61	2.71	I^-/I_3^-	[143]
70	397 ($CHCl_3$)	22 100	400 (TiO_2)	> 40% (565–649)	7.85	0.60	63	2.96	I^-/I_3^-	[143]
71	680 (CH_2Cl_2)	178 000	–	> 60% (560–670)	9.4	0.465	54	2.4	I^-/I_3^-	[144]
130	546 (CH_2Cl_2)	57 073	–	≈ 65% (475)	6.98	0.415	59	1.72	I^-/I_3^-	[195]

[a] 0.1 M 4-*tert*-butyl-pyridine in the electrolyte.

faster electron transfer and a better charge-separation in the device.

3.1.2. Polymer Dyes

The stepwise evolution of sensitizers has finally outlined organic dyes as the winning choice for high photovoltaic performance.[13] Meantime, polymer dyes have also been investigated to evaluate devices' efficiencies. Polymer dye-sensitized solar cell (PSSC) shows the same structure and operation principles of the above-described DSSCs with the only difference residing on the polymeric nature of the dye.

Many examples of PSSC were reported using polythiophenes, polyanilines, phenyl-conjugated oligoenes, polyfluorenes, diketopyrrolopyrrole-based copolymer, polytriphenyl-based polymers among the others as key component.[132–139] The main advantages of the polymeric matrix rely on good thermal and environmental stabilities, solution processability, excellent mobility and conductivity, satisfying exciton generation under illumination, easy deposition on substrates, broad absorption, and high extinction coefficients.[140,141] These properties have also been widely exploited in solid-state dye solar cells, that will be later analyzed.[30]

Perylene diimide derivatives were also employed in these devices as reported by Niu et al. by synthetizing perylene-containing polyamides **67** and **68** that were later adsorbed on TiO_2 for 48 h (Scheme 4).[142] Unfortunately, these two sensitizers were soluble just in high boiling point solvents such as *m*-cresol, DMAc, and NMP that could undesirably dope the dyed TiO_2 film. To avoid this effect additional washing of the film with ethanol and acetonitrile was required. Finally, a solution of 1-butyl-3-methylimidazolium iodide (BMII) (0.6 M), LiI (0.1 M), I_2 (0.05 M), 4-*tert*-butylpyridine (4-TBP) (0.5 M) in acetonitrile was used as electrolyte. Nevertheless, the poor recorded efficiencies of the PSSC cells with **67** and **68** were of 0.116% and 0.083% respectively, most likely due to the lack of chemical bonds between the dyes and the TiO_2 (photovoltaic parameters of *N719* standard: J_{sc} = 14.1 mA cm^{-2}, V_{oc} = 0.735 V, FF = 0.52, PCE = 5.94%.[142]

Slightly better efficiencies were reported by Patra et al. with perylene diimide and thiophene-based copolymers **69** and **70** functionalized with alkyl or perfluoroalkyl chains (Scheme 4).[143] The polymers were adsorbed on the semiconductor surface for 8 h from chloroform and the electrolyte consisted of 1-butyl-3-methylimidazolium iodide (BMII) (0.6 M), I_2 (0.03 M), guanidinium thiocyanate (0.10 M) and 4-*tert*-butylpyridine (4-TBP) (0.05 M) in 85/15 (v/v) acetonitrile/valeronitrile solution. Efficiencies of 2.71% and 2.96% has been reached with **69** and **70**, respectively. The higher photovoltaic performance of the perfluoroalkyl-containing polymer dye **70** was attributed to various reasons: i) the introduction of perfluoroalkyl chain can enhance the internal dipole moment within the polymer backbone; ii) the functionality helped to provide an ordered microstructure at the donor-acceptor interface, which would lower the charge recombination and improve the exciton dissociation at the TiO_2/dye/electrolyte interface; iii) the enhanced π-stacking interactions with TiO_2 surface. It is important to highlight that the efficiency reported for **70** is, up to date, the highest value reordered among the polymer dye-sensitized solar cells.

3.2. Terrylene Sensitizers

The possibility to take an advantage of the photophysical properties of expanded rylene homologs represents an interesting strategy to improve the photovoltaic performance. As previously discussed, the extension of the perylene core via additional naphthalene units along the molecular longitudinal axis leads a gradual bathochromic shift along with improving the molar absorptivity values (Figure 4).

Following this strategy, Hagfeldt et al. have reported a terrylene monoimide monoanhydride decorated with four bulky phenoxy groups **71** that showed a strong absorption band at 680 nm with an outstanding molar absorption coefficient of 178 000 M^{-1}cm^{-1} in dichloromethane (Scheme 4).[144] Dye **71** has been linked on an 8 μm thick TiO_2 film on FTO glass through the anhydride group and an efficiency of 2.4% has been recorded under AM 1.5 solar light by using 0.5 M LiI and 0.05 M I_2 in acetonitrile as electrolyte. A comparison with similar less extended perylene-based dyes **45** and **48** highlights slightly improvement in the terrylene derivatives. A possible reason for the lower performances of the smaller dye might reside on the incompatibility with additives such as 4-*tert*-butylpyridine, usually used to improve the photovoltaic performance. The limited device improvement, the worse processability along with a more challenging synthesis, limited the development of these sensitizers. To date, this is the only example of expanded-rylene dye applied in DSSCs.

3.3. Perylene Monoimide Derivatives

The imide electron-withdrawing nature and the resulting lack of strong electronic push-effects, as already described for the perylene diimide derivatives, compromises the electron injection in the semiconductor and thus the overall photovoltaic performance. Perylene monoimide derivatives have been employed with the aim to overcome these limitations in a similar way as was done by introduction the ruthenium-complexes in DSSC (**Scheme 5**). These complexes have demonstrated that charge separation in the sensitizers is a fundamental feature to provide an efficient charge transfer. Spatial separation of the positive charge left on the dye and the injected electrons after the MLCT (metal-to-ligand charge transfer) considerably lowers the rate of recombination phenomena between injected electrons and oxidized dye molecules.[145] Transposing this concept in the organic dyes domain, the orbital partitioning can only be achieved by a push-pull design, as for example, by combining a strong donor with a strong acceptor and thus creating a strong intramolecular dipole. In the monoimide perylene derivatives, an appropriate molecular design can lead to a LUMO located on the perylene core and on the anchoring group, thus close to the metal oxide, and concurrently a HOMO preferentially located on the donor moiety, close to the electrolyte. This design, at first, helps the intramolecular charge transfer and the electron injection from the LUMO of the excited dye to the conduction band of the metal semiconductor, next, it is also useful for the dye's regeneration by the electrolyte.

In addition to a strong desired push-pull effect, the dye's aggregation has been considered as an extremely incident factor on the overall efficiency. The perylene monoimide derivatives have been already known for their strong tendency to aggregate.[146]

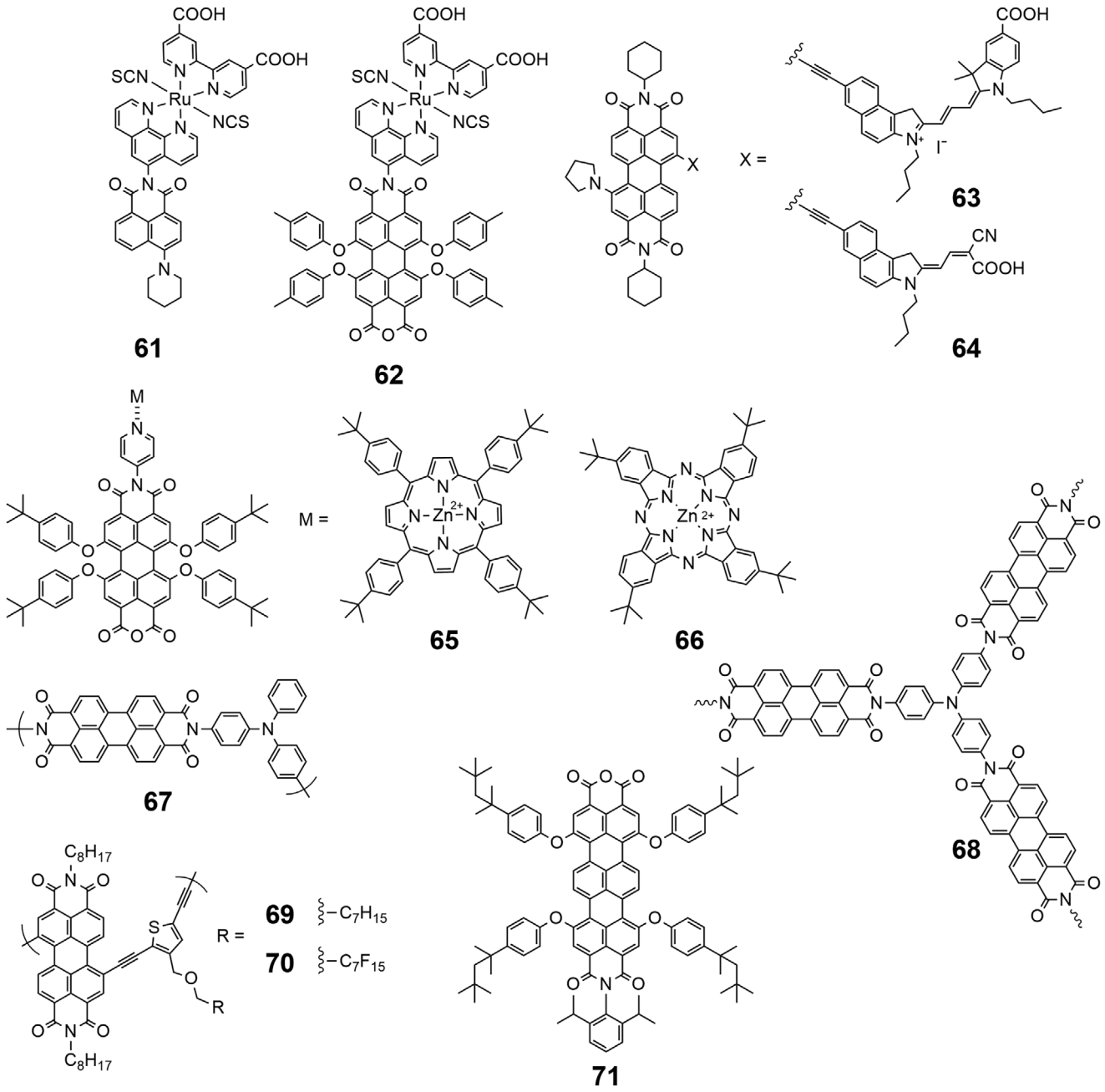

Scheme 4. Perylene diimide-based for multi-chromophores and polymer systems.

Taking advantage of this information, the attachment of bulky strong electron-donating groups in position 9 has been the first structural modification applied on the perylene monoimide core to control this phenomenon.

The first-ever application of monoimide perylene derivative in DSSCs has been reported by Gregg et al. showing how both the photocurrents and power conversion efficiencies can be improved by 100 times by UV treatment.[147,148] Four sensitizers were prepared to evaluate the effect of the bulky alkyl chain and the type and position of the anchoring group. Dyes **72** and **73** are classical push-pull molecules where the alkyl amine attached at the peri-position caused a strong coupling of the HOMO on the electron-donating amine group while the LUMO was located on the perylene monoanhydride core. The greatest steric effect of the *N,N*-dioctylamine substituent led to a better efficiency of 1.92% under AM 1.5 solar light for **73** compared to **72**. Replacing the anhydride in **73** with canonical carboxylic acid in **74** has shown variation on the relative orientation of the dye on the surface and therefore resulting in different morphologies of the film (Scheme 5). Moreover, the photophysical features of the dye on the TiO_2 surface were also affected producing a small bathochromic shift in **74** upon adsorption. The anhydride anchoring group led to

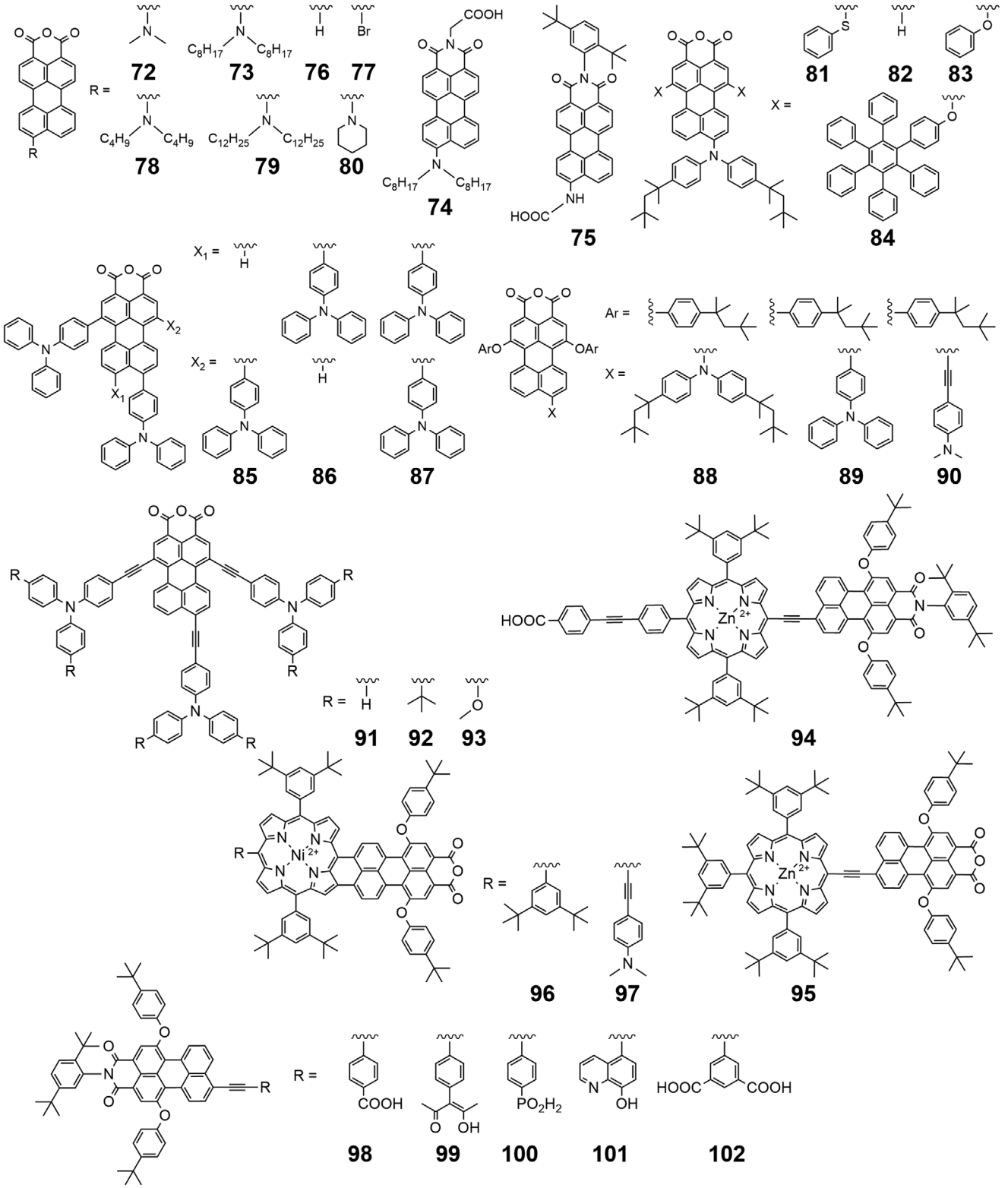

Scheme 5. Perylene monoimide-based dyes.

a better photovoltaic performance proved by the experimental results where dye **74** achieved higher photocurrent than **73** (J_{sc} = 9.7 mA cm^{-2}) but lower voltage (V_{oc} = 400 mV) resulting in lower efficiency of 1.2%. Finally, the position of the anchoring group was evaluated by recording how **75**, bearing a carbamic acid-anchoring group at the peri-position instead of an electron-donating moiety showed similar photovoltaic performance as **74**, resulting an efficiency of 1.3% (photovoltaic parameters of *N3* standard: J_{sc} = 21.0 mA cm^{-2}, V_{oc} = 0.590 V, PCE = 4.4%).[147] It is worth nothing that the molecular design of **75** is the common structure of the dyes applied in the *p*-type dye-sensitized solar cells, which will be discussed later.

The same dyes **72** and **73** along with four other monoanhydride perylene derivatives **76–79** were reported by Matsui et al. in ZnO based device (Scheme 5).[149] Quite surprisingly the best photovoltaic performances in the series were achieved by the bromo-substituted **77** that showed an efficiency of 0.52%. This unexpected result could be related to the higher fluorescence quantum yield of the series dyes compared to the one of **77** promoting alternative pathways for the electrons rather than injection.

A major improvement was achieved by Otsuki et al. with a similar molecular design in **80** bearing a piperidine-substituent as electron-donating group and achieving an efficiency of 3.1% under AM 1.5 solar light (Scheme 5).[150]

The push-pull character conferred by bulky electron-donating substituents in position 9 of PMIs improves their efficiency, but the simple HOMO-LUMO separation is not sufficient to achieve useful photovoltaic performances. A minimum driving force, quantified around at least 0.2 eV, is required to promote both an efficient electron injection and a quick dye regeneration process.[13] This concept translates in proper molecular design to tune the HOMO and LUMO level by insert proper substituents on the bay positions in PMI modulating at the same time the photophysical and the electrochemical features while preventing undesired aggregation phenomena.[59,146]

Following this concept, Nazeeruddin et al. synthetized **81** bearing a bis(4-(2,4,4-trimethylpentan-2-yl)phenyl)amine donor in the peri-position and phenylthio-groups in the bay-positions (Scheme 5).[151] The optimized device has shown an outstanding power conversion efficiency of 6.8% under standard AM 1.5 solar conditions. To date, this is the highest value obtained for DSSCs with sensitizers based on PMI derivatives. Another extraordinary result obtained by **81** was an IPCE up to 87% (> 50% between 400 and 625 nm) using a solution of 1-butyl-3-methylimidazolium iodide (0.6 M), I_2 (0.05 M), LiI (0.1 M) and 4-*tert*-butylpyridine (0.5 M) in 85/15 (v/v) acetonitrile/valeronitrile as electrolyte. Solid-state DSSCs have also been assembled with **81** and by replacing the liquid electrolyte by spiro-MeOTAD proving an efficiency of 1.8%.

Structurally similar compounds **82–84**, functionalized with no to large and even larger bay-substituents have been prepared by Müllen et al. to investigate the relationship between the photovoltaic performance and the substituents steric hindrance (Scheme 5).[152] The dyes in the series shared similar absorption spectra but, strong decrease in the absorption spectra were observed to be directly related to the dyes size and molecular weight, upon adsorption on the TiO_2.Moreover, the unsubstituted **82** exhibited a broad absorption spectrum compared to **83** and **84**, suggesting a higher aggregation rate due to the smallest size of the dye, which was compensated by a greater dye loading of **82** on TiO_2 versus **83** and **84**. The photovoltaic performance showed a direct correlation between the efficiency and the dyes molecular size with the smallest PMI showing the best result. The devices with **82**, **83**, and **84** have reached the efficiencies of 2.9%, 2.7%, and 2.5%, respectively under 1 sun (**Table 2**).

The amount and type of substituents on the PMI core affects the photovoltaic performances as it was shown by Valiyaveettil et al. with a series of sensitizers **85–87** bearing a different number of triphenylamine moieties in different positions (Scheme 5).[153]

The comparison between the tri-substituted **85** and **86** pointed out that the different positions of the triphenylamine group on the dye core had no effect on the efficiency, which was 0.95 and 0.85% for the two dyes respectively. On the other hand, increasing the number of substituents as in **87** led to an improved efficiency up to 1.14% due to the higher intramolecular charge transfer character in the PMI.

Not only the number and the position but also the distance between the donor and the acceptor part of the sensitizer is a critical factor for the photovoltaic application. A spacer can play dual role in the dyes molecular design. It can enhance the absorption by taking part in the conjugation between the donor and acceptor or it can generate a stronger orbital separation by hindering the conjugation and therefore improve the intramolecular charge transfer.

Following this concept, Edvinsson et al. reported a series of sensitizers **82**, **88–90** for pioneering the evaluation of the effect of various spacers on the photovoltaic performance.[154] A rigid conjugated acetylene spacer and a flexible phenylene bridge, were employed in **89** and **90**, respectively.

The phenylene spacer in **89** increased the distance between the amine donor and the anhydride acceptor while weakening the donor ability of the diphenylamine by twisting it out of the plane and lowering the conjugation, reflected in a less efficient intramolecular charge process in **89** compared to **90**. The prepared devices with **82**, **88–90** have reached the efficiencies of 3.9%, 3.2%, 2.4%, and 2.2%, respectively (photovoltaic parameters of *N719* standard: PCE = 6.0%).[154] Interestingly, dye **82** bearing only a peri-substituent without any spacer nor bay-functionalization, showed the best result compared to the other sensitizers of the series, probably due to the higher concentration on TiO_2 surface. Therefore, the spacer is an effective tool in the molecular design but, since multiple parameters are involved in the real devices, the dyes design requires to find the right molecular compromises to achieve the best possible results.

Additional evidence of the spacer effect on the photovoltaic performance was reported by Imahori et al. in the dyes **91–93**, where an acetylene spacer was introduced between three substituted triphenylamine and the acceptor PMI core (Scheme 5).[155] The presence of the acetylene bridge in **91–93** betters separated and forces the alignment between the phenylene moieties and the conjugation plane of the perylene the increasing donor strength in comparison to the previously discussed similar dye **89**. In accordance with the improved electron donation effect, the best efficiency of 2.9% was recorded with the dye **93** while the other sensitizers **91** and **92** showed both an efficiency of 2.1%. Finally, a comparison between **91** and the analogue without the acetylene spacer **85** characterized by and efficiency of 0.95%, clearly demonstrates the spacer effect on the device features.

Table 2. Photovoltaic performance of DSSCs employing perylene monoimide-based dyes.

Dye	λ_{MAX} (sol) [nm]	ε [$M^{-1}cm^{-1}$]	λ_{MAX} (film) [nm]	IPCE [%] [range/nm]	J_{SC} [mA cm^{-2}]	V_{OC} [V]	FF	PCE [%]	Electrolyte	References
72	556 (ACN)	–	< 480 (TiO_2)	–	4.0	0.41	–	0.59	I^-/I_3^-	[147]
					1.0 [a]	0.54 [a]	–	0.26 [a]		
	561 (DMSO)	25 000	444 (ZnO)	9.2%	0.66	0.37	67	0.16	I^-/I_3^-	[149]
73	560 (ACN)	–	452 (TiO_2)	62% (450) [148]	8.9	0.54	–	1.92	I^-/I_3^-	[147]
					3.1 [a]	0.63 [a]	–	0.92 [a]		
	564 (DMSO)	22 700	458 (ZnO)	12.3%	0.70	0.44	63	0.20	I^-/I_3^-	[149]
74	500 (ACN)	–	531 (TiO_2)	25% (550) [148]	9.7	0.40	–	1.2	I^-/I_3^-	[147]
	550 (CH_2Cl_2)				0.16 [a]	0.54 [a]	–	0.052 [a]		
75	506 (CH_2Cl_2)	–	500 (TiO_2)	> 40% (450–540) [148]	9.8	0.41	–	1.3	I^-/I_3^-	[147]
					2.7 [a]	0.50 [a]	–	0.68 [a]		
76	495 (DMSO)	38 100	424 (ZnO)	29.5%	1.44	0.45	65	0.42	I^-/I_3^-	[149]
	489 ($CHCl_3$)	10 000	450 (TiO_2)	80% (450)	7.6	0.45	63	2.2		[150]
77	503 (DMSO)	35 200	431 (ZnO)	35.5%	1.78	0.46	64	0.52	I^-/I_3^-	[149]
78	561 (DMSO)	22 100	462 (ZnO)	14.0%	0.81	0.41	64	0.21	I^-/I_3^-	[149]
79	566 (DMSO)	22 400	458 (ZnO)	12.3%	0.70	0.44	63	0.20	$I^-/I_3^{\cdot}$	[149]
80	544 ($CHCl_3$)	16 000	450 (TiO_2)	70% (470)	7.7	0.57	70	3.1	I^-/I_3^-	[150]
81	620 (CH_2Cl_2)	22 700	506 (TiO_2)	87% (550)	12.6	0.73	74	6.8	I^-/I_3^-	[151]
82	605 (CH_2Cl_2)	21 000	478 (TiO_2)	60% (500)	10.4	0.651	58	3.9	I^-/I_3^-	[154]
	605 (CH_2Cl_2)	21 000	473 (TiO_2)	65% (500)	8.99	0.58	55	2.9		[152]
83	606 (CH_2Cl_2)	25 200	473 (TiO_2)	55% (500)	7.52	0.64	57	2.7	I^-/I_3^-	[152]
84	606 (CH_2Cl_2)	18 800	481 (TiO_2)	50% (515)	6.99	0.63	56	2.5	I^-/I_3^-	[152]
85	582 ($CHCl_3$)	–	–	–	2.22	0.59	69.5	0.95	I^-/I_3^-	[153]
86	595 ($CHCl_3$)	–	–	–	2.07	0.57	69	0.85	I^-/I_3^-	[153]
87	624 ($CHCl_3$)	–	–	–	3.08	0.53	66.8	1.14	I^-/I_3^-	[153]
88	599 (CH_2Cl_2)	32 000	470 (TiO_2)	47% (500)	7.96	0.696	59	3.2	I^-/I_3^-	[154]
89	540 (CH_2Cl_2)	35 000	430 (TiO_2)	54% (475)	6.13	0.651	55	2.2	I^-/I_3^-	[154]
90	568 (CH_2Cl_2)	35 000	450 (TiO_2)	54% (485)	7.50	0.598	54	2.4	I^-/I_3^-	[154]
91	574 (CH_2Cl_2)	–	–	> 30% (410–570)	5.0	0.58	74	2.1	I^-/I_3^-	[155]
92	588 (CH_2Cl_2)	–	–	> 40% (435–550)	5.6	0.60	74	2.1	$I^{\cdot}/I_3^{\cdot}$	[155]
93	595 (CH_2Cl_2)	–	–	> 40% (420–570)	6.5	0.61	72	2.9	I^-/I_3^-	[155]
94	448 (THF)	116 000	–	–	0.349	0.439	44	0.07	I^-/I_3^-	[156]
95	437 (THF)	157 000	–	–	–	–	–	< 0,02	I^-/I_3^-	[156]
96	805 ($CHCl_3$)	89 000	–	31% (772)	7.11	0.329	54	1.26	I^-/I_3^-	[157]
97	847 ($CHCl_3$)	81 000	–	30% (790)	7.66	0.333	52	1.36	I^-/I_3^-	[157]
98	536 (DMF)	49 000	503 (TiO_2)	–	0.85	0.470	69	0.28	I^-/I_3^-	[159]
					2.87 [b]	0.440 [b]	72 [b]	0.90 [b]		
99	538 (DMF)	54 000	514 (TiO_2)	–	0.24	0.380	60	0.06	I^-/I_3^-	[159]
					0.53 [b]	0.390 [b]	68 [b]	0.14 [b]		
100	538 (DMF)	38 000	503 (TiO_2)	–	0.70	0.450	35	0.13	I^-/I_3^-	[159]
					4.20 [b]	0.480 [b]	70 [b]	1.42 [b]		
101	545 (DMF)	56 000	538 (TiO_2)	–	1.37	0.510	68	0.47	I^-/I_3^-	[159]
					5.60 [b]	0.460 [b]	71 [b]	1.80 [b]		
102	536 (DMF)	40 000	503 (TiO_2)	–	1.30	0.480	69	0.42	I^-/I_3^-	[159]
					3.28 [b]	0.430 [b]	71 [b]	1.00 [b]		
131	590 (CH_2Cl_2)	25 000	550 (TiO_2)	> 20% (400-600)	4.2	0.440	66	1.2	I^-/I_3^-	[196]

[a] Photovoltaic parameters achieved without UV treatment; [b] Photovoltaic parameters achieved with an acetonitrile-based electrolyte.

In summary, the reported works demonstrated the easy tunability of the photophysical and electrochemical properties of the PMI derivatives. As seen, i) the modification of the peri-position allows to reach more suitable push-pull designs for a better localization of the HOMO and LUMO levels; ii) the modification of the bay-positions helps to prevent the dye aggregation, but excessively bulky substituents could dramatically reduce the dye loading; iii) the insertion of an appropriate spacer could improve push-pull effect on the molecule, promoting better efficiencies. Therefore, the PMI derivatives generally provide improved photovoltaic performance compared to the previous class of PDI sensitizers.

3.3.1. Porphyrin-Based Perylene Monoanhydride Dyes

In this paragraph, the application of differently functionalized PMI with a porphyrin core will be discussed as an efficient strategy to improve photovoltaic efficiency similarly to the multichromophoric systems described in Section 3.1.1.

Yeh et al. designed the dyads **94** and **95** to evaluate the influence on the photovoltaic performance of dye orientation on the TiO_2 surface.[156] In **94** a PMI was linked through acetylene spacer to a Zn-porphyrin that was decorated at the *meso* positions with bulky substituents to prevent aggregation and with a benzoic acid, by another acetylene spacer, to provide an anchoring group. On dye **95**, instead, the anchoring group was provided by the anhydride moiety on the PMI derivative, and the porphyrin functionalized with three bulky groups. The photovoltaic performances were measured for both the sensitizers but only **94** showed an appreciable efficiency of 0.07% while **95** was affected by poor adsorption on the TiO_2 surface most likely because of the hindered dye structure that lowered the dye-loading efficiency.

Despite the initial poor reported efficiency, the porphyrin-based dyad concept was further investigated by Wang et al. with a remarkable improvement, by extending the conjugated system fusing perylene monoanhydride core to a Ni-based porphyrin.[157] Sensitizers **96** and **97** exhibited an outstanding NIR response beyond 900 nm and the dye-loading was improved by mixing with the dyes an unfunctionalized perylene monoanhydride. The devices with **96** and **97** reached the efficiencies of 1.26 and 1.36%, respectively and the latter result was related to the greater electron-donor strength of the amine-based substituent in **97** in respect to the di-*tert*-butylphenyl group in **96**.

3.3.2. Perylene Monoimide in Water-Based DSSCs

The electrolyte plays a key role in DSSC. Commonly employed electrolyte solutions consist of organic solvent containing in small percent iodide/iodine redox couple along with additives to tune the open circuit voltage and the photocurrent. Acetonitrile, valeronitrile, 3-methoxypropionitrile, are broadly used as solvents for electrolytes solutions despite their volatility and toxicity.[158] The possibility of designing water-based DSSCs represents a valuable alternative to avoid organic solvents. Water-based DSSCs present the same structure and operation principles as classical DSSC with the only difference of the organic solvent-based electrolyte replacement with a water-based one. These devices unfortunately have not reached yet comparable efficiencies to those with the organic-base electrolyte, but they represent a safer and cheaper alternative in which also PMI dyes have been tested.[29]

Odobel et al. reported a series of PMI dyes to correlate the photovoltaic performance of a water-based DSSCs to the presence of different anchoring group such as carboxylic acid **98**, acetylacetone **99**, phosphonic acid **100**, hydroxyquinoline **101**, and dipicolinic acid **102** (Scheme 5).[159] The perylene monoimide core was decorated with bulky hydrophobic units to prevent deleterious dye aggregation and to minimize desorption in the media. The prepared devices with **98** and **102** reached efficiencies of 0.06 and 0.47% in aqueous electrolyte while slightly better results were achieved with acetonitrile-based ones. The hydroxyquinoline-based dye **101** shows the best efficiency due to a broader absorption compared to the others, both in water and in acetonitrile-based electrolyte. On the other hand, the acetylacetone dye **99** showed the lower efficiencies in both the electrolytes due to the perpendicular orientation of the anchoring group with respect to the perylene core, preventing the electron-withdrawing effect from the anchoring site and thus, reducing the electron density close to the TiO_2 surface. Interestingly, dye holding the phosphonic acid anchor **100** showed a significant different behavior depending on the electrolyte. The dye produced higher photocurrent and thus a better efficiency by switching from aqueous to acetonitrile-based media, probably due to high recombination phenomena involving the interactions of water with the phosphonic acid and the surface of TiO_2. Despite the lower efficiency compared to top performing systems, the application of PMI derivatives has been successfully introduced in water-based DSSCs and might be of inspiration for further implementation.

3.4. Perylene Monoimide Derivatives in p-Type DSSCs

In addition to the classic *n*-type configuration, another type of device configuration, namely known as *p*-type DSSCs with an inverted structure and an opposite operating principle has been deeply investigated over the years in the DSSC community. While in the *n*-type cell the TiO_2-based anode is the photoactive electrode, in a *p*-type cell the photoactive electrode is a cathode based on NiO.[160] In a *p*-DSSC the dye's light excitation leads to the formation of its excited state that subsequently decays by a hole injection into the valance band of the p-type semiconductor generating the charge separation (**Figure 7**a). A redox shuttle, as triiodide/iodide, reacts with the reduced sensitizer to restore the ground state of the dye and transports the electron to the counter electrode where it is handed to the external electric circuit.

It is obvious that the molecular design of a *p*-type sensitizer needs to fulfil different requirements compared to the dyes used in *n*-type DSSC. Dyes with push-pull design bearing an electron-withdrawing moiety localized on the opposite side of the anchoring groups are particularly suitable in *p*-type DSSCs.[157] This structure concept allows an electron flow from the anchoring group to the opposite side of the dye, resulting in a better interaction with the redox shuttle. Despite the lower efficiencies reached in comparison to the more consolidate *n*-type DSSCs, the development of efficient *p*-type cells is the missing key point for the assembly of tandem-DSSCs.[160]

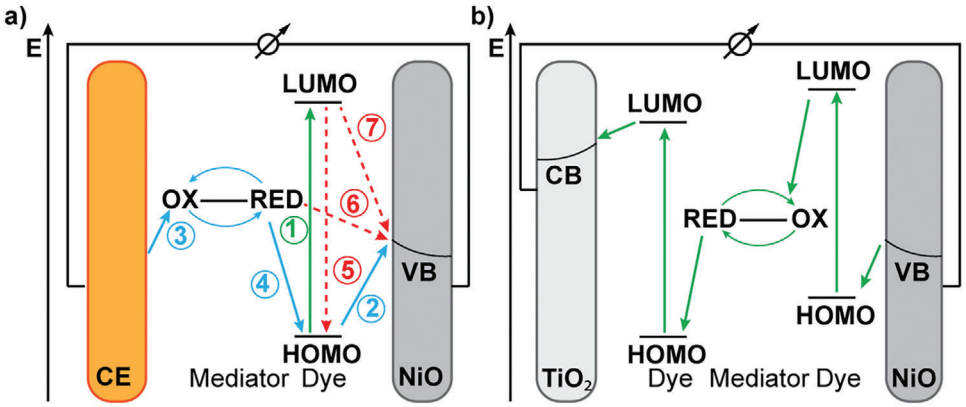

Figure 7. a) Schematic overview of charge transfer processes in a p-type DSSCs. Solid blue arrows describe the hole transfer processes, solid green arrow describes the electron transfer process upon dye excitation, and dashed red arrows describe the undesired charge transfers. 1) Photoexcitation, 2) hole injection into the valance band, 3) regeneration of the oxidized redox shuttle, 4) restore of the dye's ground state, 5) deactivation of the excited state, 6) non-geminate electron recombination, 7) geminate electron recombination. b) Schematic overview of a tandem DSSC.

The tandem DSSCs are a multi-junction device in which a photoanode and a photocathode are coupled in a sandwich configuration (Figure 7b) that can lead to better photovoltaic efficiencies and overcome the intrinsic Shockley-Queisser limit of 33.7% for a single-junction cell.[162] Further insights on the recent advances in *p*-type and tandem DSSCs can be found in recent literature.[160,161,163] In this context, perylene imide derivatives (**Scheme 6**) have played a fundamental role to the technology development being the best performing sensitizers in this type of cells.

The first ever application of a perylene imide derivative in a *p*-type DSSCs was reported by Odobel et al. where two PMI dyes **103** and **104** were decorated with three phenoxy-substituents in the bay and 9 positions to tune the reduction potential and to prevent the dye aggregation.[164,165] The bay-substituents were bearing t*ert*-butyl groups while the one in the 9-position was functionalized with carboxylic anchoring group. An electron-withdrawing moiety, localized at the opposite side of the anchoring groups, is particularly suitable in *p*-type DSSCs, therefore in **104** a naphthalene diimide unit was inserted as secondary electron acceptor. The comparison of the devices with **103** and **104** showed how an additional electron-withdrawing group led to a longer charge separation lifetime and a higher IPCE value (4%) compared to **103** (1.3%). The same dye **104** used in combination with a Co-based electrolyte (tris(4,4′-di-*tert*-butyl-2,2′-bipyridine)cobalt$^{II/III}$) by Hammarström et al. allowed to obtain an outstanding open circuit voltage of 0.35 V and an efficiency of 0.20% that was four time higher than the previous record reported by Mori et al.[165,166] Obviously, the remarkable improvements within the *p*-type counterpart were converted to an improvement in tandem DSSCs performance. Employing a TiO_2 photoanode sensitized with coumarin 343 (C343) and a NiO photocathode sensitized with **104**, open circuit voltage of 0.91 V and an efficiency of 0.55% (*n*-type side) were obtained, overcoming the previous record reported by Lindquist et al.[167]

Following the same molecular concept, Odobel et al. synthetized a series of dyes **105–107** to evaluate the insertion of a phenylene spacer between the PMI and the additional acceptor-group and to examine a new strongly electron-withdrawing group such a fullerene C_{60}.[168] In the dyad **106** and **107** a longer separated charges were proven but the presence of the spaces did not lead to a considerable improvement of the photovoltaic performances compared to the results reported for **104**. The devices with dyes **105–107** achieved efficiencies of 0.043%, 0.074%, and 0.058% respectively. However, dye **107** with the fullerene acceptor showed an interesting IPCE of 57% and a high short circuit current density of 1.88 mA cm^{-2}, probably due to lower excited state of C_{60} compared to NDI. A comparison between different electrolyte such as I^-/I_3^- and Co(III/II) complexes has also been investigated highlighting that the Co-based electrolyte facilitated the regeneration process in competition with the undesired recombination pathway particularly for the dyad **106** and **107**.

Not only the redox shuttle, but also the solvent type in the electrolyte can affect the overall device photovoltaic performance. In detailed studies by Gibson et al. and Hammarström et al. the effect of solvents such as acetonitrile, propionitrile, and propylene carbonate were investigated with dyes **80**, **81**, **108–111**.[169,170] Both the hole injection from NiO to the electrolyte and the dye regeneration processes were strongly solvent-dependent: the best efficiencies for all dyes **80**, **81**, **108–111** were obtained using propylene carbonate-based electrolyte.

As seen, the *p*-type cell has an opposite operating principle compared to the *n*-type cell, therefore the electronic properties of the optimal binding group for NiO are different from those for TiO_2-based photoanodes. NiO is a *p*-type semiconductor and is composed of Ni(II) cation that is a weaker Lewis acid than Ti(IV) in TiO_2.[171] The HOMO of the dye must fit with the valence band to achieve a fast hole injection into the NiO valence band and, in this fashion, the anchoring group orbitals can give a significant contribution to the HOMO. A comprehensive study of a series of PMI **98–102** decorated with different anchoring group was reported by Hammarström et al. to evaluate this property (Scheme 6).[166,172] The phosphonic acid group **100** resulted the strongest anchoring group leading to the highest dye loading, while the acetylacetone **99** and hydroxyquinoline **101** groups were the weakest. Dyes decorated with weakest anchoring group showed better photovoltaic performance since the lower dye-loading was translated into a lower degree of

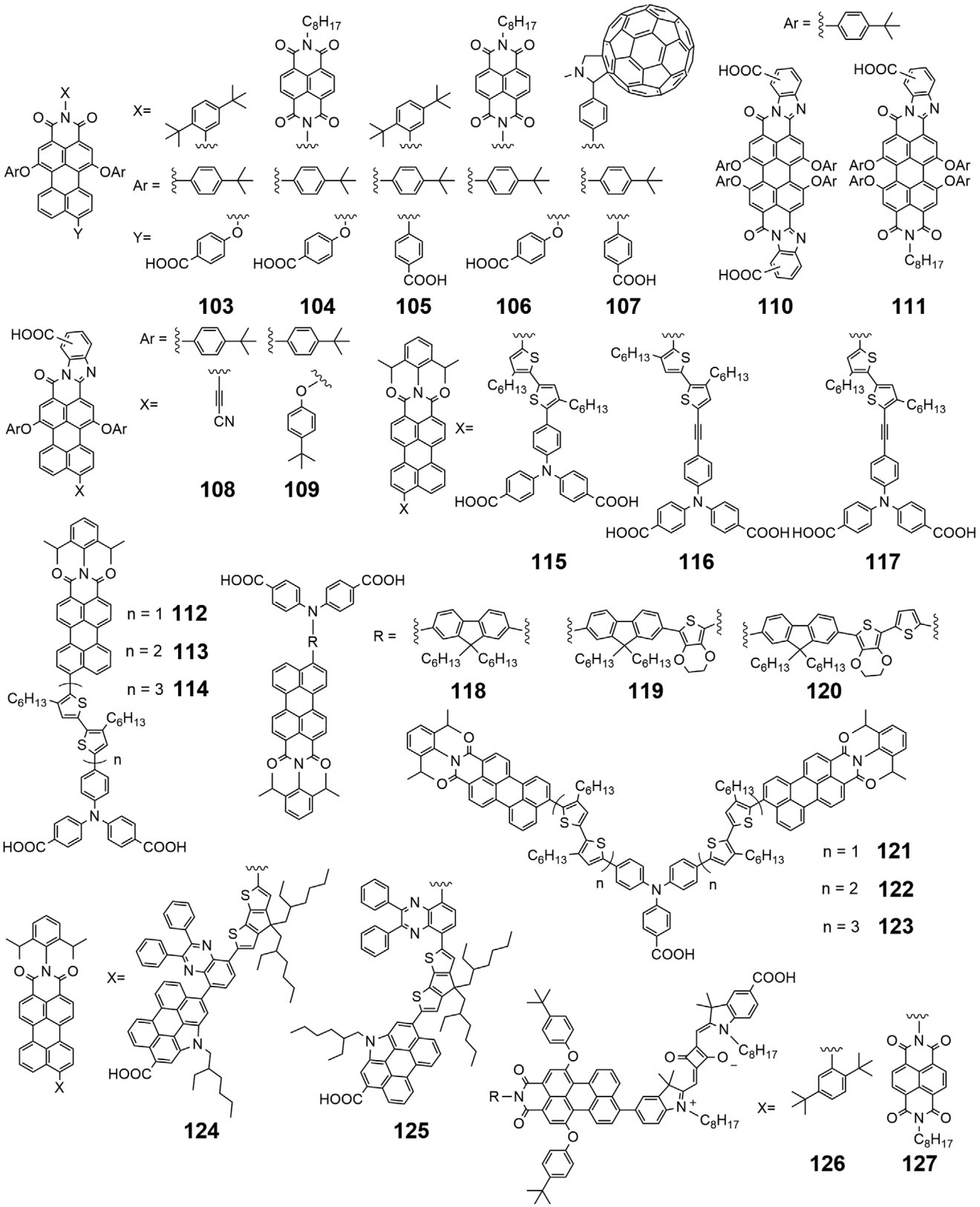

Scheme 6. Perylene imide-based dyes for *p*-type DSSCs.

aggregation. The devices with dyes **99** and **101** both achieved an efficiency of 0.086%. Interestingly, the same dyes have been also successfully used in the first ever application of PMI derivatives in water-based DSSCs as previously discussed.[159]

An outstanding breakthrough on *p*-type DSSCs has been achieved by Bach et al. with dyes **112–114** in which a regioregularly alkylated oligo-3-hexylthiophene spacer was added between the PMI acceptor and triphenylamine donor group.[173] In these dyes, the LUMO was located exclusively on the PMI core and the side thiophene ring, while the HOMO was distributed more evenly over the entire conjugated system. The sharing on PMI core decreased with the increasing oligothiophene-spacer length, while a better charge separation was obtained along with the desired reduction of charge recombination rates. Dye **114** based on sexithiophene-spacer showed the outstanding efficiency of 0.41%, doubling the previous record achieved with dye **113**.[165] Furthermore, **114** could convert absorbed photons into electrons with a yield of up to 96% and when used to sensitize the NiO photocathode, in a tandem combination with a *N719* sensitized TiO_2 photoanode an overall efficiency of 1.91% and an outstanding open-circuit voltage of 1.079 V was achieved.

Later, Bach et al. further improved the photovoltaic performance showed by **114** by modifying the redox shuttle introducing the tris(1,2-diaminoethane)cobalt(II)/(III) complexes as redox couple raising the previous efficiency from 0.41% to 1.30%.[174,175] The significant improving was mainly due to the greater open-circuit voltage of 0.709 V compared to previous 0.218 V reported with iodide/triiodide redox couple. A further improvement was reached using a cheaper and safer tris(acetylacetonato)iron(III)/(II) complexes as redox couple.[175] To date, the efficiency of 2.51% achieved by dye **114** with an iron-base electrolyte was the best value for a *p*-type DSSCs.

Following the same concept, different spacers were tested by Bäuerle et al. in **115–117** to evaluate the effect of different bithiophene bridge regioisomers and the presence of an additional acetylene spacer between the bridging bithiophene unit and the triphenylamine donor (Scheme 6).[176] In regioisomer **115** the steric repulsion decreased resulting in a smaller torsion angle, instead of creating a distortion between the PMI core and the adjacent 3-hexylthiophene unit as previously seen in dye **113**. On the other side, the steric hindrance between the triphenylamine and the bithiophene bridge increased. The comparison of dyes **113** and **115** showed that the planarization of the PMI core and the bithiophene bridge led to worse photovoltaic parameters as depicted by the **113**-device efficiency of 0.09%, twice that of **115**. Moreover, the insertion of an acetylene additional spacer was evaluated showing and improvement of the photophysical feature in **116** compared to **115** due to the extension of the conjugated system, along with and increment of the distance between the acceptor moiety and the NiO surface resulting in an efficiency of 0.10%. These results proved the importance of the charge separation, suggesting that distortion between the acceptor and donor moieties may be required to achieve better efficiencies.

He et al.[177] have reported a series of sensitizers **118–120** decorated with different fluorene-based spacers (Scheme 6). The photophysical properties and the charge injection efficiency were tuned by the further insertion on fluorene-core of different electron-rich heterocyclic aromatic groups such as 3,4-ethylenedioxythiophene and thiophene. The direct comparison with dyes **112** and **115** suggested that the fluorene spacer provided better results than the bithiophene-based spacer as noted by the achieved efficiencies of 0.184%, 0.160%, and 0.148% with sensitizer **118–120**.

Combining the structure of the record holder **114** and the "double acceptor" design Sun et al. and Wu et al. have reported a series of sensitizers **121–123**, replacing one of the carboxylic acid anchoring group with an additional oligothiophene-PMI arm.[178,179] The double acceptor structure led to better photophysical properties than dyes **112** and **114** improving the molar extinction coefficient up to outstanding values of almost 10^5 $M^{-1}cm^{-1}$, rising the efficiency up to 0.13% with **121**. Interestingly, while in a "single acceptor" design the sexithiophene-based spacer led to better efficiencies, in the case of a "double acceptor" design, the quaterthiophene-based spacer provided the best photovoltaic results. The device with dye **122** achieved an efficiency of 0.28%, higher than the 0.24% of **124** most likely due to the smaller size that resulted in greater dye-loading on the NiO surface (Scheme 6).

The strategy of additional electron-acceptor group to increase the charge separation in push-pull sensitizers was already discussed.[165,168] However the relative position of the further acceptor group on the molecular structure can address the results in a different manner like in the case of a D–A–π–A configuration that can facilitate to broaden the absorption band in respect to D–π–A–A configuration.[180] Following this concept, Hua et al. synthetized the dyes **124** and **125** to study the effect of the two molecular configurations on the photovoltaic performance where a classical PMI and a quinoxaline were selected as acceptor moieties, while a *N*-annulated perylene worked as donor.[181] Dyes based on this latter portion will be discussed later in details. The comparison between the photophysical properties of **124** and **125**, proved that the configuration D–A–π–A affected the absorption spectra with **124** showing a broader and more red-shifted absorption than **125**, however the latter was characterized by a higher molar extinction coefficient. Dye **125** provided the best device efficiency of 0.316% due to the better interaction with the redox shuttle and thanks to a higher dye-loading on NiO surface compared to dye **124** (spin-coating step-by-step deposition of NiO-a four-layer photocathode).

The multichromophoric approach was investigated also in the design of *p*-type DSSCs with the aim to improve the photovoltaic performance. Odobel et al. have developed multichromophoric dyes **126** and **127** starting by already studied sensitizers **112** and **113** and combining them with the well-known squaraine derivatives (Scheme 6).[182,183] Dyes **126** and **127** showed better photophysical properties compared to the benchmark structures **112** and **113** since the squaraine moiety led to a strong absorption band near 665 nm improving the overall panchromatic behavior. Additionally, both dyes were characterized by a long-lived charge separation resulting in slower charge recombination processes. The main difference between the performance of the multichromophoric sensitizers and those of the reference were due to the different photophysical operation mechanism. The presence of a secondary electron acceptor near the squaraine sensitizer unit allowed a competing intramolecular electron transfer over the desired hole injection from sensitizer excited-state or energy transfer from the PMI excited-state. Consequently, recombination of the resulting charge separated state could compete with the hole

injection from the oxidized sensitizer lowering the overall photovoltaic performances.[184] The device with multichromophoric dye **127** achieved an efficiency of 0.083%, improving the result of 0.033% for dye **113** in the same conditions (**Table 3**).

In summary, the key role of the PMI derivatives in the development of high-efficiency *p*-type DSSCs has been clearly established. Good sensitizers for *p*-type devices require a push-pull molecule with an opposite orientation in which the donor group is adjacent to the photocathode while acceptor group interacts with the electrolyte. The insertion of an appropriate spacer improves the overall photovoltaic performances due to the long-lived charge separation and slower recombination processes. Finally, adding another acceptor group or another chromophoric moiety is a potential strategy to improve the photophysical properties and thus the efficiencies. Despite the lower photovoltaic performance of the *p*-type DSSCs, their improvement could lead in the incoming years to a development of high-efficiency tandem devices.

3.5. Perylene Imides in Solid-State DSSCs

The liquid electrolyte is among the weakness of DSSCs and even though in water-based DSSCs the solvent's toxicity can be overcome, the difficult task of junctions sealing to prevent the electrolyte evaporation still persists.[185] Solid state dye-sensitized solar cells (SS-DSSCs) overcome this limitation by replacing the liquid electrolyte by solid charge transport materials.[29,30,141] A solid-state DSSC has the same structure as the liquid one with the only difference of employing a solid redox electrolyte or a hole transport material (HTM). While in the liquid-electrolyte DSSCs, the charge transfer between the photoanode and counter electrode is mediated by a redox electrolyte, in the solid-state DSSCs a solid hole transporting material infiltrates the porous metal oxide. The working principle is fundamentally the same, SS-DSSCs show dye-regeneration progress from its oxidized-state with a higher fast rate (few hundred picoseconds) than in the liquid DSSCs due to a faster regeneration process related to a direct hole transfer into the HOMO level of a solid-state hole transporter from the oxidized state of the dye molecule.[30] To date, many examples of small molecule as spiro-OMeTAD, inorganic-hole transport material as CuSCN, $CsSnI_3$, copper complexes, and polymers as P3HT, PEDOT have been successfully applied in solid-state DSSCs.[186–192] In this context, perylene imide derivatives show again interesting results that are discussed in this section (**Table 4**).

Icli et al. reported in 2005 the first application of a PMI derivative in solid-state DSSCs where dye **128** was deposited on a 10 µm thick TiO_2 film on ITO glass while poly-(3-hexylthiophene) (P3HT) or poly(3-octylthiophene) (P3OT) were used as HTM.[193] A thin aluminum film, deposited by chemical vapor deposition, was used as the counter electrode and both devices showed similar photovoltaic parameter with an overall efficiency of 0.02%. These results could be caused by a poor contact area of hole conductor polymer and TiO_2 or, more likely, by the unsuitable structure of the sensitizer. This latter hypothesis was supported by the low efficiency of 0.03% obtained in liquid DSSC with **128** (**Scheme 7**).

Similar dye-structure in **129** was proposed by Sharma et al. for the application in a quasi-solid-state device, simultaneously demonstrating how the TiO_2 doping by Al_2O_3 could shifts the conduction band potential toward the negative direction and enhance the power conversion efficiency.[194] Quasi-solid-state devices have the same structure and the same working operation concept, but the only difference consists in the use of a gel polymer electrolytes (GPEs) that are liquid electrolytes encapsulated in a polymer framework resulting in a trade-off situation that exploit the advantages of both liquid and solid configuration. GPEs can hold large amounts of the electrolyte, their excellent contacting and filling properties between the electrodes result in fast dye regeneration and their high conductivity ensures fast charge transport to the counter electrode.[29,30,141] Dye **129** was deposited on a 6 µm thick TiO_2 film modified with Al_2O_3, a quasi-solid-state polymer (in particular polyethylene oxide, PEO) containing 0.5 M KI and 0.05 M I_2 was used as electrolyte and spin-coated to form a hole conducting layer. A thin film of protonated poly-(3,4-ethylenedioxythiophene)-polystyrene (PEDOT:PSS) was used as counter electrode, over graphite-coated FTO glass substrates. The device achieved an interesting efficiency of 3.42% highlighting a remarkable improvement thanks to the quasi-solid-state nature of the electrolyte. Interestingly, the sensitizer **129** proved once more that the molecular design concepts required to reach high efficiency in a liquid DSSC, such as the presence of an appropriate anchoring group, does not necessarily translate into good photovoltaic performance in a solid-state DSSC. In support of this evidence, interesting results were reported by Salbeck et al. with the sensitizer **130** bearing a diphenylamine-functionalized spirobifluorene group applied in a liquid DSSCs and in a solid-state one (Scheme 7).[195] Liquid DSSCs achieved an efficiency of 1.72%, comparable to results reported by sensitizers with similar scaffolds such as **59** and **60**.[127] Contrarily, dye **130** in solid-state DSSCs achieved a poor efficiency of 0.2%, confirming how the sensitizers for the solid-state devices require different molecular-design concept.

In the solid-state DSSCs, as in the liquid devices, the transition from the perylene diimide dyes to the PMI led to a generally improvement of the photovoltaic performances. The first ever application of PMI derivatives was reported by Nazeeruddin et al. reaching an efficiency of 1.78% and an outstanding value of open circuit voltage (V_{OC} = 0.838 V) applying dye **81**.[151]

Starting from this encouraging result reported, Boschloo et al. synthetized the PMI **131** with a new molecular design concept where a carboxylic acid spaced by a methylene bridge was attached to an imide nitrogen instead of the anhydride anchoring group.[196,197] Applying **131** in both liquid and solid-state devices, the efficiencies of 1.2 and 3.2%, were respectively achieved, enforcing the requirement of a different molecular design for solid-state application and showing a remarkable efficiency improvement using a novel anchoring group. In addition, extensive studies on the interfacial properties of **131** in a solid-state DSSCs with spiro-OMeTAD as hole transporter were also reported by Boschloo et al.[197]

Following the same concept **131**, Müllen et al. studied the PMI **132** bearing a branched terthiophene spacer group that led to a stronger orbital partitioning lowering the unwanted recombination process and thus improving the photovoltaic performance (Scheme 7).[198] The dendritic structure of the spacer was justified

Table 3. Photovoltaic performance of *p*-type DSSCs employing perylene-based dyes.

Dye	λ_{MAX} (sol) [nm]	ε [$M^{-1}cm^{-1}$]	λ_{MAX} (film) [nm]	IPCE [%] [range/nm]	J_{SC} [mA cm^{-2}]	V_{OC} [V]	FF	PCE [%]	Electrolyte	References
98	536 (DMF)	4 9000	495 (NiO)	≈ 20% (508)	1.52	0.161	25.4	0.062	I^-/I_3^-	[172]
99	538 (DMF)	54 000	497 (NiO)	≈ 32% (513)	2.08	0.169	27.9	0.086	I^-/I_3^-	[172]
100	538 (DMF)	38 000	495 (NiO)	≈ 20% (504)	1.27	0.181	17.7	0.041	I^-/I_3^-	[172]
101	545 (DMF)	56 000	514 (NiO)	≈ 21% (527)	2.21	0.164	23.8	0.086	I^-/I_3^-	[172]
102	536 (DMF)	40 000	497 (NiO)	≈ 26% (498)	1.33	0.168	24.6	0.055	I^-/I_3^-	[172]
103	515 (CH_2Cl_2)	32 000	525 (NiO)	≈ 3% (490–530)	0.26	0.08	26	0.006	$[Co(dtb)_3]^{2+/3+}$	[165]
	521 (CH_2Cl_2)	–	–	–	0.250	0.085	28.9	0.006	$[Co(dtb)_3]^{2+/3+}$	[168]
				≈ 26% (490)	1.316	0.110	31.6	0.046	I^-/I_3^-	
	517 (CH_2Cl_2)	31 900	–	20% (517) [a]	1.14 [a]	0.105 [a]	32 [a]	0.04 [a]	I^-/I_3^-	[169]
				36% (517) [b]	1.71 [b]	0.090 [b]	30 [b]	0.05 [b]		
				22% (517) [c]	1.42 [c]	0.085 [c]	34 [c]	0.04 [c]		
104	525 (CH_2Cl_2)	29 000	–	31% (505)	1.66	0.35	34	0.20	$[Co(dtb)_3]^{2+/3+}$	[165]
				–	0.97 [d]	0.91 [d]	62 [d]	0.55 [d]	$[Co(dtb)_3]^{2+/3+}$	
				–	0.88 [e]	0.53 [e]	80 [e]	0.37 [e]	$[Co(dtb)_3]^{2+/3+}$	
	530 (CH_2Cl_2)	–	–	≈ 28% (520)	1.20	0.285	41.0	0.141	$[Co(dtb)_3]^{2+/3+}$	[168]
				≈ 32% (515)	1.76	0.120	34.5	0.073	I^-/I_3^-	
105	522 (CH_2Cl_2)	–	–	–	0.342	0.085	23.6	0.007	$[Co(dtb)_3]^{2+/3+}$	[168]
				≈ 26% (510)	1.418	0.100	30.3	0.043	I^-/I_3^-	
	522 (CH_2Cl_2)	7500	–	18% (522) [a]	0.70 [a]	0.100 [a]	32 [a]	0.02 [a]	I^-/I_3^-	[169]
				25% (522) [b]	1.42 [b]	0.100 [b]	30 [b]	0.04 [b]		
				23% (522) [c]	1.41 [c]	0.070 [c]	33 [c]	0.03 [c]		
106	517 (CH_2Cl_2)	–	–	≈ 14% (500)	0.78	0.210	29.3	0.048	$[Co(dtb)_3]^{2+/3+}$	[168]
				≈ 31% (490)	1.64	0.130	34.6	0.074	I^-/I_3^-	
107	522 (CH_2Cl_2)	–	–	≈ 23% (485)	0.58	0.180	38.8	0.040	$[Co(dtb)_3]^{2+/3+}$	[168]
				≈ 43% (490)	1.88	0.095	32.4	0.058	I^-/I_3^-	
108	566 (CH_2Cl_2)	10 000	–	14% (566) [a]	0.97 [a]	0.100 [a]	32 [a]	0.03 [a]	I^-/I_3^-	[169]
				17% (566) [b]	1.33 [b]	0.100 [b]	33 [b]	0.04 [b]		
				14% (566) [c]	1.41 [c]	0.085 [c]	30 [c]	0.04 [c]		
109	560 (CH_2Cl_2)	37 400	–	8% (560) [a]	0.48 [a]	0.100 [a]	35 [a]	0.02 [a]	I^-/I_3^-	[169]
				16% (560) [b]	1.04 [b]	0.095 [b]	33 [b]	0.04 [b]		
				5% (560) [c]	1.07 [c]	0.080 [c]	33 [c]	0.03 [c]		
110	607 (CH_2Cl_2)	62 700	–	2% (607) [a]	0.39 [a]	0.095 [a]	30 [a]	0.02 [a]	I^-/I_3^-	[169]
				18% (607) [b]	0.83 [b]	0.105 [b]	34 [b]	0.03 [b]		
				5% (607) [c]	0.94 [c]	0.070 [c]	33 [c]	0.02 [c]		
111	602 (CH_2Cl_2)	66 000	–	3% (602) [a]	0.41 [a]	0.095 [a]	41 [a]	0.02 [a]	I^-/I_3^-	[169]
				9% (602) [b]	0.75 [b]	0.085 [b]	33 [b]	0.02 [b]		
				3% (602) [c]	0.54 [c]	0.075 [c]	33 [c]	0.01 [c]		
112	370 ($CHCl_3$)	53 400	–	≈ 11% (355)	2.06	0.153	29	0.09	I^-/I_3^-	[173]
	361 (CH_2Cl_2)	61 800	358 (NiO)	≈ 22% (380, 503)	1.77	0.146	30	0.08	I^-/I_3^-	[176]
113	362 ($CHCl_3$)	50 600	–	> 15% (330–540)	3.40	0.176	32	0.19	I^-/I_3^-	[175]
114	367 ($CHCl_3$)	52 300	–	≈ 48% (430)	5.35	0.218	35	0.41	I^-/I_3^-	[173]
				–	2.40 [d]	1.079 [d]	74 [d]	1.91 [d]	I^-/I_3^-	
				> 55% (390–530)	4.44	0.709	42	1.30	$[Co(en)_3]^{2+/3+}$	[174]
				> 55% (400–530)	7.65	0.645	51	2.51	$[Fe(acac)_3]^{0/-1}$	[175]
115	358 (CH_2Cl_2)	53 800	353 (NiO)	≈ 10% (370)	1.06	0.122	29	0.04	I^-/I_3^-	[176]
116	362 (CH_2Cl_2)	61 800	358 (NiO)	≈ 15% (370, 500)	2.24	0.147	30	0.10	I^-/I_3^-	[176]
117	362 (CH_2Cl_2)	59 700	358 (NiO)	≈ 12% (370)	1.23	0.136	28	0.05	I^-/I_3^-	[176]

(*Continued*)

Table 3. (Continued)

Dye	λ_{MAX} (sol) [nm]	ε [$M^{-1}cm^{-1}$]	λ_{MAX} (film) [nm]	IPCE [%] [range/nm]	J_{SC} [mA cm^{-2}]	V_{OC} [V]	FF	PCE [%]	Electrolyte	References
118	357 (THF)	53 100	507 (NiO)	43% (367)	4.36	0.112	38	0.184	I^-/I_3^-	[177]
119	361 (THF)	64 700	334 (NiO)	48% (370)	4.00	0.111	36	0.160	I^-/I_3^-	[177]
120	407 (THF)	55 000	540 (NiO)	43% (373)	3.80	0.109	36	0.148	I^-/I_3^-	[177]
121	520 (CH_2Cl_2)	84 000	–	–	4.3	0.097	31	0.13	I^-/I_3^-	[179]
122	515 (CH_2Cl_2)	96 000	–	–	7.4	0.128	30	0.28	I^-/I_3^-	[179]
123	488 (CH_2Cl_2)	96 000	–	–	4.4	0.095	31	0.13	I^-/I_3^-	[179]
124	564 (THF)	39 078	525 (NiO)	≈ 20% (500)	5.85	0.126	33.16	0.244	I^-/I_3^-	[181]
125	528 (THF)	46 782	490 (NiO)	≈ 15% (415)	6.69	0.135	35.03	0.316	I^-/I_3^-	[181]
126	665 (CH_2Cl_2)	–	660 (NiO)	≈ 15% (490)	1.31	0.065	31	0.026	I^-/I_3^-	[184]
				≈ 25% (610)	0.34	0.095	28	0.009	$[Co(dtb)_3]^{2+/3+}$	
127	665 (CH_2Cl_2)	–	664 (NiO)	≈ 17% (520)	2.73	0.095	32	0.083	I^-/I_3^-	[184]
				≈ 23% (625)	1.17	0.175	27	0.055	$[Co(dtb)_3]^{2+/3+}$	

[a] Photovoltaic parameters achieved with a propionitrile-based electrolyte; [b] Photovoltaic parameters achieved with a propylene carbonate-based electrolyte; [c] Photovoltaic parameters achieved with an acetonitrile-based electrolyte; [d] Tandem-cell (*n*-side); [e] Tandem-cell (*p*-side).

for a fine tuning of the energy levels. Despite of the weaker conjugation due to the α-β connection between the thiophene unit, the second triphenylamine donor group provided a considerable increasing of the LUMO energy level and thus a better electron injection process. Moreover, the branched spacer increased the bulkiness of the **132** preventing the aggregation contributing to reach an efficiency of 3.8% under standard AM 1.5 solar condition in combination with spiro-OMeTAD as hole transporter. To date, this is the highest value achieved among the solid-state DSSCs with sensitizers based on PMI derivatives.

To improve the electron injection another electron-donor group was proposed and tested by Laquai et al. introducing a bis(9,9-dimethyl-9*H*-fluoren-2-yl) amine as donor group in **133** and reaching an efficiency of 3.7% in the testing condition just described for **132**.[199] Dye **133** shows better results than **131** mainly due to the presence of phenylene spacer that led to a stronger orbital partitioning while provide comparable efficiency to **132**.

Good sensitizer for solid-state application required a slightly different molecular design. While the concepts of push-pull structure and the spacer employment remain useful, the typical anhydride anchoring group is substituted by a more suitable carboxylic acid group. Despite the lower photovoltaic performance, solid-state DSSCs are, nowadays, good candidates to overcome the limitations of liquid electrolyte-based devices.

4. *N*-annulated Perylene-Based Dyes in DSSCs

In the previous sections, it was discussed how PDI-based sensitizers suffer from the lack of preferential directed photogenerated charge transfer from the chromophore toward the conduction band of the metal oxide, while the PMI-based devices are affected by strong intrinsic self-aggregation phenomenon that compromises the photovoltaic performances. In the case of the PDI-based sensitizers, the improvement of photovoltaic performances was addressed by synthetizing the corresponding PMI-base structure, while for PMI-based sensitizers, partial improvements of the performances were recorded upon the rational insertion of bulky electron donor group in the dye structures. However, the intrinsic self-aggregation of the PMI-based sensitizers was not the only drawbacks preventing the achievement of higher photovoltaic performances. The anhydride anchoring group was also demonstrated to be responsible for the limited performances of PMI-based sensitizers because of the intrinsic cluttered

Table 4. Photovoltaic performance of solid state DSSCs employing perylene-based dyes.

Dye	λ_{MAX} (sol) [nm]	ε [$M^{-1}cm^{-1}$]	λ_{MAX} (film) [nm]	IPCE [%] [range/nm]	J_{SC} [mA cm^{-2}]	V_{OC} [V]	FF	PCE [%]	HTM	Refs.
128	524 (ACN)	97 200	489 (TiO_2)	–	0.076	0.82	26	0.02	P3OT	[193]
				–	0.081	0.70	26	0.02	P3HT	
129	510 (THF)	–	525 (TiO_2)	–	8.92	0.65	59	3.42	I^-/I_3^- in PEO	[194]
130	546 (CH_2Cl_2)	57 073	517 (TiO_2)	≈ 7% (475)	0.48	0.822	50	0.2	spiro-MeOTAD	[195]
131	590 (CH_2Cl_2)	25 000	550 (TiO_2)	> 40% (435–670)	8.7	0.640	57	3.2	spiro-MeOTAD	[196]
132	365 (CH_2Cl_2)	41 000	500 (TiO_2)	> 40% (400–600)	8.7	0.680	63	3.8	spiro-MeOTAD	[198]
133	360 (CH_2Cl_2)	–	510 (TiO_2)	–	9.03	0.68	60	3.7	spiro-MeOTAD	[199]

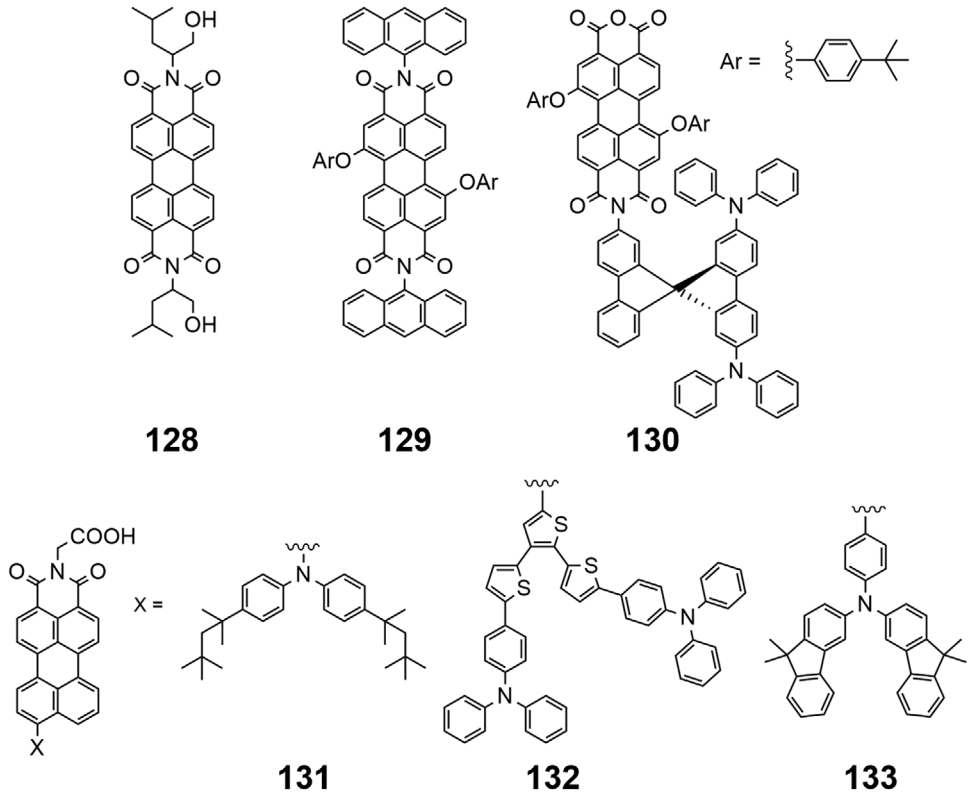

Scheme 7. Perylene imide-based dyes for solid-state DSSCs.

anchoring mode that affected the dye-loading process and by exhibiting relevant undesired phenomena of electron recombination of the injected charge.[103] These limitations were clearly depicted by values of photocurrent density <10.0 mA cm^{-2} in the PMI-based sensitized devices.

In this section, the *N*-annulated perylene-based sensitizers (NP) will be discussed showing how the rational investigation of novel structures and the optimization of the anchoring moiety allowed to double the value of photocurrent density achieving values over 20.0 mA cm^{-2} and therefore better the device performances (**Scheme** 8).

The first application of *N*-annulated perylene-based sensitizers in DSSCs was reported by Wang et al.[200] Following the porphyrin-based multichromophoric systems results discussed in Section 3.3.1, a series of multichromophoric dyes **134–137** were synthesized combining a *N*-annulated perylene unit and a Zn-based porphyrin similar to the well-known *YD2-o-C8*.[201] All sensitizers were linked to the TiO_2 surface by a 4-ethynylbenzoic acid anchoring group, known for its rigid structure allowing an efficient π-conjugation between the donor and acceptor moieties. In the sensitizers **134** and **135** the dyes were directly connected to each other, in **135** the porphyrin unit was fused with NP core, while **136** and **137** presented an acetylene spacer between the two chromophoric centres. The different connection between the porphyrin and the NP units significantly affected the dyes' optical properties. The absorption spectrum of **134** was the linear combination of the absorption of the two chromophores, while the presence of the acetylene spacer in **136** and **137** increased the π-conjugation, red-shifting the absorption component of NP unit and lowering the absorption intensity of the Soret band. This trend was particularly evident in **135** where the two units were fused with a consequent increase of the π-conjugate system leading to panchromatic absorptions spectra but also to a lowering of the LUMO energy levels. The comparison of the photovoltaic performance showed a dramatically difference between **135** and the other dyes. The low LUMO energy level of **135** was depicted by weak electron injection force from the excited state to the TiO_2 conduction band, resulting in a 0.3% device efficiency under simulated AM 1.5 sunlight. The improved photophysical properties of dyes **137** and **128** compared to **134** demonstrated the beneficial effect of the acetylene spacer resulting in higher short circuit photocurrents. Dye **134** achieved an efficiency of 5.6% while **136** and **137** reached outstanding values of 10.3% and 10.5%, respectively (photovoltaic parameters of *YD2-o-C8* standard: J_{sc} = 16.33 mA cm^{-2}, V_{oc} = 0.868 V, FF = 0.74, PCE = 10.5%).[200] The slight difference between **136** and **137** was due to the presence of the didodecoxyphenyl groups that better suppressed the dye aggregation and also lifted up the LUMO level of **137**.[200,201]

The outstanding device efficiencies above 10% reported by Wang et al. did not demonstrate the potentiality of the NP unit since the multichromophoric system was based on very efficient well-known dye *YD2-o-C8*.[200,201] The first real evidence was reported by Wang et al. by creating a push-pull dye **138** on a NP core by using a bis(4-(hexyloxy)phenyl)amino moiety as donor, a cyanoacrylic acid as acceptor/anchoring group and a 2-heptylundecyl hindered alkyl group on the amino position to prevent aggregation.[202] The device with dye **138** achieved an

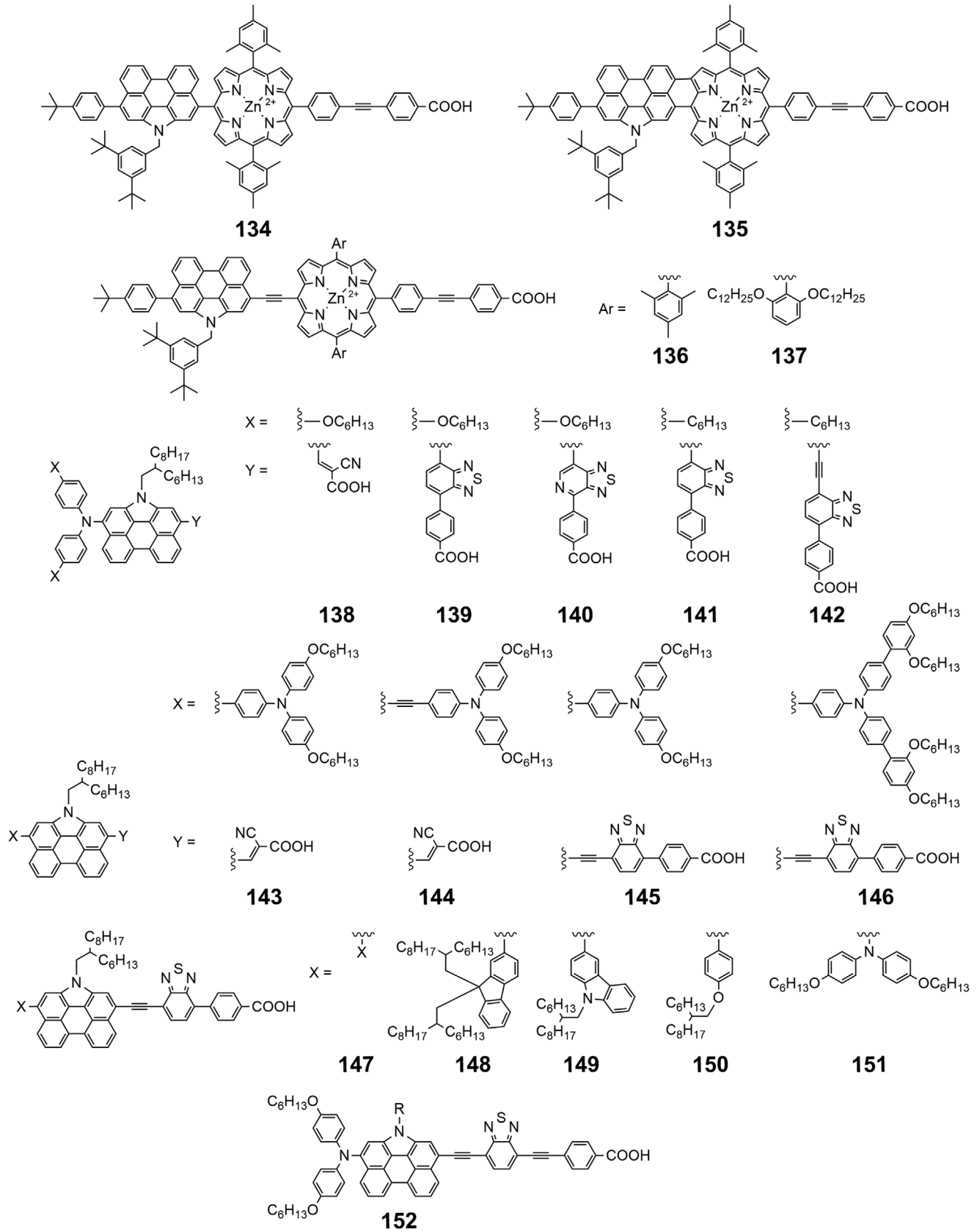

Scheme 8. *N*-annulated perylene dyes for solid-state DSSCs.

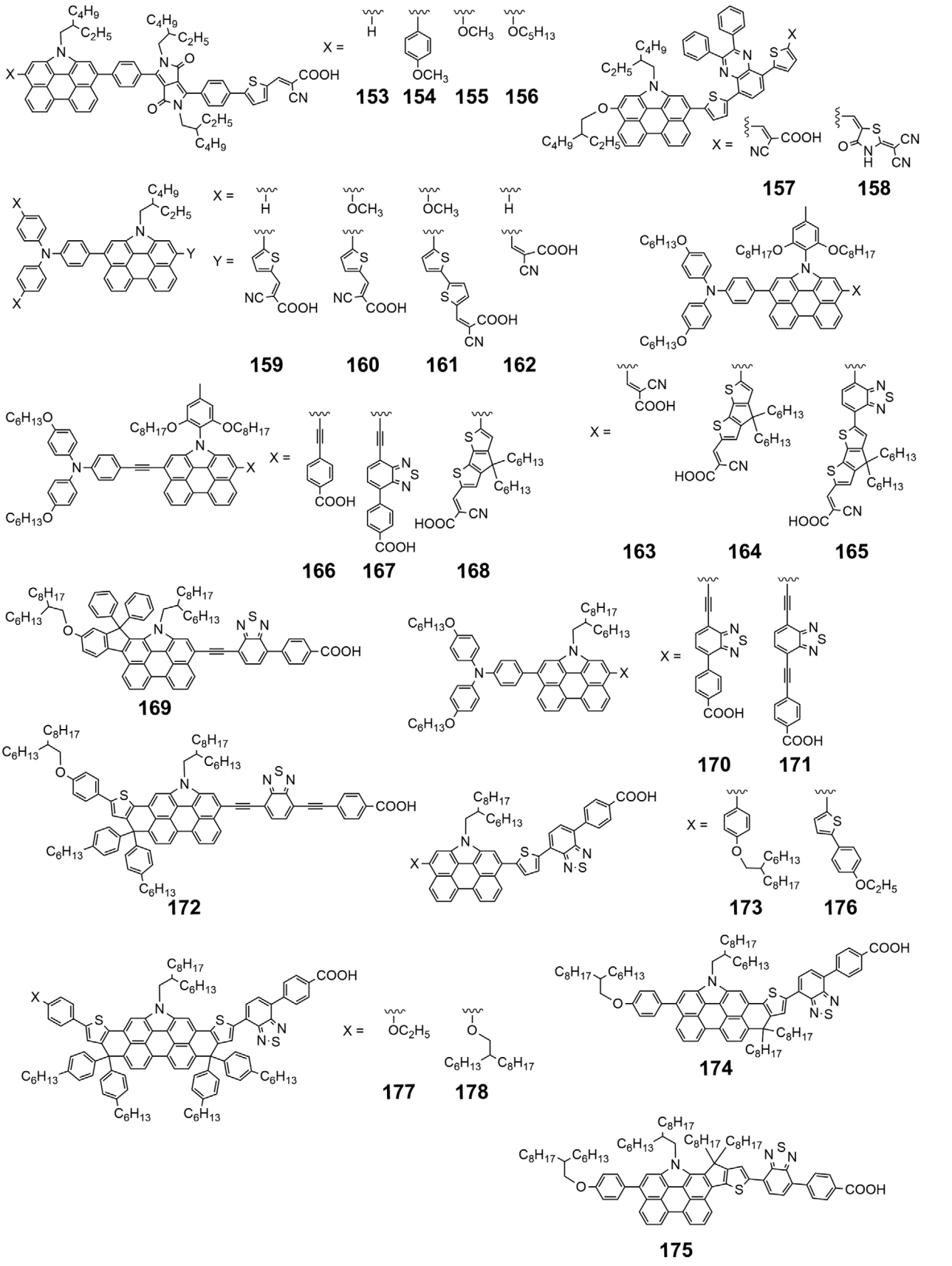

Scheme 8. *Continued*

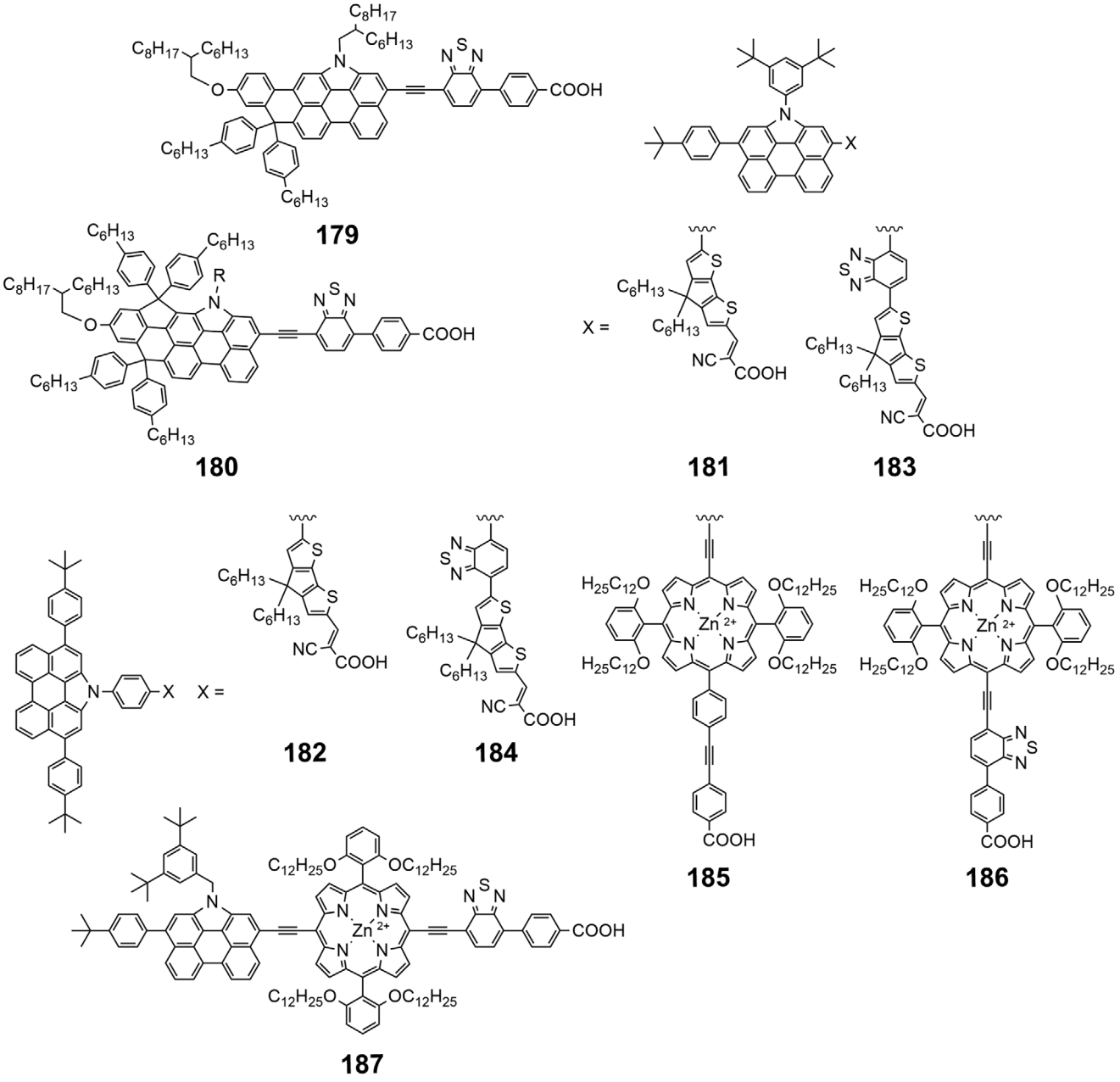

Scheme 8. *Continued*

outstanding efficiency of 8.8% under standard AM 1.5 sunlight, exceeding the previous record of 6.8% for a perylene-based dye in DSSCs obtained with **81**.[151]

The same group performed further investigation following this trend to improve the photovoltaic performance replacing the cyanoacrylic acceptor with a well-performing benzothiadiazole-benzoic acid (BTBA) group.[203,204] Preliminary theoretical calculations allowed to predict a large torsion angle between the perylene core and the benzothiadiazole unit in **139**, leading to a blue-shifted absorption peak compared to the reference **138**. To balance this behavior, the benzothiadiazole unit was also replaced with a more electron-withdrawing pyridothiadiazole in **140** reducing the energy gap and enhancing the light absorption. The devices with **139** and **140** achieved efficiencies of 7.3% and 5.0%, respectively employing tris(2,2′-bipyridine)cobalt (Co-bpy) complex as electrolyte. The better performance of **139** was due to the higher IPCE (81%) compared to 45% registered with **140**. Compared to the reference dye **138**, **139** had similar photovoltaic parameters with a slightly lower efficiency probably due to the worse photophysical properties or for the smaller band gap between the Fermi level of the redox couple (−4.80 eV) and the HOMO level of the dye (−4.98 eV for **138** and −4.87 eV for **139**). To overcome this limitation the alkyl chains replaced the alkoxyl in **141** along with a space increase between the NP core and the

benzothiadiazole unit was introduced by placing an acetylene bridge.[205] The replacement of the alkoxyl chains with the alkyl ones lowered the HOMO level (−4.99 eV for **141** vs −4.87 eV for **139**) enlarging the band gap with respect to the Fermi level (−4.80 eV) of the redox mediator and improving the driving force of the hole injection. Dye **141** achieved an efficiency of 8% resulting a better dye compared to **139** due to the ameliorated interactions with the electrolyte. Further improvement was achieved by introducing an acetylene spacer in **142**, improving the π-conjugation between the NP core and the benzothiadiazole resulting in better photophysical features than **139**. The device with **142** registered an efficiency of 8.8% under standard AM 1.5 sunlight, proving the beneficial effect of both alkyl chain and acetylene spacer (**Table 5**).

Another strategy investigated by Wang et al. consisted in replacing the diphenylamine moiety with a triphenylamine electron-donor group in **143**.[108] The theoretical calculations showed a large torsion angle between the perylene core and the side donor group, similarly to the case of benzothiadiazole unit, and similarly solvable by the insertion of an acetylene spacer in **144**. A red-shifted absorption and a higher molar extinction coefficient were recorded for **144** compared to **143**, but the latter provided a device efficiency of 9.0%, slightly higher than 8.6% of **144**, most likely affected by a lower dye-loading deriving by a more tilted anchoring mode. This feature was well-associated with the reduced photovoltage output compared to **143**. The comparison between the photovoltaic parameters of the dyes **138**, **143**, and **144** highlighted the key role of the anchoring mode. The best efficiency showed by **144** mainly depended on higher open circuit voltage, which was well-associated with the conformation of the dye-layer on the TiO_2 surface.

The previous studies shown i) the beneficial effect of inserting a benzothiadiazole unit as an electron acceptor, ii) the key role of the acetylene spacer between the NP core and the acceptor group, and iii) the increased push-pull effect due to a triphenylamine-based donor group (Scheme 8). Combining these concepts, Wang et al. synthetized **145** and **146** decorated with ethynylbenzothiadiazolebenzoic acid (EBTBA) as an electron-acceptor and with two different electron-donor groups.[206] Dye **145** was modified with a triphenylamine-based donor-group while **146** with a bulky diphenylamine-based one, and the corresponding devices achieved efficiencies of 10.6% and 11.5%, respectively. The comparison between **143** and **145** showed that the EBTBA acceptor group prompted better photovoltaic performances with respect to the cyanoacrylic moiety due to a more efficient charge injection into the conduction band and to a less tilted anchoring mode of the dye on the TiO_2 surface reflected by a higher dye-loading. However, the efficiency record was achieved by **146** using a diphenylamine-based donor group, characterized by a higher open circuit voltage derived by the twisted configuration of the bulky electron-donor group. The results discussed so far indicated how the triphenylamine-based donor-groups allowed to achieve better efficiencies while sensitizer **146** belied this reported evidence (Scheme 8).

Wang et al. synthetized a series of dyes **147–150** to explore that donor-group could better the photovoltaic efficiency on the **146** scaffold.[207,208] Dye **147** without any donor-group on the NP core was taken as reference and achieved an efficiency of 7.6%, showing the worse photophysical properties in terms of photocurrent, open circuit voltage and tendency to aggregate over the whole series. Dye **148** decorated with a 9,9-bis(2-hexyldecyl)-9*H*-fluorene achieved an efficiency of 9.8% due to the presence of push-pull system, better photophysical features and less self-aggregation in comparison to **147**. Further improvements in efficiency were reached with **149** and **150** that achieved 10.7% and 10.6%, respectively, thanks to a greater dye-loading on TiO_2 surface than **148**. The dyes based on the donor-NP-EBTBA structure, namely **145**, **146**, **148–150**, showed efficiencies in the 9.8–11.5% range, proving the small improvement obtained by tuning the donor-group's properties. Nevertheless, alternative molecular design strategies were explored to achieve a concrete improvement.

In this context, Wang et al. studied dyes **151** and **152** to evaluate further modification of the well-known EBTBA acceptor group, being inspired by the insertion of acetylene spacer between the NP-core and the benzothiadiazole unit, previously proposed by the same research group in **142**, to planarize the structure and improve the π-conjugation (Scheme 8).[209] An additional acetylene spacer was added to prevent the twisting between the benzoic acid anchoring group and the molecular backbone, resulting in a red-shifted absorption but no considerable improvement on the photophysical properties. The devices with **151** and **152** achieved efficiencies of 10.2% and 10.1%, respectively, highlighting that the longer synthetic pathway to get **152** was not an effective strategy to improve the device performance.

A completely different design was studied by Tian et al. in the **153–156** series bearing the cyanoacrylic anchoring group, diketopyrrolopyrrole (DPP) as electron acceptor-group and a thiophene spacer.[210] Branched 2-ethylhexyl chains were introduced at the amine site, both on the NP and DPP moieties to improve solubility and preventing aggregation. The best efficiency of 8.30% was achieved with **154** due to the higher push-pull effect and bulky structure of the *p*-methoxyphenyl group compared to the other proposed substituents.

Similar approach was followed by Hua et al. with dyes **157** and **158** linking a NP core to a quinoxaline acceptor and using two different types of anchoring groups such as cyanoacrylic acid in **157** and 2-(1,1-dicyanomethylene) rhodamine (DCRD) in **158** (Scheme 8).[211] The Anchoring group, quinoxaline unit and NP core were connected by thiophene spacers to extend the π-conjugation while branched 2-ethylhexyl and 2-ethylhexoxyl chains were introduced at the amine and peri sites respectively to prevent the aggregation. Dye **157** showed and efficiency of 7.58%, almost double the 4.43% recorded with **158** due to the wider spectral absorption, larger molar extinction coefficient and the longer electron lifetime of dye.

Wang et al. studied a series of dyes **159–162** to understand the effect of thiophene spacer length between the NP core and the anchoring group (Scheme 8).[108] A triphenylamine was used as donor group and two methoxy substituents were attached on **160** and **161** to fine tune the energetic levels of the orbitals and improve the solubility. The comparison between **160** and **161** highlighted an increase of the molar extinction coefficients along with a decrement of the electron injection while elongating the thiophene spacer, leading to 7.74% and 7.40% efficiencies in the corresponding devices. Moreover, the methoxy substituent on the triphenylamine upshifted the LUMO levels, increasing the electron injection driving force, which was lower in the unsubstituted

Table 5. Photovoltaic performance of DSSCs employing *N*-annulated perylene-based dyes.

Dye	λ_{MAX} (sol) [nm]	ε [$M^{-1}cm^{-1}$]	λ_{MAX} (film) [nm]	IPCE [%] [range/nm]	J_{SC} [mA cm^{-2}]	V_{OC} [V]	FF	PCE [%]	Electrolyte	References
134	438 (CH_2Cl_2)	19 4700	–	≈ 73% (455)	9.81	0.744	76.7	5.6	$[Co(bpy)_3]^{2+/3+}$	[200]
135	792 (CH_2Cl_2)	75 400	–	≈ 5% (440)	3.00	0.500	29.9	0.3	$[Co(bpy)_3]^{2+/3+}$	[200]
136	441 (CH_2Cl_2)	158 500	–	≈ 82% (720)	18.43	0.766	73.3	10.3	$[Co(bpy)_3]^{2+/3+}$	[200]
137	441 (CH_2Cl_2)	153 800	–	≈ 84% (720)	17.69	0.809	73.5	10.5	$[Co(bpy)_3]^{2+/3+}$	[200]
	441 (THF)	153 800			17.16	0.840	73.8	10.6	$[Co(bpy)_3]^{2+/3+}$	[218]
138	544 (THF)	44 100	–	> 75% (450–620)	14.90	0.844	70.1	8.8	$[Co(bpy)_3]^{2+/3+}$	[202]
	573 (Toluene)	–								
139	485 (THF)	23 900	–	81% (470)	12.63	0.788	73.5	7.3	$[Co(bpy)_3]^{2+/3+}$	[203]
	489 (Toluene)	–		> 60% (460–590)	13.80	0.818	71.8	8.1	$[Co(bpy)_3]^{2+/3+}$	[209]
140	475 (THF)	–	–	45% (450)	8.83	0.742	76.8	5.0	$[Co(bpy)_3]^{2+/3+}$	[203]
141	471 (THF)	28 500	–	> 80% (420–590)	13.40	0.813	73.8	8.0	$[Co(bpy)_3]^{2+/3+}$	[205]
142	526 (THF)	41 400	–	> 80% (420-620)	15.53	0.797	71.5	8.8	$[Co(bpy)_3]^{2+/3+}$	[205]
143	526 (THF)	32 900	–	> 80% (450–575)	14.50	0.928	66.9	9.0	$[Co(bpy)_3]^{2+/3+}$	[108]
144	540 (THF)	48 500	–	> 80% (450–575)	15.13	0.819	69.3	8.6	$[Co(bpy)_3]^{2+/3+}$	[108]
145	523 (THF)	34 500	–	> 90% (450–600)	16.62	0.856	74.5	10.6	$[Co(bpy)_3]^{2+/3+}$	[206]
146	522 (THF)	40 100	–	> 90% (450–600)	16.50	0.920	75.8	11.5	$[Co(bpy)_3]^{2+/3+}$	[206]
147	498 (THF)	30 600	–	> 80%(485–545)	12.06	0.824	76.0	7.6	$[Co(phen)_2]^{2+/3+}$	[207]
148	512 (THF)	52 200	–	> 80%(425–620)	14.78	0.887	74.9	9.8	$[Co(phen)_2]^{2+/3+}$	[207]
149	517 (THF)	47 800	–	> 80%(415–630)	16.71	0.883	72.2	10.7	$[Co(phen)_2]^{2+/3+}$	[207]
150	512 (THF)	36 100	–	> 90% (470-595)	15.81	0.897	74.4	10.6	$[Co(phen)_2]^{2+/3+}$	[214]
153	400 ($CHCl_3$)	57 300	510 (TiO_2)	> 70% (440-560)	15.29	0.675	72.3	7.46	I^-/I_3^-	[210]
154	403 ($CHCl_3$)	43 900	510 (TiO_2)	> 80% (450–540)	17.14	0.698	69.4	8.30	I^-/I_3^-	[210]
155	397 ($CHCl_3$)	38 000	510 (TiO_2)	> 60% (450-550)	14.60	0.639	71.7	6.69	I^-/I_3^-	[210]
156	396 ($CHCl_3$)	46 900	510 (TiO_2)	> 65% (440-560)	15.59	0.643	69.9	7.01	I^-/I_3^-	[210]
157	525 (THF)	36 600	537 (TiO_2)	> 70% (400-580)	14.89	0.728	70	7.58	I^-/I_3^-	[211]
158	516 (THF)	28 900	533 (TiO_2)	≈ 65% (350)	10.34	0.670	64	4.43	I^-/I_3^-	[211]
159	472 (CH_2Cl_2)	26 400	478 (TiO_2)	> 55% (420–515)	10.75	0.655	70.0	4.90	I^-/I_3^-	[106]
160	472 (CH_2Cl_2)	25 200	482 (TiO_2)	> 70% (450–515)	17.05	0.687	66.1	7.74	I^-/I_3^-	[106]
161	472 (CH_2Cl_2)	30 800	472 (TiO_2)	> 65% (440–535)	16.60	0.669	66.6	7.40	I^-/I_3^-	[106]
162	512 (CH_2Cl_2)	30 100	484 (TiO_2)	> 75% (450–515)	16.50	0.734	68.4	8.28	I^-/I_3^-	[106]
163	531 ($CHCl_3$)	32 700	503 (TiO_2)	> 70% (450–565)	10.48	0.825	69.1	5.79	$[Co(bpy)_3]^{2+/3+}$	[212]
				60% (510) [a]	8.76 [a]	0.729 [a]	74.4 [a]	4.76 [a]		
164	550 ($CHCl_3$)	44 500	494 (TiO_2)	> 70% (430–545)	12.31	0.731	67.8	6.10	$[Co(bpy)_3]^{2+/3+}$	[212]
				> 70% (430–545) [a]	12.80 [a]	0.740 [a]	73.3 [a]	6.95 [a]		
165	502 ($CHCl_3$)	49 600	465 (TiO_2)	> 50% (375–540)	10.27	0.739	72.0	5.46	$[Co(bpy)_3]^{2+/3+}$	[212]
				> 55% (370–585) [a]	11.32 [a]	0.766 [a]	72.6 [a]	6.30 [a]		
166	501 (CH_2Cl_2)	41 100	485 (TiO_2)	–	7.96	0.82	72	4.71	$[Co(bpy)_3]^{2+/3+}$	[213]
				> 80% (435–525) [a]	8.73 [a]	0.76 [a]	78 [a]	5.14 [a]		
167	532 (CH_2Cl_2)	44 700	486 (TiO_2)	–	10.24	0.78	71	5.65	$[Co(bpy)_3]^{2+/3+}$	[213]
				> 80% (450–590) [a]	14.49 [a]	0.78 [a]	74 [a]	8.38 [a]		
168	525 (CH_2Cl_2)	48 600	515 (TiO_2)	–	8.77	0.75	65	4.27	$[Co(bpy)_3]^{2+/3+}$	[213]
				> 70% (430–600) [a]	13.30 [a]	0.79 [a]	74 [a]	7.78 [a]		
169	536 (THF)	51 100	–	> 90% (500–625)	17.03	0.956	77.0	12.5	$[Co(phen)_2]^{2+/3+}$	[214]
170	492 (THF)	35 800	–	> 90% (440–540)	14.69	0.843	73.7	9.0	$[Co(bpy)_3]^{2+/3+}$	[215]
171	570 (THF)	44 200	–	> 90% (510–610)	17.70	0.810	73.1	10.5	$[Co(bpy)_3]^{2+/3+}$	[215]
172	600 (THF)	65 100	–	> 90% (490–650)	19.65	0.843	72.5	12.0	$[Co(bpy)_3]^{2+/3+}$	[215]
173	461 (THF)	37 700	–	> 90% (465–580)	15.54	0.818	73.6	9.4	$[Co(bpy)_3]^{2+/3+}$	[109]
174	560 (THF)	37 700	–	> 90% (520–610)	19.42	0.820	72.4	11.5	$[Co(bpy)_3]^{2+/3+}$	[109]
175	565 (THF)	43 200	–	> 90% (500–675)	19.64	0.843	72.8	12.0	$[Co(bpy)_3]^{2+/3+}$	[109]

(*Continued*)

Table 5. (Continued)

Dye	λ_{MAX} (sol) [nm]	ε [$M^{-1}cm^{-1}$]	λ_{MAX} (film) [nm]	IPCE [%] [range/nm]	J_{SC} [mA cm^{-2}]	V_{OC} [V]	FF	PCE [%]	Electrolyte	References
176	470 (THF)	39 300	–	> 80% (450–550)	14.81	0.734	73.6	8.0	$[Co(bpy)_3]^{2+/3+}$	[217]
177	630 (THF)	58 900	–	> 90% (575–670)	21.20	0.786	70.8	11.8	$[Co(bpy)_3]^{2+/3+}$	[217]
178	–	–	–	> 90% (575–710)	21.69	0.815	73.5	13.0	$[Co(bpy)_3]^{2+/3+}$	[217]
179	544 (THF)	–	–	≈ 90% (600)	16.57	0.950	74.1	11.7	$[Co(phen)_2]^{2+/3+}$	[218]
180	552 (THF)	–	–	≈ 90% (600)	17.28	0.974	74.7	12.6	$[Co(phen)_2]^{2+/3+}$	[218]
181	488 (THF)	64 080	–	≈ 73% (490)	13.07	0.748	73.3	7.16	$[Co(bpy)_3]^{2+/3+}$	[107]
				≈ 73% (490) [a]	14.63 [a]	0.739 [a]	72.3 [a]	7.82 [a]		
182	450 (THF)	43 900	–	≈ 52% (390)	9.76	0.746	71.6	5.21	$[Co(bpy)_3]^{2+/3+}$	[107]
				≈ 52% (390) [a]	10.61 [a]	0.727 [a]	72.9 [a]	5.62 [a]		
183	450 (THF)	67 300	–	≈ 70% (440)	8.75	0.733	73.4	4.70	$[Co(bpy)_3]^{2+/3+}$	[107]
				≈ 66% (440) [a]	7.88 [a]	0.737 [a]	74.8 [a]	4.31 [a]		
184	449 (THF)	50 000	–	≈ 52% (390)	9.08	0.743	74.2	5.01	$[Co(bpy)_3]^{2+/3+}$	[107]
				≈ 50% (470) [a]	8.27 [a]	0.734 [a]	74.7 [a]	4.53 [a]		
185	454 (THF)	241 600	–	70% (450)	8.05	0.078	77.7	4.4	$[Co(bpy)_3]^{2+/3+}$	[219]
186	456 (THF)	167 600	–	40% (450, 700)	8.27	0.733	78.6	4.8	$[Co(bpy)_3]^{2+/3+}$	[219]
187	474 (THF)	132 000	–	72% (720)	15.93	0.770	75.2	9.2	$[Co(bpy)_3]^{2+/3+}$	[219]
188	520 (THF)	40 400	–	73% (505)	10.55	0.681	72.4	5.19	I^-/I_3^-	[220]
189	525 (THF)	36 900	–	70% (505)	10.08	0.654	72.4	4.76	I^-/I_3^-	[220]
190	528 (THF)	38 400	–	63% (505)	9.96	0.633	71.1	4.48	I^-/I_3^-	[220]
191	545 (THF)	47 500	–	58% (500)	11.20	0.637	73.0	5.21	I^-/I_3^-	[220]
192	541 (THF)	35 400	–	68% (540)	12.46	0.657	73.4	6.00	I^-/I_3^-	[220]

[a] Photovoltaic parameters achieved with deoxycholic acid (DCA) co-adsorbed.

159 leading to 4.90% device efficiency. Interestingly, the best result was achieved with **162** that did not present a thiophene spacer resulting in a better electron injection into the TiO_2 conduction band.

A different approach was reported by *Wu* et al. studying a series of dyes **163–165** in which a bulky *O*-alkoxy-substituted phenyl group rather than flexible alkyl chain was chosen to suppress the problematic dye aggregation (Scheme 8).[212] Using alkoxy-substituted triphenylamine as electron-donor and cyanoacrylic acid as anchoring groups, the effect of a gradual extension of the π-conjugated system by the insertion of a cyclopentadithiophene (CPDT) in **164** and a benzothiadiazole unit in **165** was investigated. Dyes **164** and **165** were characterized by higher molar extinction coefficient than **163**. However, **164** showed a slightly red-shifted absorption maximum while dye **165** an ipsochromic shift due to the larger dihedral angle between the benzothiadiazole unit and NP core. The devices with dyes **163–165** achieved efficiencies of 5.79%, 6.10%, and 5.46%, respectively with **164** providing the best efficiency due to best IPCE (75%) and better photophysical properties. The same dyes were also co-adsorbed with deoxycholic acid (DCA) to prevent self-aggregation achieving efficiencies of 4.76%, 6.95%, and 6.30%, respectively. The co-adsorption of DCA led to better results for **164** and **165** while reduced the efficiency for **163**. The larger improvement recorded for **165** strongly confirmed the dye aggregation issue without a co-adsorbent compared to **163** and **164**.

In a subsequently study, Wu et al. worked to ameliorate the photovoltaic efficiency of **164** by the insertion of an acetylene spacer between the donor group and the NP core in **168**.[213] In parallel, other different acceptor/anchor groups replacing the cyclopentadithiophene-cyanoacrylic acid moiety with the ethynylbenzoic acid (EBA) in **166** and the well-known EBTBA group in **167** were tested (Scheme 8). The insertion of acetylene spacer in dye's **168** structure led to a higher efficiency of 7.78% using DCA as co-adsorbent. The other dyes **166** and **167** achieved efficiencies of 5.14% and 8.38%, respectively, confirming the EBTBA acceptor group as good performer. In the previous work it was demonstrated how DCA could slightly improve the photovoltaic performance of dye **164** and **165**. On the other, **166–168** were negatively affected by the presence of DCA mainly due to the more planarized structure that favors the aggregation.

The breakthrough in the *N*-annulated perylene-based dyes was achieved by Wang et al. with **169** as result of a new design concept to enhance the light absorption and the photovoltage of dye by the formation of a polycyclic aromatic hydrocarbon (PAH) based on *N*-annulated indeno-perylene structure (NIP) (Scheme 8).[214] Dye **169** showed an enlarged coplanar structure that led to a red-shifted absorption and a significant improvement of the molar extinction coefficient compared to the reference **150**. In **169** the well-known EBTBA unit was used as acceptor group while branched 2-hexyldecyloxy and 2-hexyldecy alkyl chain, were respectively attached on peri- and amino-position to prevent the strongly intermolecular π-π stacking. The device with **169** achieved an outstanding efficiency of 12.5% under standard AM 1.5 sunlight (photovoltaic parameters of *YD2-o-C8* standard: J_{sc} = 14.44 mA cm^{-2}, V_{oc} = 0.917 V, FF = 0.78,

PCE = 10.4%).[214] Compared to the reference, the IPCE value did not change (≈92%) while the short circuit photocurrent and the open circuit voltage deeply improved up to 17.03 mA cm^{-2} and 0.956 V, respectively.

The innovative molecular design concept was further investigated by Wang et al. with **170** and **171** using alkoxy-substituted triphenylamine as donor group, a benzothiadiazolebenzoic acid (BTBA) in **170** and diethynylbenzothiadiazolebenzoic acid (EBTBEA) in **171** as acceptor groups (Scheme 8).[215] The comparison of these dyes further proved the beneficial effect of the acetylene spacer and was exploited for tailoring the molecular design of dye **172** where a properly functionalized thiophene was linked into the peri-position of NP-core and subsequently the *N*-annulated 6*H*-thienobenzoperylene (NTBP) structure was obtained by intramolecular Friedel-Craft cyclization. Dye **172** showed better photovoltaic performance compared to **170** and **171** achieving an efficiency of 12.0% (photovoltaic parameters of *Z907* standard: J_{sc} = 13.76 mA cm^{-2}, V_{oc} = 0.779 V, FF = 0.75, PCE = 8.01%).[215]

The different isomers resulting by the intramolecular Friedel-Craft cyclization were lately investigated in relationship to the photovoltaic performance.[109,216] The series of dyes **173–175** was synthetized starting from the reference structure **150** in which the acetylene spacer of EBTBA unit was replaced by a thiophene bridge. In dyes **174** and **175**, a properly functionalized thiophene was used to perform the intramolecular Friedel-Craft cyclization leading to the formation of the two isomers, the *N*-annulated 6*H*-thienobenzoperylene (NTBP) **174** and *N*-annulated 13*H*-thienocyclopentaperylene (NTCP) **175**. The comparison between **174**, **175**, and **173** evidenced that the cyclization red-shifted the absorption and improved the IPCE: ≈90% in the range 450–600 nm for **173** while **174** and **175** presented the same value in a larger range (450–700 nm). Lower IPCE led to an efficiency of 9.4% for dye **173** while the devices with **174** and **175** achieved efficiencies of 11.5 and 12.0%, respectively (photovoltaic parameters of *YD2-o-C8* standard: J_{sc} = 17.07 mA cm^{-2}, V_{oc} = 0.860 V, FF = 0.72, PCE = 10.6%).[109] The slightly better result of **175** compared to **174** was due to the larger amount of sensitizer dye-loaded onto the TiO_2 surface (Scheme 8).

To further reduce the optical energy gap of dye for better the absorption of near-infrared solar photons, Wang et al. decorated the peri-positions of the NP core with two properly functionalized thiophenes in **177**, and **178** to enlarge the PAH structure in comparison to similar sensitizers.[217] Dye **176**, synthetized as reference bearing an EBTBA unit as acceptor group and an ethoxyphenyl substituent as donor, showed an efficiency of 8.0%. PAH dye **177** had better photophysical properties with a higher molar extinction coefficient and a deeply red-shifted absorption. The IPCE reached value upper than 80% over 750 nm while, at this wavelength, **176** showed an IPCE near to 10%. The significant improvement of the IPCE led to an outstanding value of short circuit photocurrent of 21.20 mA cm^{-2} for **177**. Nevertheless, the extended coplanar structure in **177** induced a strong intermolecular π–π stacking reducing the open circuit voltage that was overcome in **178** by the insertion of a bulkier 2-hexyldecyloxy substituent on the phenyl group in the peri position. This novel modification improved the open circuit voltage resulting in a brilliant efficiency of 13.0% under standard AM 1.5 sunlight. To date, this is not only the highest value among DSSCs with perylene-based dyes, but it is also one of the highest values ever reached.

Following the same concept, Wang et al. studied another PAH structure exploiting a double intramolecular cyclization on the same thiophene to obtain a *N*-annulated benzoindenopentaphene (NBIP) structure **180** (Scheme 8).[218] Compared to the mono-cyclized isomers **169** and **179**, dye **180** showed a slightly red-shifted absorption and IPCE. The di-cyclized **180** provided an efficiency of 12.6% higher than the 11.7% registered with **179**. The performance improvement was due to the better photophysical properties but also to the extra bulky alkyl chains that reduced the aggregation and the recombination processes. Interestingly, the comparison between the two isomers **169** and **179** further proved the better performance achieved by the *N*-annulated indeno-perylene structure.

Finally, also the linkage mode of NP core on the TiO_2 surface was explored. So far, the NP core was decorated with a large variety of anchoring unit but always exploiting the peri position. Wu et al. synthetized **183** and **184** in which the amino position was exploited to attach the anchoring group.[107]

Dye **181** was synthetized as reference using a cyclopentadithiophene (CDP) spacer and a cyanoacrylic acid group as anchoring group, while **182** was decorated with a further benzothiadiazole acceptor group between the NP core and the CPD spacer (Scheme 8). The comparison between the two dyes showed that **181** drove to a better photovoltaic performance with an efficiency of 7.82%. Benzothiadiazole unit in **182** improved the charge separation but the larger dihedral angle present, reduced the π-conjugated system and lead to a lower molar extinction coefficient. Dyes **183** and **184** presented the same anchoring units but they were attached to the amino positions of NP core via a phenyl spacer. The different linkage mode led to lower photovoltaic performance due to the worse IPCE of these dyes compared to **181** and **182**. Interestingly, the comparison between dyes **183** and **184** showed how the dye with the benzothiadiazole unit achieved a better efficiency of 4.53% compared to the 4.31% of **183**.

The same concept was exploited in a multichromophoric-system based on a Zn-porphyrin **137** and **185–187** (Scheme 8).[219] Dyes **137** and **187** were synthetized as reference using an ethynylbenzoic acid (EBA) and an EBTBA unit as anchoring groups, respectively. A Zn-porphyrin-based moiety bridged the NP core and the anchoring group exploiting the peri position while in **185** and **186** the Zn-porphyrin was attached on the amino group of NP core. Confirming the evidence reported by Wu et al., the linkage via the amino site led to a worse photovoltaic performance.[107] Reference dyes **137** and **187** achieved efficiencies of 10.6% and 9.2% respectively, while dyes **185** and **186** achieved just of 4.4% and 4.8% respectively.

In summary, the key role of the *N*-annulated perylene-based dyes in the development of high-efficiency DSSCs was demonstrated. As seen, i) the bulky triphenylamine donor groups led to a better push-pull effect and thus to a larger photovoltaic performance, ii) the use of the acetylene spacer could provide better performance or decrease the charge injection depending by the context in which is employed, iii) the enlargement of NP core to a PAH structure led to a huge improvement of the photovoltaic performance and iv) the linkage mode via the amino position of the NP worsened the photophysical properties and also the charge

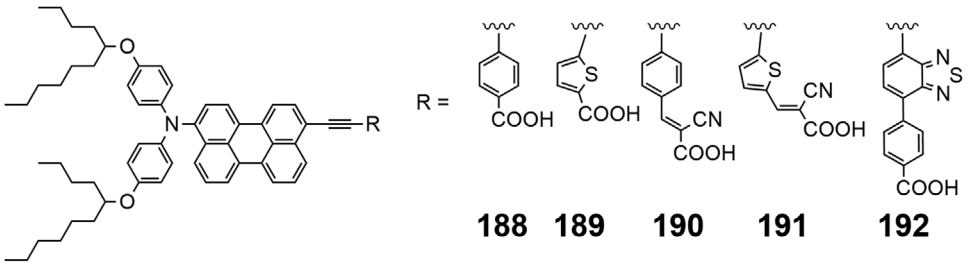

Scheme 9. *N*-annulated perylene dyes for solid-state DSSCs.

injection resulting in a lower efficiencies compared to the classic linkage via the peri position.

5. Perylene-Based Dyes in DSSCs

Besides to the most performant *N*-annulated rylene sensitizers, some dyes based on the simple perylene structure were tested in DSSCs.[220–223] Dyes **188**–**192** were based on a perylene core functionalized with a hindered diphenylamine donor-group and various anchoring moieties. An acetylene spacer between the perylene and the anchoring moiety was used to planarize the structure and improve the π-conjugation. Dyes **188** and **189** bared a carboxylic acid group as anchoring while **190** and **191** exploited the cyanoacrylic acid group. The different anchoring groups and spacers did not have any significant effect on the device efficiency with the family dyes reporting comparable results except for **192** that achieved the best efficiency of 6.00% with the well-known anchoring moiety EBTBA (**Scheme 9**).

6. Outlook

The structural evolution of perylene-based dyes has been reported in detail in this review. The fine-tuning of their structure allows to successfully achieve efficiency near 13% that remains, up to now, among the highest in the DSSCs' panorama. The stability and the possibility to tune the photophysical properties is the key value of DSSCs. However, the challenging synthetic approach, above all for the monoimide- and the *N*-annulated perylene-based dyes, is one of the critical points that limits their use in comparison to other more common but less efficient sensitizers. Further improvements from the synthetic point of view will therefore be needed to specifically either achieve higher yields in the desired product or lower the reaction's step to prepare the scaffolds. In this regards the initial synthetic step involving the controlled halogenation plays a key role in the overall process, since side reactions, forming perhalogenated products or undesired isomers, are always occurring. Similarly, the imide formation reaction requires to be strictly controlled in for the optimal synthesis of either asymmetrical perylene derivatives or mono imide scaffolds. Later, the device optimization should be heavily addressed to optimize the dye-loading methods, evaluating the best electrolyte formulation and the possible use of co-adsorbents. A general methodology can unlikely work for the whole library on the perylene derivatives due to the high variability of the possible substituent and functional groups present both on the bay and edge positions. On the other hand, the robustness and tolerance of the perylene scaffold to many synthetic conditions allows to explore an endless number of functionalization both on the dye core and on the imide side. This feature can be easily translated in novel sensitizer, co-sensitizer and dyes characterized higher suitability for the application in DSSC in the next years.

Moreover, the perylene-based dyes allow the fabrication of devices operating over the whole visible spectrum by simply expanding the perylene core and obtaining highly conjugated planar structures able to absorb light also in the NIR region. These prospects can lead to the development not only of more efficient DSSC but also colourless DSSCs capable of improving the possibility of realizing building integrated photovoltaics systems BIPV.

Acknowledgements

The authors acknowledge support from the project CH4.0 under the MUR program "Dipartimenti di Eccellenza 2023–2027" (CUPD13C22003520001). C.B. acknowledges support from "IMPRESSIVE" project that received funding from the European Union's Horizon2020 research and innovation program under grant agreement number n°826013 and from "CANVAS" project that received funding from the Italian Ministry of the Environment and the Energy Security, through the Research Fund for the Italian Electrical System (CSEAA_00009).

Open access publishing facilitated by Universita degli Studi di Torino, as part of the Wiley - CRUI-CARE agreement.

Conflict of Interest

The authors declare no conflict of interest.

Keywords

dye-sensitized solar cells, energy, perylene dyes

Received: June 26, 2024
Revised: September 11, 2024
Published online:

[1] IEA (2022), World Energy Outlook 2022, IEA Publications, Paris, **2022**, https://www.iea.org/reports/world-energy-outlook-2022.
[2] Q. Schiermeier, J. Tollefson, T. Scully, A. Witze, O. Morton, *Nature* **2008**, *454*, 816.
[3] N. Lewis, *Science* **2007**, *315*, 798.
[4] V. Smil, *General Energetics: Energy in the Biosphere and Civilization*, John Wiley, New York **1991**, p. 240.

[5] A. Goetzberger, J. Luther, G. Willeke, *Sol. Energy Mater. Sol. Cells* **2002**, *74*, 1.
[6] A. Cristobal, A. M. Vega, A. L. López, *Next Generation of Photovoltaics: New Concepts*, Springer, Berlin Heidelberg **2012**.
[7] D. Chapin, C. Fuller, G. Pearson, *J. Appl. Phys.* **1954**, *25*, 676.
[8] M. A. Green, Y. Hishikawa, W. Warta, E. D. Dunlop, D. H. Levi, J. Hohl-Ebinger, A. W. H. Ho-Baillie, *Prog. Photovoltaics Res. Appl.* **2017**, *25*, 668.
[9] A. Hagfeldt, N. Vlachopoulos, in *The Future of Semiconductor Oxides in Next-Generation Solar Cells*, (Ed: M. Lira-Cantu), Elsevier, Amsterdam, Netherlands **2018**, p. 183.
[10] A. Shah, P. Torres, R. Tscharner, N. Wyrsch, H. Keppner, *Science* **1999**, *285*, 692.
[11] M. Grätzel, *J. Photochem. Photobiol. C* **2003**, *4*, 145.
[12] M. Grätzel, *Acc. Chem. Res.* **2009**, *42*, 1788.
[13] A. Hagfeldt, G. Boschloo, L. Sun, L. Kloo, H. Pettersson, *Chem. Rev.* **2010**, *110*, 6595.
[14] H. Hoppe, N. Sariciftci, S. Niyazi, *Mater. Res.* **2004**, *19*, 45.
[15] L. Dou, J. You, Z. Hong, Z. Xu, G. Li, R. A. Street, Y. Yang, *Adv. Mater.* **2013**, *25*, 6642.
[16] J. Hou, O. Inganas, R. H. Friend, F. Gao, *Nat. Mater.* **2018**, *17*, 119.
[17] A. J. Nozik, *Physica* **2002**, *14*, 115.
[18] P. Kamat, *J. Phys. Chem. Lett.* **2013**, *4*, 909.
[19] G. H. Carey, A. L. Abdelhady, Z. Ning, S. M. Thon, O. M. Bakr, E. H. Sargent, *Chem. Rev.* **2015**, *115*, 12732.
[20] M. A. Green, A. Ho-Baillie, H. J. Snaith, *Nat. Photonics* **2014**, *8*, 506.
[21] J. Correa-Baena, A. Abate, M. Saliba, W. Tress, J. T. Jesper, M. Grätzel, A. Hagfeldt, *Energy Environ. Sci.* **2017**, *10*, 710.
[22] Y. Ren, D. Zhang, J. Suo, Y. Cao, F. T. Eickemeyer, N. Vlachopoulos, S. M. Zakeeruddin, A. Hagfeldt, M. Grätzel, *Nature* **2023**, *613*, 60.
[23] H. Pettersson, T. Gruszecki, *Sol. Energy Mater. Sol. Cells* **2001**, *70*, 203.
[24] M. Freitag, G. Boschloo, *Curr. Opin. Electrochem.* **2017**, *2*, 111.
[25] A. B. Muñoz-García, I. Benesperi, G. Boschloo, J. J. Concepcion, J. H. Delcamp, E. A. Gibson, G. J. Meyer, M. Pavone, H. Pettersson, A. Hagfeldt, M. Freitag, *Chem. Soc. Rev.* **2021**, *50*, 12450.
[26] T. M. W. J. Bandara, J. M. C. Hansadi, F. Bella, *Ionics* **2022**, *28*, 2563.
[27] C. Dupraz, H. Marrou, G. Talbot, L. Dufour, A. Nogier, Y. Ferad, *Renew. Energ.* **2011**, *36*, 2725.
[28] F. Grifoni, M. Bonomo, W. Naim, N. Barbero, T. Alnasser, I. Dzeba, M. Giordano, A. Tsaturyan, M. Urbani, T. Torres, C. Barolo, F. Sauvage, *Adv. Energy Mat.* **2021**, *11*, 2101598.
[29] J. Wu, Z. Lan, J. Lin, M. Huang, Y. Huang, L. Fan, G. Luo, *Chem. Rev.* **2015**, *115*, 2136.
[30] I. Benesperi, H. Michaels, M. Freitag, *J. Mater. Chem. C* **2018**, *6*, 11903.
[31] M. Giordano, G. Volpi, M. Bonomo, P. Mariani, C. Garino, G. Viscardi, *New J. Chem.* **2021**, *45*, 15303.
[32] B. O'Regan, M. Grätzel, *Nature* **1991**, *353*, 737.
[33] M. Grätzel, *Nature* **2001**, *414*, 338.
[34] A. Listorti, B. O'Regan, J. R. Durrant, *Chem. Mater.* **2011**, *23*, 3381.
[35] C. Martín, M. Ziółek, A. Douhal, *J. Photochem. Photobiol. C* **2016**, *26*, 1.
[36] R. Katoh, A. Furube, *J. Photochem. Photobiol. C* **2014**, *20*, 1.
[37] K. Kakiage, Y. Aoyama, T. Yano, K. Oya, J. Fujisawa, M. Hanaya, *Chem. Commun.* **2015**, *51*, 15894.
[38] J.-M. Ji, H. Zhou, Y. K. Eom, C. H. Kim, H. K. Kim, *Adv. Energy Mater.* **2020**, *10*, 2000124.
[39] T. Higashino, H. Imahori, *ACS Energy Lett.* **2022**, *7*, 1926.
[40] S. Zhang, F. Huang, X. Guo, Y. Xiong, Y. Huang, H. Ågren, L. Wang, J. Zhang, *Angew. Chem., Int. Ed.* **2023**, *62*, 202302753.
[41] J. N. Clifford, E. Martínez-Ferrero, A. Viterisi, E. Palomares, *Chem. Soc. Rev.* **2011**, *40*, 1635.
[42] A. Islam, H. Sugihara, H. Arakawa, *J. Photoch. Photobio. A* **2003**, *158*, 131.
[43] A. O. Adeloye, P. A. Ajibade, *Molecules* **2014**, *19*, 12421.
[44] S. Mathew, A. Yella, P. Gao, R. Humphry-Baker, B. F. E. Curchod, N. Ashari-Astani, I. Tavernelli, U. Rothlisberger, M. K. Nazeeruddin, M. Grätzel, *Nat. Chem.* **2014**, *6*, 242.
[45] L.-L. Li, E. W. G. Diau, *Chem. Soc. Rev.* **2013**, *42*, 291.
[46] S. Eu, T. Katoh, T. Umeyama, Y. Matano, H. Imahori, *Dalton Trans.* **2008**, *40*, 5476.
[47] M. V. Martinez-Diaz, G. de la Torre, T. Torres, *Chem. Commun.* **2010**, *46*, 7090.
[48] K. Hara, M. Kurashige, Y. Dan-ho, C. Kasada, A. Shinpo, S. Suga, K. Sayama, H. Arakawa, *New J. Chem.* **2003**, *27*, 783.
[49] T. Horiuchi, H. Miura, K. Sumioka, S. Uchida, *J. Am. Chem. Soc.* **2004**, *126*, 12218.
[50] D. P. Hagberg, T. Edvinsson, T. Marinado, G. Boschloo, A. Hagfeldt, L. Sun, *Chem. Commun.* **2006**, 2245.
[51] A. Burke, L. Schmidt-Mende, S. Ito, M. Grätzel, *Chem. Commun.* **2007**, *3*, 234.
[52] D. Saccone, S. Galliano, N. Barbero, P. Quagliotto, G. Viscardi, C. Barolo, *Eur. J. Org. Chem.* **2016**, *2016*, 2244.
[53] W. Herbst, K. Hunger, *Industrial Organic Pigments: Production, Properties, Applications*, 2nd ed., WILEY-VCH, Weinheim **1997**.
[54] C. Huang, S. Barlow, S. R. Marder, *J. Org. Chem.* **2011**, *76*, 2386.
[55] B. A. Jones, A. Facchetti, M. R. Wasielewski, T. J. Marks, *J. Am. Chem. Soc.* **2007**, *129*, 15259.
[56] G. Horowitz, F. Kouki, P. Spearman, D. Fichou, C. Nogues, X. Pan, F. Garnier, *Adv. Mater.* **1996**, *8*, 242.
[57] F. Würthner, *Chem. Commun.* **2004**, *14*, 1564.
[58] S. Becker, A. Böhm, K. Müllen, *Chem.-Eur. J.* **2000**, *6*, 3984.
[59] C. Li, J. Schöneboom, Z. H. Liu, N. G. Pschirer, P. Erk, A. Herrmann, K. Müllen, *Chem.-Eur. J.* **2009**, *15*, 878.
[60] H. Langhals, *Heterocycles* **1995**, *40*, 477.
[61] A. Hermann, K. Müllen, *Chem. Lett.* **2006**, *35*, 978.
[62] Y. Avlasevich, C. Li, K. Müllen, *J. Mater. Chem.* **2010**, *20*, 3814.
[63] L. Chen, C. Li, K. Müllen, *J. Mater. Chem. C* **2014**, *2*, 1938.
[64] A. Nowak-Król, F. Würthner, *Org. Chem. Front.* **2019**, *6*, 1272.
[65] W. Jiang, H. Qian, Y. Li, Z. Wang, *J. Org. Chem.* **2008**, *73*, 7369.
[66] W. S. Shin, H. H. Jeong, M. K. Kim, S. H. Jin, M. R. Kim, J. K. Lee, J. W. Lee, Y. S. Gal, *J. Mater. Chem.* **2006**, *16*, 384.
[67] C. Li, H. Wonneberger, *Adv. Mater.* **2012**, *24*, 613.
[68] E. Kozma, M. Catellani, *Dyes Pigm.* **2013**, *98*, 160.
[69] Z. Liu, D. Zeng, X. Gao, P. Li, Q. Zhang, X. Peng, *Sol. Energ. Mat. Sol. C* **2019**, *189*, 103.
[70] A. Gerniski Macedo, L. Patricio Christopholi, A. E. X. Gavim, J. Ferreira de Deus, M. A. M. Teridi, A. R. M. Yusoff, W. J. da Silva, *J. Mater.* **2019**, *30*, 15803.
[71] X. Zhan, A. Facchetti, S. Barlow, T. J. Marks, M. A. Ratner, M. R. Wasielewski, S. R. Marder, *Adv. Mater.* **2011**, *23*, 268.
[72] T. Weil, T. Vosch, J. Hofkens, K. Peneva, K. Müllen, *Angew. Chem., Int. Ed.* **2010**, *49*, 9068.
[73] C. Ji, W. Cheng, Q. Yuan, K. Müllen, M. Yin, *Acc. Chem. Res.* **2019**, *52*, 2266.
[74] J. Liu, N. Zheng, Z. Hu, Z. Wang, X. Yang, F. Huang, Y. Cao, *Sci. China Chem.* **2017**, *60*, 1136.
[75] J. Yi, J. Wang, Y. Lin, W. Gao, Y. Ma, H. Tan, H. Wang, C.-Q. Ma, *Dyes Pigm.* **2017**, *136*, 335.
[76] M. Yi, J. Yi, J. Wang, L. Wang, W. Gao, Y. Lin, Q. Luo, H. Tan, C.-Q. Ma, H. Wang, *Dyes Pigm.* **2017**, *139*, 498.
[77] M. Matussek, M. Filapek, P. Gancarz, S. Krompiec, J. G. Małecki, S. Kotowicz, M. Siwy, S. Maćkowski, A. Chrobok, E. Schab-Balcerzak, A. Słodek, *Dyes Pigm.* **2018**, *159*, 590.
[78] W. E. Benjamin, D. R. Veit, M. J. Perkins, E. Bain, K. Scharnhorst, S. McDowall, D. L. Patrick, J. D. Gilbertson, *Chem. Mater.* **2014**, *26*, 1291.
[79] H. Chang, Z. Chen, X. Yang, Q. Yin, J. Zhang, L. Ying, X.-F. Jiang, B. Xu, F. Huang, Y. Cao, *Org. Electron.* **2017**, *45*, 227.

[80] W. Xiong, X. Meng, T. Liu, Y. Cai, X. Xue, Z. Li, X. Sun, L. Huo, W. Ma, Y. Sun, *Org. Electron.* **2017**, *50*, 376.
[81] T. Adhikari, Z. Ghoshouni Rahami, J.-M. Nunzi, O. Lebel, *Org. Electron.* **2016**, *34*, 146.
[82] G. Li, Y. Zhao, J. Li, J. Cao, J. Zhu, X. W. Sun, Q. Zhang, *J. Org. Chem.* **2015**, *80*, 196.
[83] M. Kardos, *German Patent, DE 276357*, **1913**.
[84] M. Kardos, *German Patent, DE 276956*, **1913**.
[85] L. D. Wescott, D. L. Mattern, *J. Org. Chem.* **2003**, *68*, 10058.
[86] A. Rademacher, S. Märkle, H. Langhals, *Chem. Ber.* **1982**, *115*, 2927.
[87] V. Rogovik, L. Gutnik, *Zh. Org. Khim.* **1988**, *24*, 635.
[88] P. Osswald, F. Würthner, *J. Am. Chem. Soc.* **2007**, *129*, 14319.
[89] M. Queste, C. Cadiou, B. Pagoaga, L. Giraudet, N. Hoffmann, *New J. Chem.* **2010**, *34*, 2537.
[90] M. Sadrai, L. Hadel, R. R. Sauers, S. Husain, K. Krogh-Jespersen, J. D. Westbrook, G. R. Bird, *J. Phys. Chem.* **1992**, *96*, 7988.
[91] A. Böhm, H. Arms, G. Henning, P. Blaschka, *(BASF AG), Ger. Pat. Appl., DE 19547209 A1* **1997**.
[92] F. Würthner, V. Stepanenko, Z. Chen, C. R. Saha-Möller, N. Kocher, D. Stalke, *J. Org. Chem.* **2004**, *69*, 7933.
[93] P. Rajasingh, R. Cohen, E. Shirman, L. J. W. Shimon, B. Rybtchinski, *J. Org. Chem.* **2007**, *72*, 5973.
[94] Y. Zhao, M. R. Wasielewski, *Tetrahedron Lett.* **1999**, *40*, 7047.
[95] Y. Nagao, T. Misono, *Bull. Chem. Jpn.* **1981**, *54*, 1191.
[96] Y. Nagao, T. Misono, *Bull. Chem. Jpn.* **1981**, *54*, 1575.
[97] L. Feiler, H. Langhals, K. Polborn, L. Ann, **1995**, 7, 1229.
[98] K. Tomizaki, P. Thamyongkit, R. S. Loewe, J. S. Lindsey, *Tetrahedron* **2003**, *59*, 1191.
[99] Z. Yuan, S.-L. Lee, L. Chen, C. Li, K. S. Mali, S. De Feyter, K. Müllen, *Chem.-Eur. J.* **2013**, *19*, 11842.
[100] H. Quante, K. Müllen, *Angew. Chem., Int. Ed.* **1995**, *34*, 1323.
[101] N. G. Pschirer, C. Kohl, F. Nolde, J. Qu, K. Müllen, *Angew. Chem., Int. Ed.* **2006**, *45*, 1401.
[102] M. Grzybowski, K. Skonieczny, H. Butenschçn, D. T. Gryko, *Angew. Chem., Int. Ed.* **2013**, *52*, 9900.
[103] L. Zhang, J. M. Cole, *ACS Appl. Mater. Interfaces* **2015**, *7*, 3427.
[104] J. E. Anthony, *Chem. Rev.* **2006**, *106*, 5028.
[105] J. J. Looker, *J. Org. Chem.* **1972**, *37*, 3379.
[106] L. Yang, Z. Zheng, Y. Li, W. Wu, H. Tian, Z. Wang, *Chem. Commun.* **2015**, *51*, 4842.
[107] J. Luo, X. Wang, L. Fan, G. Li, Q. Qi, K.-W. Huang, T. L. D. Tam, J. Zhang, Q. Wang, J. Wu, *J. Mater. Chem. C* **2016**, *4*, 3709.
[108] C. Yan, W. Ma, Y. Ren, M. Zhang, P. Wang, *ACS Appl. Mater. Interfaces* **2015**, *7*, 801.
[109] Z. Yao, M. Zhang, R. Li, L. Yang, Y. Qiao, P. Wang, *Angew. Chem., Int. Ed.* **2015**, *54*, 5994.
[110] B. Burfeindt, T. Hannappel, W. Storck, F. Willig, *J. Phys. Chem-Us* **1996**, *100*, 16463.
[111] S. Ferrere, A. Zaban, B. A. Gregg, *J. Phys. Chem. B* **1997**, *101*, 4490.
[112] S. Wang, Y. L. Li, C. M. Du, Z. Q. Shi, S. X. Xiao, D. B. Zhu, E. Q. Gao, S. M. Cai, *Synth. Met.* **2002**, *128*, 299.
[113] C. Zafer, M. Kus, G. Turkmen, H. Dincalp, S. Demic, B. Kuban, Y. Teoman, S. Icli, *Sol. Energ. Mat. Sol. C* **2007**, *91*, 427.
[114] J. E. Kroeze, N. Hirata, S. Koops, M. K. Nazeeruddin, L. Schmidt-Mende, M. Grätzel, J. R. Durrant, *J. Am. Chem. Soc.* **2006**, *128*, 16376.
[115] L. Zhang, J. M. Cole, *J. Mater. Chem.* **2017**, *5*, 19541.
[116] Y. Shibano, T. Umeyama, Y. Matano, H. Imahori, *Org. Lett.* **2007**, *9*, 1971.
[117] J. Fortage, M. Severac, C. Houarner-Rassin, Y. Pellegrin, E. Blart, F. Odobel, *J. Photochem. Photobiol. A* **2008**, *197*, 156.
[118] M. Planells, F. J. Céspedes-Guirao, L. Goncalves, A. Sastre-Santos, F. Fernandez-Lazaro, E. Palomares, *J. Mater. Chem.* **2009**, *19*, 5818.
[119] H. J. Snaith, S. M. Zakeeruddin, L. Schmidt-Mende, C. Klein, M. Grätzel, *Angew. Chem.* **2005**, *44*, 6413.
[120] M. Planells, F. J. Céspedes-Guirao, A. Forneli, A. Sastre-Santos, F. Fernández-Lázaro, E. Palomares, *J. Mater. Chem.* **2008**, *18*, 5802.
[121] G. D. Sharma, R. Kurchania, R. J. Ball, M. S. Roy, J. A. Mikroyannidis, *Int. J. Photoenergy* **2012**, *2012*, 983081.
[122] A. Kay, M. Grätzel, *J. Phys. Chem.* **1993**, *97*, 6272.
[123] H. Dinçalp, Z. Askar, C. Zafer, S. Icli, *Dyes Pigm.* **2011**, *91*, 182.
[124] M. Liang, W. Xu, F. Cai, P. Chen, B. Peng, J. Chen, Z. Li, *J. Phys. Chem. C* **2007**, *117*, 4465.
[125] G. Li, K. Jiang, Y. Li, S. Li, L. Yang, *J. Phys. Chem. C* **2008**, *112*, 11591.
[126] Z. Ning, Q. Zhang, W. Wu, H. Pei, B. Liu, H. Tian, *J. Org. Chem.* **2008**, *73*, 3791.
[127] C. A. Echeverry, R. Cotta, A. Insuasty, A. Ortíz, N. Martín, L. Echegoyen, B. Insuasty, *Dyes Pigm.* **2018**, *153*, 182.
[128] B. Liu, W. H. Zhu, W. J. Wu, K. M. Ri, H. Tian, *J. Photochem. Photobiol. A* **2008**, *194*, 268.
[129] Y. H. Jin, J. L. Hua, W. J. Wu, X. M. Ma, F. S. Meng, *Synth. Met.* **2008**, *158*, 64.
[130] D. K. Panda, F. S. Goodson, S. Ray, R. Lowell, S. Saha, *Chem. Commun.* **2012**, *48*, 8775.
[131] D. K. Panda, F. S. Goodson, S. Ray, S. Saha, *Chem. Commun.* **2014**, *50*, 5358.
[132] S. Yanagida, G. K. R. Senadeera, K. Nakamura, T. Kitamura, Y. Wada, *J. Photochem. Photobiol. A* **2004**, *166*, 75.
[133] G. K. R. Senadeera, K. Nakamura, T. Kitamura, Y. Wada, S. Yanagida, *Appl. Phys. Lett.* **2003**, *83*, 5470.
[134] Y. Kim, J. Walker, L. A. Samuelson, J. Kumar, *Nano Lett.* **2003**, *3*, 523.
[135] Y. Z. Hao, M. Z. Yang, S. M. Cai, *Sol. Energy Mater. Sol. Cells* **1998**, *56*, 75.
[136] T. Kitamura, M. Ikeda, K. Shigaki, T. Inoue, N. A. Anderson, X. Ai, T. Lian, S. Yanagida, *Chem. Mater.* **2004**, *16*, 1806.
[137] X. Liu, R. Zhu, Y. Zhang, B. Liu, S. Ramakrishna, *Chem. Commun.* **2008**, *32*, 3789.
[138] C. Kanimozhi, P. Balraju, G. D. Sharma, S. Patil, *J. Phys. Chem. C* **2010**, *114*, 3287.
[139] Z. Fang, A. A. Eshbaugh, K. S. Schanze, *J. Am. Chem. Soc.* **2011**, *133*, 3063.
[140] S. Yuna, J. N. Freitas, A. F. Nogueira, Y. Wang, S. Ahmad, Z. S. Wang, *Prog. Polym. Sci.* **2016**, *59*, 1.
[141] M. S. Su'ait, M. Y. A. A. Rahman, A. Ahmad, *Sol. Energy* **2015**, *115*, 452.
[142] H. Niu, J. Luo, W. Wu, J. Mu, C. Wang, X. Bai, W. Wang, *J. Appl. Polym. Sci.* **2012**, *125*, 200.
[143] D. Giri, S. K. Raut, S. K. Patra, *Dyes Pigm.* **2020**, *174*, 108032.
[144] T. Edvinsson, N. Pschirer, J. Schöneboom, F. Eickemeyer, G. Boschloo, A. Hagfeldt, *Chem. Phys.* **2009**, *357*, 124.
[145] M. K. Nazeeruddin, F. De Angelis, S. Fantacci, A. Selloni, G. Viscardi, P. Liska, S. Ito, B. Takeru, M. Grätzel, *J. Am. Chem. Soc.* **2005**, *127*, 16835.
[146] N. Tasios, C. Grigoriadis, M. R. Hansen, H. Wonneberger, C. Li, H. W. Spiess, K. Müllen, G. Floudas, *J. Am. Chem. Soc.* **2010**, *132*, 7478.
[147] S. Ferrere, B. A. Gregg, *J. Phys. Chem. B* **2001**, *105*, 7602.
[148] S. Ferrere, B. A. Gregg, *New J. Chem.* **2002**, *26*, 1155.
[149] T. Dentani, K. Funabiki, J. Y. Jin, T. Yoshida, H. Minoura, M. Matsui, *Dyes Pigm.* **2007**, *72*, 303.
[150] J. T. Otsuki, Y. Takaguchi, D. Takahashi, P. Kalimuthu, S. P. Singh, A. Islam, L. Han, *Adv. Optoelectron.* **2011**, *2011*, 860486.
[151] C. Li, J. H. Yum, S. J. Moon, A. Herrmann, F. Eickemeyer, N. G. Pschirer, P. Erk, J. Schöneboom, K. Müllen, M. Grätzel, M. K. Nazeeruddin, *ChemSusChem* **2008**, *1*, 615.
[152] C. Li, Z. H. Liu, J. Schöneboom, F. Eickemeyer, N. G. Pschirer, P. Erk, A. Herrmann, K. Müllen, *J. Mater. Chem.* **2009**, *19*, 5405.

[153] A. Keerthi, Y. Liu, Q. Wang, S. Valiyaveettil, *Chem.-Eur. J.* **2012**, *18*, 11669.
[154] T. Edvinsson, C. Li, N. Pschirer, J. Schöneboom, F. Eickemeyer, R. Sens, G. Boschloo, A. Herrmann, K. Müllen, A. Hagfeldt, *J. Phys. Chem. C* **2007**, *111*, 15137.
[155] S. Mathew, H. Imahori, *J. Mater. Chem.* **2011**, *21*, 7166.
[156] H. Chen, H. Lu, C. Lee, S. Chuang, E. W. Diau, C. Yeh, *J. Chin. Chem. Soc.* **2010**, *57*, 1141.
[157] C. Jiao, N. Zu, K. Huang, P. Wang, J. Wu, *Org. Lett.* **2011**, *13*, 3652.
[158] F. Bella, C. Gerbaldi, C. Barolo, M. Grätzel, *Chem. Soc. Rev.* **2015**, *44*, 3431.
[159] J. Warnan, J. Willkomm, Y. Farré, Y. Pellegrin, M. Boujtita, F. Odobel, E. Reisner, *Chem. Sci.* **2019**, *10*, 2758.
[160] F. Odobel, Y. Pellegrin, E. A. Gibson, A. Hagfeldt, A. L. Smeigh, L. Hammarström, *Coord. Chem. Rev.* **2012**, *256*, 2414.
[161] F. Odobel, L. L.e Pleux, Y. Pellegrin, E. Blart, *Acc. Chem. Res.* **2010**, *43*, 1063.
[162] W. Shockley, H. J. Queisser, *J. Appl. Phys.* **1961**, *32*, 510.
[163] F. Odobel, Y. Pellegrin, *J. Phys. Chem. Lett.* **2013**, *4*, 2551.
[164] A. Morandeira, J. Fortage, T. Edvinsson, L. L.e Pleux, E. Blart, G. Boschloo, A. Hagfeldt, L. Hammarström, F. Odobel, *J. Phys. Chem. C* **2008**, *112*, 1721.
[165] E. A. Gibson, A. L. Smeigh, L. L.e Pleux, J. Fortage, G. Boschloo, E. Blart, Y. Pellegrin, F. Odobel, A. Hagfeldt, L. Hammarström, *Angew. Chem., Int. Ed.* **2009**, *48*, 4402.
[166] S. Mori, S. Fukuda, S. Sumikura, Y. Takeda, Y. Tamaki, E. Suzuki, T. Abe, *J. Phys. Chem. C* **2008**, *112*, 16134.
[167] J. He, H. Lindström, A. Hagfeldt, S. Lindquist, *Sol. Energy Mater. Sol. Cells* **2000**, *62*, 265.
[168] L. L.e Pleux, A. L. Smeigh, E. Gibson, Y. Pellegrin, E. Blart, G. Boschloo, A. Hagfeldt, L. Hammarström, F. Odobel, *Energy Environ. Sci.* **2011**, *4*, 2075.
[169] E. A. Gibson, L. L.e Pleux, J. Fortage, Y. Pellegrin, E. Blart, F. Odobel, A. Hagfeldt, G. Boschloo, *Langmuir* **2012**, *28*, 6485.
[170] A. L. Smeigh, L. L.e Pleux, J. Fortage, Y. Pellegrin, E. Blart, F. Odobel, L. Hammarström, *Chem. Commun.* **2012**, *48*, 678.
[171] R. Jose, A. Kumar, V. Thavasi, K. Fujihara, S. Uchida, S. Ramakrishna, *Appl. Phys. Lett.* **2008**, *93*, 023125.
[172] Y. Farré, F. Maschietto, J. Föhlinger, M. Wykes, A. Planchat, Y. Pellegrin, E. Blart, I. Ciofini, L. Hammarström, F. Odobel, *ChemSusChem* **2022**, *13*, 1844.
[173] A. Nattestad, A. J. Mozer, M. K. R. Fischer, Y. B. Cheng, A. Mishra, P. Bauerle, U. Bach, *Nat. Mater.* **2010**, *9*, 31.
[174] S. Powar, T. Daeneke, M. T. Ma, D. Fu, N. W. Duffy, G. Goti, M. Weidelener, A. Mishra, P. Bäuerle, L. Spiccia, U. Bach, *Angew. Chem., Int. Ed.* **2013**, *52*, 602.
[175] I. R. Perera, T. Daeneke, S. Makuta, Z. Yu, Y. Tachibana, A. Mishra, P. Bäuerle, C. A. Ohlin, U. Bach, L. Spiccia, *Angew. Chem., Int. Ed.* **2015**, *54*, 3758.
[176] M. Weidelener, A. Mishra, A. Nattestad, S. Powar, A. J. Mozer, E. Mena-Osteritz, Y.-B. Cheng, U. Bach, P. Bäuerle, *J. Mater. Chem.* **2012**, *22*, 7366.
[177] Z. Liu, D. Xiong, X. Xu, Q. Arooj, H. Wang, L. Yin, W. Li, H. Wu, Z. Zhao, W. Chen, M. Wang, F. Wang, Y.-B. Cheng, H. He, *ACS Appl. Mater. Interfaces* **2014**, *6*, 3448.
[178] P. Qin, H. Zhu, T. Edvinsson, G. Boschloo, A. Hagfeldt, L. Sun, *J. Am. Chem. Soc.* **2008**, *130*, 8570.
[179] K. A. Click, D. R. Beauchamp, B. R. Garrett, Z. Huang, C. M. Hadad, Y. Wu, *Phys. Chem. Chem. Phys.* **2014**, *16*, 26103.
[180] Y. Wu, W.-H. Zhu, S. M. Zakeeruddin, M. Grätzel, *ACS Appl. Mater. Interfaces* **2015**, *7*, 9307.
[181] X. Li, F. Yu, S. Stappert, C. Li, Y. Zhou, Y. Yu, X. Li, H. Ågren, J. Hua, H. Tian, *ACS Appl. Mater. Interfaces* **2016**, *8*, 19393.
[182] C.-H. Chang, Y.-C. Chen, C.-Y. Hsu, H.-H. Chou, J. T. Lin, *Org. Lett.* **2012**, *14*, 4726.
[183] M. Bonomo, N. Barbero, G. Naponiello, M. Giordano, D. Dini, C. Barolo, *Front. Chem.* **2019**, *7*, 99.
[184] J. Warnan, J. Gardner, L. L.e Pleux, J. Petersson, Y. Pellegrin, E. Blart, L. Hammarström, F. Odobel, *J. Phys. Chem. C* **2014**, *118*, 103.
[185] S. K. Yadav, S. Ravishankar, S. Pescetelli, A. Agresti, F. Fabregat-Santiago, A. Di Carlo, *Phys. Chem. Chem. Phys.* **2017**, *19*, 22546.
[186] U. Bach, D. Lupo, P. Comte, J. E. Moser, F. Weissörtel, J. Salbeck, H. Spreitzer, M. Grätzel, *Nature* **1998**, *395*, 583.
[187] Z. Shen, B. Xu, P. Liu, Y. Hu, Y. Yu, H. Ding, L. Kloo, J. Hua, L. Sun, H. Tian, *J. Mater. Chem. A* **2017**, *5*, 1242.
[188] E. V. A. Premalal, N. Dematage, G. R. R. A. Kumara, R. M. G. Rajapakse, M. Shimomura, K. Murakami, A. Konno, *J. Power Sources* **2012**, *203*, 288.
[189] I. Chung, B. Lee, J. He, R. P. H. Chang, M. G. Kanatzidis, *Nature* **2012**, *485*, 486.
[190] Y. Cao, Y. Saygili, A. Ummadisingu, J. J. Teuscher, J. Luo, N. Pellet, F. Giordano, S. M. Zakeeruddin, J.-E. Moser, M. Freitag, A. Hagfeldt, M. Grätzel, *Nat. Commun.* **2017**, *8*, 15390.
[191] M. Chevrier, H. Hawashin, S. Richeter, A. Mehdi, M. Surin, R. Lazzaroni, P. Dubois, B. Ratier, J. Bouclé, S. Clément, *Synth. Met.* **2017**, *226*, 157.
[192] J. Zhang, L. Yang, Y. Shen, B.-W. W. Park, Y. Hao, E. M. J. Johansson, G. Boschloo, L. Kloo, E. Gabrielsson, L. Sun, A. Jarboui, C. Perruchot, M. Jouini, N. Vlachopoulos, A. Hagfeldt, *J. Phys. Chem. C* **2014**, *118*, 16591.
[193] C. Zafer, C. Karapire, N. S. Sariciftci, S. Icli, *Sol. Energy Mater. Sol. Cells* **2005**, *88*, 11.
[194] J. A. Mikroyannidis, M. M. Stylianakis, M. S. Roy, P. Suresh, G. D. Sharma, *J. Power Sources* **2009**, *194*, 1171.
[195] C. Noumissing Sao, K. Onken, T. P. I. Saragi, T. Fuhrmann-Lieker, J. Salbeck, *Synth. Met.* **2012**, *162*, 888.
[196] U. B. Cappel, M. H. Karlsson, N. G. Pschirer, F. Eickemeyer, J. Schöneboom, P. Erk, G. Boschloo, A. Hagfeldt, *J. Phys. Chem. C* **2009**, *113*, 14595.
[197] U. B. Cappel, A. L. Smeigh, S. Plogmaker, E. M. J. Johansson, H. Rensmo, L. Hammarström, A. Hagfeldt, G. Boschloo, *J. Phys. Chem. C* **2011**, *115*, 4345.
[198] H. Wonneberger, N. Pschirer, I. Bruder, J. Schöneboom, C. Q. Ma, P. Erk, C. Li, P. Bäuerle, K. Müllen, *Chem. Asian J.* **2011**, *6*, 1744.
[199] I. A. Howard, M. Meister, B. Baumeier, H. Wonneberger, N. Pschirer, R. Sens, I. Bruder, C. Li, K. Müllen, D. Andrienko, F. Laquai, *Adv. Energy Mater.* **2014**, *4*, 1300640.
[200] J. Luo, M. Xu, R. Li, K.-W. Huang, C. Jiang, Q. Qi, W. Zeng, J. Zhang, C. Chi, P. Wang, J. Wu, *J. Am. Chem. Soc.* **2014**, *136*, 265.
[201] A. Yella, H. Lee, H. N. Tsao, C. Yi, A. Chandiran, M. K. Nazeeruddin, E. W.-G. Diau, C. Y. Yeh, S. M. Zakeeruddin, M. Grätzel, *Science* **2011**, *334*, 629.
[202] Z. Yao, C. Yan, M. Zhang, R. Li, Y. Cai, P. Wang, *Adv. Energy Mater.* **2014**, *4*, 1400244.
[203] M. Zhang, Z. Yao, C. Yan, Y. Cai, Y. Ren, J. Zhang, P. Wang, *ACS Photonics* **2014**, *1*, 710.
[204] M. Zhang, Y. Wang, M. Xu, W. Ma, R. Li, P. Wang, *Energy Environ. Sci.* **2013**, *6*, 2944.
[205] L. Yang, Y. Ren, Z. Yao, C. Yan, W. Ma, P. Wang, *J. Phys. Chem. C* **2015**, *119*, 980.
[206] L. Yang, S. Chen, J. Zhang, J. Wang, M. Zhang, X. Dong, P. Wang, *J. Mater. Chem. A* **2017**, *5*, 3514.
[207] H. Wu, L. Yang, Y. Li, M. Zhang, J. Zhang, Y. Guo, P. Wang, *J. Mater. Chem. A* **2016**, *4*, 519.

[208] Y. Li, J. Wang, Y. Yuan, M. Zhang, X. Dong, P. Wang, *Phys. Chem. Chem. Phys.* **2017**, *19*, 2549.
[209] L. Yang, Z. Yao, J. Liu, J. Wang, P. Wang, *ACS Appl. Mater. Interfaces* **2016**, *8*, 9839.
[210] X. Li, Z. Zheng, W. Jiang, W. Wu, Z. Wang, H. Tian, *Chem. Commun.* **2015**, *51*, 3590.
[211] F. Yu, S.-C. Cui, X. Li, Y. Peng, Y. Yu, K. Yun, S.-C. Zhang, J. Li, J.-G. Liu, J. Hua, *Dyes Pigm.* **2007**, *139*, 7.
[212] Q. Qi, X. Wang, L. Fan, B. Zheng, W. Zeng, J. Luo, K.-W. Huang, Q. Wang, J. Wu, *Org. Lett.* **2015**, *17*, 724.
[213] Q. Qi, J. Zhang, S. Das, W. Zeng, J. Luo, J. Zhang, P. Wang, J. Wu, *R. S. C. Adv.* **2016**, *6*, 81184.
[214] Z. Yao, M. Zhang, H. Wu, L. Yang, R. Li, P. Wang, *J. Am. Chem. Soc.* **2015**, *137*, 3799.
[215] Y. Ren, Y. Li, S. Chen, J. Liu, J. Zhang, P. Wang, *Energy Environ. Sci.* **2016**, *9*, 1390.
[216] P. Xu, C.-R. Zhang, Y.-Z. Wu, L.-H. Yuan, Y.-H. Chen, Z.-J. Liu, H.-S. Chen, *J. Phys. Chem. A* **2020**, *124*, 3626.
[217] Z. Yao, H. Wu, Y. Li, J. Wang, J. Zhang, M. Zhang, Y. Guo, P. Wang, *Energy Environ. Sci.* **2015**, *8*, 3192.
[218] J. Wang, H. Wu, L. Jin, J. Zhang, Y. Yuan, P. Wang, *Chem Sus Chem* **2017**, *10*, 2962.
[219] J. Luo, J. Zhang, K.-W. Huang, Q. Qi, S. Dong, J. Zhang, P. Wang, J. Wu, *J. Mater. Chem. A* **2016**, *4*, 8428.
[220] H.-H. Chou, Y.-C. Liu, G. Fang, Q.-K. Cao, T.-C. Wei, C.-Y. Yeh, *ACS Appl. Mater. Interfaces* **2017**, *9*, 37786.
[221] A. Arunkumar, S. Shanavas, R. Acevedo, P. M. Anbarasan, *Opt. Quantum. Electron.* **2020**, *52*, 164.
[222] D. Nicksonsebastin, P. Pounraj, M. Prasath, *J. Mol. Model.* **2022**, *28*, 102.
[223] D. Nicksonsebastin, P. Pounraj, N. Mani, M. Selvapandiyan, M. Prasath, *J. Mol. Model.* **2022**, *28*, 373.

Marco Giordano received his Ph.D. in Chemical and Material Science from the University of Torino in 2023. In 2021 he joined for 6 months as visiting Ph.D. student the Laboratory of Photonics and Interfaces (LPI) at the École Polytechnique Fédérale de Lausanne. His research interest includes the synthesis of NIR sensitizers, fluorophore, and redox couples for photovoltaics and biological applications.

Francesca Cardano graduated in Medicinal Chemistry and Pharmaceutical Technology from the University of Genova (Italy) in 2015. She got her Ph.D. in 2020 at the same University in affiliation with the Italian Institute of Technology (IIT) and the University of Miami, afterward she moved to the University of Torino and the University of Milano as a Postdoc Researcher. Since December 2022 she is a Research Fellow at the University of Torino. Her research interest focuses on the investigation of molecular photoswitches, functional dyes, and fluorophores for application in photopharmacology, chemical biology, and material science.

Claudia Barolo graduated in Industrial Chemistry in 1997 and obtained her Ph.D. in Chemical Science in 2001. She is now Full Professor in Industrial Chemistry and Deputy Director (Research) at the Department of Chemistry of the University of Torino (Italy). Her research activity is mainly devoted to the synthesis and characterization of functional molecules and materials (i.e., chromogens and polymers) for innovative technological applications with special attention to the energy field (photovoltaics and lighting). In 2023 she was the recipient of the Italian Society of Chemistry – Organic Division prize "Organic Chemistry for Environment, Energy and Nanoscience".

Guido Viscardi was a Full Professor in Organic Chemistry in the Department of Chemistry and the NIS (Nanostructured Interfaces and Surfaces) Centre of Excellence at the University of Torino till 2023. His research activity was mainly focused on the synthesis, characterization of all-organic and organometallic functional dyes for applications in solar energy conversion, micro- and nano-sensors, optoelectronics, chemical biology, and analytical chemistry. In 2011, he received the Ravani-Pellati Award from the Academy of Sciences of Torino in recognition of his scientific contribution to the field of functional dyes.

Andrea Fin graduated in Chemistry from the University of Torino (Italy) in 2008 and obtained his Ph.D. in 2012 at the University of Geneva (Switzerland) He later moved to the University of California San Diego (USA) as SNSF fellow and in 2017 he was appointed Research Scientist at Institute of Bioengineering and Nanotechnology (Singapore). In 2018 he returned to the University of Torino where he is currently Associate Professor in Organic Chemistry. His main research focuses on the development of functional dye and fluorophores for application in smart materials and chemical biology.